Investigation of magnetized radio frequency plasma sources for electric space propulsion

Jan Dennis Gerst

▶ To cite this version:

UNIVERSITÉ D'ORLÉANS

THÈSE présentée par :

Jan Dennis GERST

soutenue le : **08 novembre 2013**

pour obtenir le grade de : **Docteur de l'université d'Orléans**

Discipline/ Spécialité : Physique

Investigation of Magnetized Radio Frequency Plasma Sources for Electric Space Propulsion

---

Acknowledgments

The last three years have been an adventure for me. I couldn't have accomplished all of that without the help and support of my colleagues, family and friends. Therefore I want to thank them for the support they have given me.

First of all I want to thank my advisor, Stéphane Mazouffre for making all of this possible. He gave me the chance to write my Diplomarbeit under his supervision and found afterward a Ph.D. grant for me. He was always there for me when I needed advice and help.

I would like to thank my Ph.D. jury, especially my two rapporteur, for taking the time to read my manuscript, come to my Ph.D. defense and giving me comments how to improve my work.

Another thank you goes to all my colleagues in ICARE and the LPP who made it possible for me to do this huge amount of work over that short period of time. Thank you also to my former co-Ph.D. students Käthe, Guillaume, Julien and Denis with who I shared hours of discussions and the occasional beer. Thank you also to Sedina, Mihaela and Aurélien for your advice and participation in my work. Thank you to all the interns and especially Stéphane and Friederike who took a great amount of work of my shoulders.

I would like to thank my parents Hans-Dieter and Biggi, who were always there for me and supported me with everything I did in my life. I would not be the person I am today without you! I would like to extend this thanks to the whole of my family and especially to my brothers Freddy and Alex who had also a great influence on who I am today.

At last I would like to thank all my friends, the ones I made when I was going to school and to university in Germany to the ones I made here in France, for the great times I had, for all the adventures we had together and for many experiences we shared!

Contents

List of Figures

xiii

List of Tables

1 General Introduction

"A Rocket into Cosmic Space" was the name of an article published by K. E. Tsiolkovsky [1] in 1903. This is the date now considered the beginning of modern rocket science and astronautics. Probably the most important part of this article is what is known as the Tsiolkovsky rocket equation. This equation describes the motion of a vehicle exhausting mass carried within the itself for propulsion. This equation states that the maximum change of speed depends on the ratio between the initial mass to the final mass and the effective exhaust velocity. Tsiolkovsky himself recognized the limits of the exhaust velocity in chemical propulsion and wrote 8 years later *"It is possible that in time we may use electricity to produce a huge velocity for the particles ejected from the rocket device"* in his article "Investigation of Universal Space by Means of Reactive Devices".

The serious development of chemical rocket engines started in the late 40s of the 20th century. The speed of development accelerated fast in the 50s where the launch of the Sputnik satellite by the Soviet Union on October 4, 1957 triggered the space race. From this point on, the Soviet Union and the United states did compete for supremacy in space and goals like first human in space, first spacewalk to the end when Neil Armstrong put his foot on the moon on July 20, 1969.

From the time of Tsiolkovsky's prediction it has taken over 50 years until 1964 NASA launched the SERT-1 mission with a Kaufman type ion thruster and proved Tsiolkovsky right. The NASA demonstrated the propulsion of a space probe by means of electrostatic accelerated particles. Since then electric propulsion developed fast. Where early missions used mercury or cesium as propellant [2], xenon is now the standard for most of the modern electric thruster. A large number of different electric thrusters concepts have been developed in the last 50 years. Out of all these concepts two types of engines have shown the most promise, the ion thruster and the Hall thruster. These two concepts clearly monopolize the market and have been space proven in a large amount of missions. They both offer a performance in terms of thrust efficiency and specific impulse that

cannot physically be reached with chemical propulsion. This allows for mission scenarios not been possible before.

The Deep Space 1 mission of NASA carried out a flyby on the asteroid Braille and the comet Borrelly with the help of its NSTAR ion thruster. The Japanese Hayabusa mission used microwave ion thrusters to go rendezvous with the the asteroid Itokawa get a sample of material and return it to earth. The GOCE mission of the European ESA uses a pair of T5 ion thruster to counteract the drag force of the atmosphere in order to precisely measure the earth's gravitational field.

Both thruster types, the Hall thruster and the ion thruster, though relying on different architectures and physical principles, share a common point they accelerate only positive ions. Therefore they have the need for an external neutralizing cathode to provide the electrons to balance the charges in the accelerated plasma. Furthermore, positive ions and electrons have a recombination length of several hundred meters and a possible interaction with the components of the spacecraft such as solar panels or optics cannot be avoided.

The PEGASES thruster (Plasma Propulsion with Electronegative Gases) goes another way. The concept is under development by the LPP (Laboratoire de Physique des Plasmas) of the Ecole Polytechnique in Paris since 2005. The PEGASES thruster accelerates positive and negative ions. The ions are produced by a radio frequency (RF) source with an electronegative gas such as SF_6. The plasma passes a magnetic field to cool down the electrons and increase the creation of negative ions. The strongly electronegative plasma is then accelerated by alternatively biased grids. A neutralization cathode is not needed since positive and negative chargers exit the thruster and a quasi neutrality is given. The recombination length between positive and negative ions is only a fraction of that between electrons and positive ions. This avoids the backscattering of the charged particles which can lead to degradation of the solar panels or the optics of the payload.

1.1 Motivation and Goals

Despite the apparent simplicity of the concept a lot of work remained to be done. We started our experiments with a capacitive coupled RF discharge at 13.56 MHz inside a quartz tube with the goal to investigate the magnetic field layouts for the PEGASES thruster. While performing the experiments we discovered a strip-like structure inside

the plasma. A similar structure had just been predicted in numerical simulations. This led to a new priority in our research and we tried to answer the following questions: Where does that structure come from? What does it mean for the PEGASES thruster? Can it be avoided? In the end it turned out that this structure has also been observed inside the PEGASES thruster.

After the second PEGASES thruster prototype, designed by the team of the LPP Ecole Polytechnique in Paris, became available to us. We integrated it into our new vacuum chamber which was specially constructed for the thruster. We started to research this thruster with all probe systems available to us in order to obtain the performance level with xenon to compare it to radio-frequency ion thrusters (RIT).

We needed a tool to measure the ion velocity distribution function (VDF) as well as the molecular ion fraction and the amount of multiply charged ions inside the plume of the thruster. For this, we started to develop an E×B probe which is smaller than a mass spectrometer, can be placed inside the vacuum chamber and is easier to use. The goal was to use the probe in a variety of gases and ultimately in SF_6, the proposed propellant for the PEGASES prototype.

1.2 Chapter Summary

Chapter 2 gives an introduction into the fundamentals of space propulsion followed by a presentation of Hall thruster and ion thrusters. A more detailed description is given for the ion thrusters as they are closely related to the object of research. The chapter continues with a description of the PEGASES thruster concept and its elements, the RF plasma source, the magnetic barrier and the acceleration system. The chapter closes with a description of the dedicated vacuum test bench used in the experiments.

Chapter 3 presents the plasma probes used in the frame of the work. It briefly introduces the planar probe, the capacitive probe, the Langmuir probe, the emissive probe and the retarding potential analyzer and the underlying theories used for processing the obtained data.

Chapter 4 gives a more detailed introduction into the theory and the construction of the E×B probe. Numerical simulations of the magnetic and electric field inside the probe are presented as well as ion trajectory simulations. A detailed description of the construction of the probe system is given. The chapter concludes with the presentation

of first measurements which have been performed in a Hall thruster and the PEGASES ion thruster.

Chapter 5 describes the investigation of a strip-like structure found in a RF plasma with a transverse magnetic field. Measurements with a variety of probes reveal the properties of the plasma. The strip-like structure is a narrow region of high electron density and temperature and large plasma potential. The strip makes the plasma strongly inhomogeneous. The E×B drift is identified as the most likely origin for the drift structure. The latter can be seen as an open drift in which the electron flow interacts with the walls. A Faraday shield is used to change the discharge conditions from capacitive to inductive and avoid the strip.

Chapter 6 contains the experiments performed with the PEGASES thruster. The properties of the thruster are characterized inside the discharge cavity and the power transfer efficiency is given. Measurements with the E×B probe, a planar probe and an RPA in the plume of the thruster operating in xenon are presented. A thrust estimate based on the measured ion flux is given. The chapter concludes with experiments performed with the magnetic barrier in SF_6 and xenon.

Chapter 7 presents the conclusion of the performed work and gives a prospect for future research.

2 Electric Propulsion

2.1 Fundamentals of Space Propulsion

The purpose of a propulsion system is the generation and delivery of thrust in order to move it. This is true for cars and airplanes as well as for rockets and satellites. The principle of the thrust generation of a rocket engine is to create a momentum exchange between the propellant which is ejected with a high velocity and the rocket or spacecraft. This can be described with:

$$T = \frac{dm}{dt} v_e = \dot{m} v_e, \tag{2.1}$$

where T is the thrust , m is the propellant mass, $\dot{m}$ is the propellant mass flow rate and v_e is the effective propellant exhaust velocity.

Satellites and space probes are getting increasingly complex. The numbers of systems and experiments on board are constantly increasing and the frontier of what is possible is constantly pushed. But as the cost of putting an object is still very high, the requirements for the propulsion system can be summarized in one statement, fulfill the mission goals with the least amount of mass. The mission requirements might demand for a high thrust like for the start of a rocket but once in space another factor gets more important. The Δv, the change of speed of the spacecraft by its propulsion system when no other additional force is applied. It originates in Konstantin Tsiolkovsky rocket equation [1],

$$\Delta v = v_e \cdot \ln \frac{m_0}{m_1}, \tag{2.2}$$

where m_0 is the initial mass of the spacecraft and m_1 the mass at the end of the maneuver.

To calculate the achievable Δ_v of the spacecraft, the equation can be rewritten as,

$$\Delta v = v_e \cdot \ln \frac{m_d + m_p}{m_d}, \tag{2.3}$$

where m_d is the final delivered mass and m_p is the total propellant mass.

This equation can be rearranged to show the relation between the propellant mass and the Δv requirement,

$$m_p = m_d \left(e^{\Delta v/v_e} - 1 \right), \tag{2.4}$$

from this equation we can clearly see that the propellant mass increases exponentially with the required Δv. The only feasible solution to increase the mission Δv above a certain grade is therefore to increase the propellant exhaust velocity. The literature [2, 3] gives, for chemical propulsion, a maximum achievable effective exhaust velocity of $4 - 4.5 \,\mathrm{km/s}$. The performance of a propulsion system is usually given in form of the specific impulse I_{sp},

$$I_{sp} = \frac{T}{\dot{m}g_o} = \frac{v_e}{g_0}, \tag{2.5}$$

where g_0 is the gravitational constant. The higher the I_{sp} the less propellant mass is needed to achieve a certain Δv.

The exhaust velocity in chemical propulsion is achieved by expansion of a hot gas through a nozzle. The gas has to be brought to a high pressure in order for the process to be effective. This is usually achieved by burning the gas and is limited by the energy contained in the propellant and the mechanical constrains of the materials used. The solution to break the restrains of chemical propulsion lies in introducing the energy in another form. This is the idea of electric space propulsion.

While the energy of chemical propulsion is stored in the chemical bonds of the propellant the energy of the electric propulsion system introduce the energy into the propellant by an external source. Although there are many ways to generate and store energy on a spacecraft the most common source nowadays are solar panels. In electric propulsion there are several ways to deposit the power into the propellant:

- The electrothermal thrusters are using the electric energy to heat and increase the
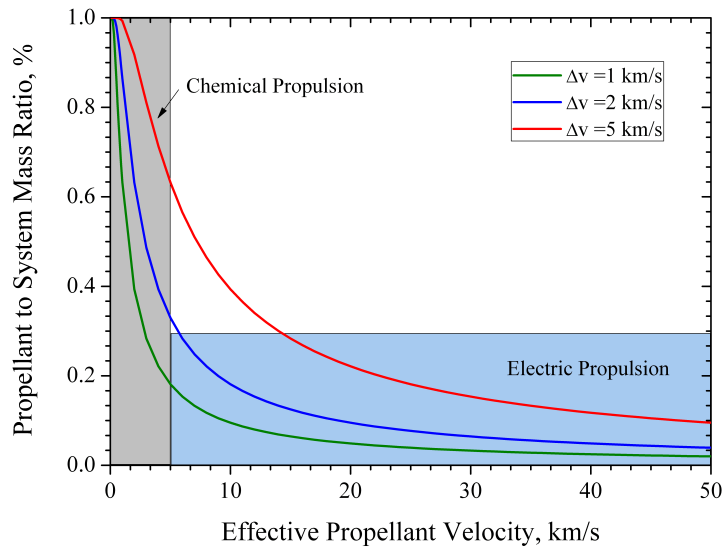
Figure 2.1: Propellant to system mass ration for common Δv requirements over the effective exhaust velocity.

pressure of the propellant and then converting it into kinetic energy by expansion in a nozzle similar to chemical propulsion systems. Arcjets and resitor jets belong to this category.

- The electromagnetic thrusters accelerate the ionized propellant by either the Lorentz force or by an electromagnetic field. Magnetoplasmadynamic thrusters and pulsed plasma thrusters belong to this group.

- The electrostatic thrusters like the Hall thruster or the ion thruster use an electrostatic field in the direction of thrust vector to accelerate the ionized plasma.

Figure 2.1 shows the propellant to mass ratio for several common Δv requirements over the effective exhaust velocity using the Tsiolkovsky rocket equation (Eq. B.1). This explains that a low propellant to mass ratio can only be achieved with the high exhaust velocities provided by electric propulsion.

Out of a variety of different ideas of electrical propulsion two concepts clearly emerged and have already been used on several missions, the Hall thruster and the gridded ion thruster.
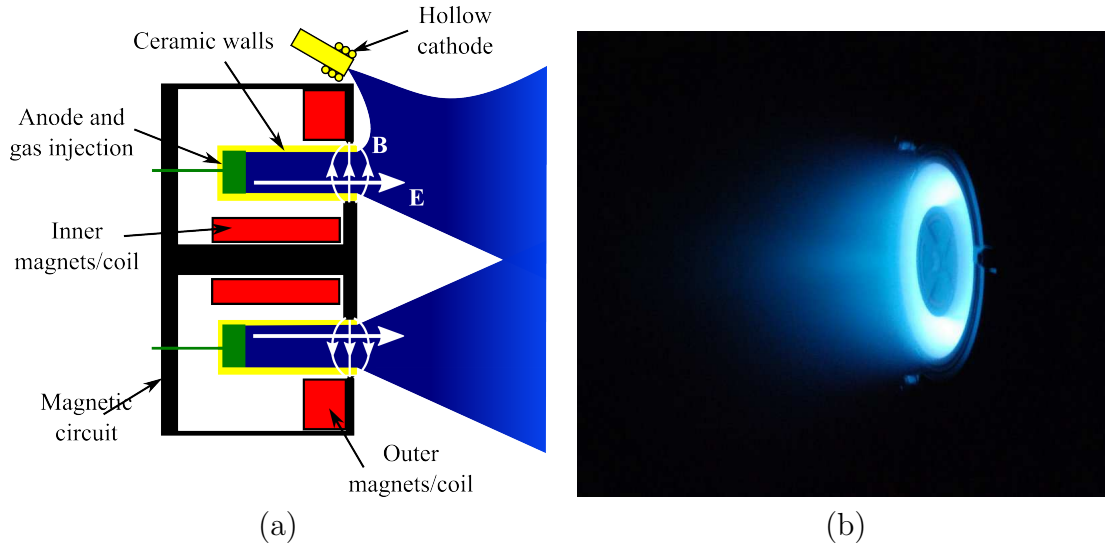
Figure 2.2: The schematic function of a Hall thruster is shown in (a) and (b) shows the PPI Hall thruster in the NeXet test chamber at the ICARE.

2.2 Hall Thruster

The Hall thruster or stationary plasma thruster is an electric thruster where the propellant is ionized and then accelerated by an electric field. A Hall thruster consists of a annular channel in which the gas, usually Xenon, is ionized. In this channel a radial magnetic field is generated by coils or permanent magnets. The magnetic field and an electric field between the thruster anode, located in the annular channel, and the cathode potential plasma in front of the thruster, forces the electrons to spiral in $E \times B$ direction around the thruster axis. This current is responsible for the ionization and is called the Hall current. A schematic drawing of the Hall thruster and a picture of the PPI Hall thruster in the NeXet test chamber at the ICARE (Institut de Combustion Aérothermique Réactivité et Environnement) is presented in Fig. 2.2.

The magnetic field is designed to influence the electrons but is not strong enough to deflect the heavier ions. The ions are accelerated parallel to the channel axis by the electric field between the anode in the thruster and the cathode in front of the thruster. The externally mounted cathode provides electrons to neutralize the beam [2].

The Hall thruster is a well researched thruster and has been flown in space regularly since its first mission in 1971 on board the Russian Meteor satellite [2]. Hall thrusters are routinely used for station keeping and orbit insertion on geostationary communications satellites.

2.3 Ion Thruster

2.3.1 Introduction

The PEGASES thruster used in this thesis is closely related to the ion thruster (or gridded electrostatic ion thruster) and therefore a more detailed introduction will be given.

Ion thrusters work by electrostatically accelerating ions extracted from a plasma generator and then neutralizing them. The first ever in space flown electric thruster was an mercury operated ion thruster in the SERT-1 mission of the NASA in 1964. Since then a few thrusters have been operated in space. The NASA demonstrated with the Deep Space 1 mission in 1998 that ion thrusters can be used reliably as a primary propulsion system for space probes. A picture of the NSTAR ion thruster integrated in the Deep Space 1 probe is shown in Fig. 2.3 (a). A picture of a hot fire test of the NSTAR thruster in the NASA JPL laboratory is shown in Fig. 2.3 (b).The NSTAR thruster was operated so successfully that a cluster of three thrusters has been integrated in NASAS's DAWN mission which has visited and orbited the asteroid Vesta and is currently on it's way to the dwarf planet Ceres.

The Hayabusa mission of the Japanese JAXA used a cluster of four microwave xenon ion thrusters. During this mission the satellite performed a gravity assist maneuver on the earth, approached the asteroid Itokawa took samples and returned them to earth. On the way the thrusters operated more than $35,000\,\mathrm{h}$ per unit [4].

Another notable ion thruster mission is GOCE (Gravity Field and Steady-State Ocean Circulation Explorer) launched by the ESA in 2009. Two QinetiQ T5 ion thrusters are used to overcome the air resistance and to keep the the satellite drag free to improve the measurements of the earths gravitational field. Each of the thrusters can provide a thrust between $0.6 - 20.6\,\mathrm{mN}$ with a resolution of $12\,\mathrm{\mu N}$ [5].

Figure 2.4 shows a schematic drawing of electron bombardment ion thruster with a hollow cathode. The thruster has a ring cusp confined source similar to the one used in the NSTAR thruster and a two grid acceleration system. The electrons needed to keep the plasma quasi neutral are provided by an external neutralizing cathode. Ion thrusters are best broken down and described in three stages: the plasma generation, the plasma acceleration and the neutralization stage:

(a)   (b)
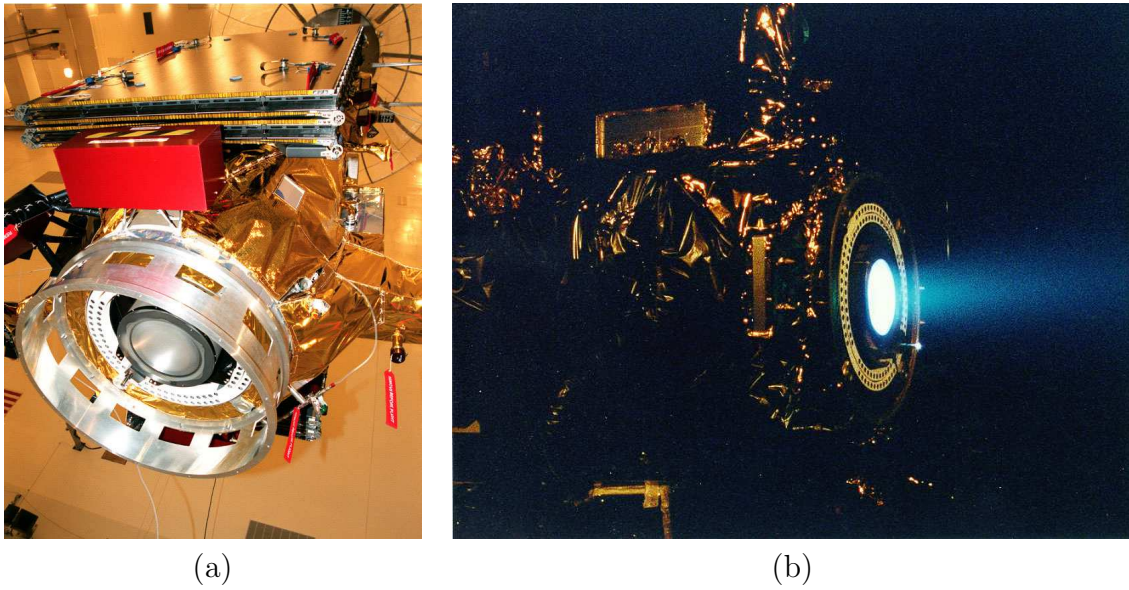
Figure 2.3: (a) shows a picture of the integrated NSTAR ion thruster in the Deep Space
1 probe. (b) shows the NSTAR ion thruster during a hot fire test at NASA's
JPL lab Pasadena, California. (Image credit: NASA)
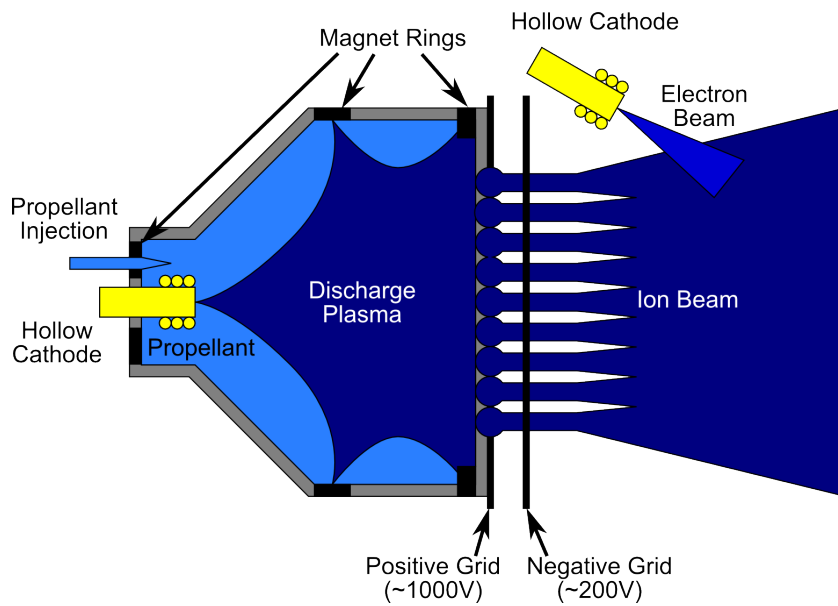
Figure 2.4: Electron bombardment ion thruster with a hollow cathode and ring cusps as
source, a two grid acceleration system and a neutralizing cathode.

2.3.2 Plasma Generation

Three different kinds of plasma generators are commonly used for ion thrusters.

- DC discharge plasma generation where a thermoionic hollow cathode in combination with a DC power supply is used to generate electrons. The electrons are extracted from the cathode and accelerated into the discharge chamber where they ionize the propellant gas. To increase the electron path length and therefore the ionization, magnetic fields are used to confine the electrons. Out of a long list, two types of magnetic confinement are commonly used. The Kaufman type source shown in Fig. 2.5 (a), named after its inventor Harold R. Kaufman, uses a mildly divergent magnetic field to keep the electron on axis of the thruster. In order to reach the anodes which are located close to the walls of the discharge chamber, the electrons have to undergo collisions [2]. The T5 engine used on the GOCE spacecraft and its successor the T6 engine uses this kind of configuration. The second magnetic field layout is called the ring-cusp field configuration and is shown in Fig. 2.5 (b). It is similar to the configuration shown in Fig. 2.4 and is used in the NSTAR thruster of the Deep Space 1 mission. The ring-cusp geometry uses rings of permanent magnets with an alternate polarity. The electrons injected by the cathode follow the field lines and demagnetize sufficiently to bounce of the surface magnetic field until they lose their energy due to collision and ionize the propellant gas or are lost to one of the cusps [2].

- Microwave ion generators use microwave frequencies to generate electromagnetic fields which excite the propellant gas to generate ions. This avoids life time issues which can be a problem with a hollow cathode and reduces sputter erosion in the thruster. The disadvantage is that to start a plasma a relatively high pressure is required. This can decreases the efficiency of such a thruster. The $\mu 10$ thrusters that propelled the Japanese Hayabusa space probe are of this design.

- RF ion thrusters use an inductive coupled plasma (ICP) source to generate an ionized gas. A low frequency RF voltage is applied to a coil, typically wrapped around an insulating chamber, to heat the electrons in the propellant gas which then ionize the atoms. The applied frequency is typically around 1 MHz [6, 7]. The advantage of the 1 MHz frequency over the industry standard frequency of 13.56 MHz is that the inductive reactance in the coil decreases with the frequency. This leads to a lower voltage and a higher current in the coil and reduces the

11
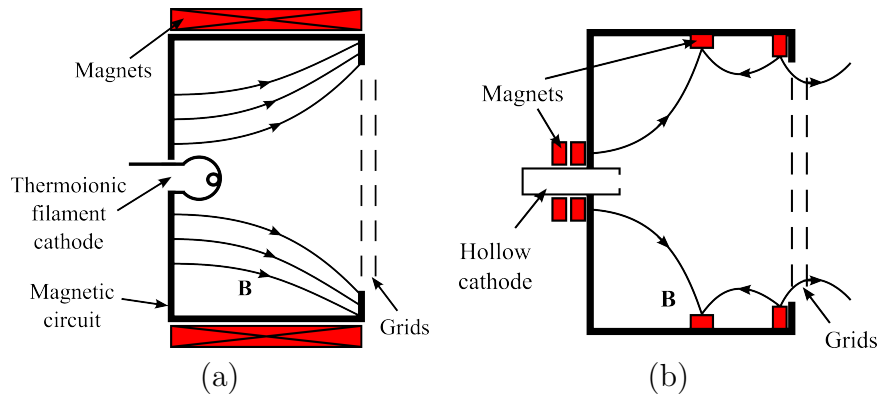
Figure 2.5: Magnetic field types of ion thruster: (a) Kaufman type thruster with a mildly diverging magnetic field and (b) ring-cusp field type.

capacitive coupling. A pair of two RIT-10 thrusters, made by EADS Astrium have been used in ESA's Artemis mission. After the the upper stage of the Ariane 5G carrier did not bring the full power, the satellite was deposed in a 17500 km orbit. In 18 months the RIT-10 thrusters, shown in Fig. 2.6, elevated the orbit to the planed 36000 km geostationary orbit and saved the mission. The RIT-XT is the successor of the RIT-10 and is displayed in Fig. 2.7 [7]. The V-shape of the thruster minimizes the interaction of the plasma with the surface and aims to reduce the ion production costs. The PEGASES thruster is technically a RF ion thruster. Although the plasma generation is similar the rest of it differs quite strongly when used like intended. In this thesis the PEGASES thruster will be used with xenon in the classical mode which means it is similar to a RF ion thruster.
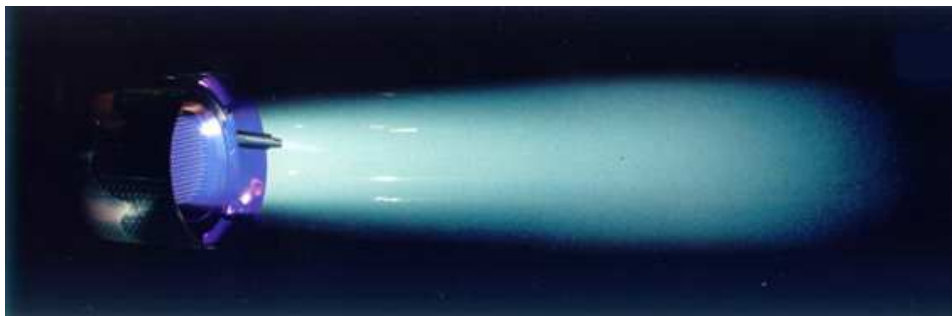
Figure 2.6: The RIT-10 thruster made by Astrium used to save ESA's Artemis mission (Image Credits Astrium).

2.3.3 Plasma Acceleration

The acceleration in ion thrusters is performed electrostatically by biasing a set of multi-aperture grids. This assembly of grids is called the ion optics. A three gridded ion thruster is most commonly used. The electrical schematics and the potential of the plasma along the x-axis are shown in Fig. 2.8. Two and 4-grid designs of the thruster are also in use. In the 2-grid design a deceleration grid is not used. This limits the ion current which can be extracted with the same amount of power. In the 4-grid design a slightly negatively polarized grid is added behind the deceleration grid to avoid backscattering of the electrons emitted by the cathode. The ion optics are designed to accelerate and focus the beam of ions and to minimize the loss onto the grids. In the same time they must warrant a long lifetime. The focusing has to be achieved over the whole range of ion densities which are the result of the different operating conditions. The transparency of the grid directly influences the discharge loss and therefore has to be minimized. In order to minimize the losses the grids should have a high ion transparency to pass a high amount of current but a low neutral transparency to confine the neutral atoms and allow for their ionization. This can be achieved with larger screen grid holes and smaller acceleration grid holes. The form of the grids also directly influences the divergence of the beam. The divergence of the beam should be minimized to generate the maximum amount of thrust. The material determines the lifetime of a grid, as erosion is etching the grids slowly away. The erosion can occur due to secondary ions which are created in the plume of the thruster by resonant charge exchange between the ions and neutral atoms. These ions are attracted to the negatively charged acceleration grid and can hit with sufficient energy to erode the grid. A well designed screen grid focuses the beam and reduces the amount of ions propelled onto the acceleration grid. However ions created between the grids, through charge exchange, are not focused and contribute to the erosion of the acceleration grid. Molybdenum is used as grid material for its positive properties. It has a low sputter erosion rate and it can be chemically etched which makes the production of the grids more cost efficient. Other materials like carbon composites and pyrolytic graphite have also good properties and can be considered as grid material [2].
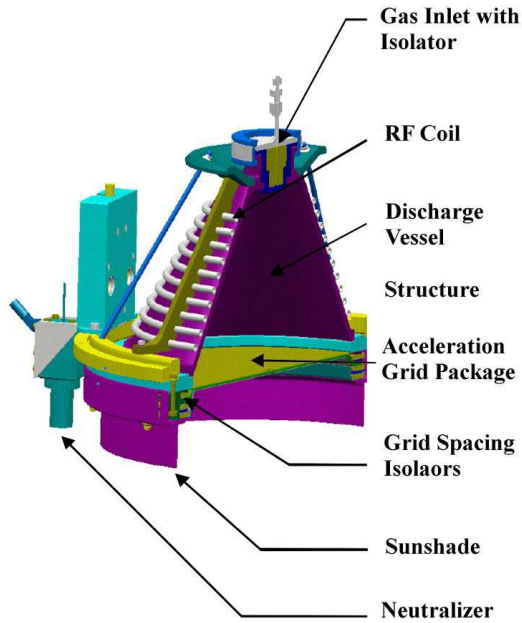
Figure 2.7: The RIT-XT thruster of Astrium (Image Credits Astrium) [7].
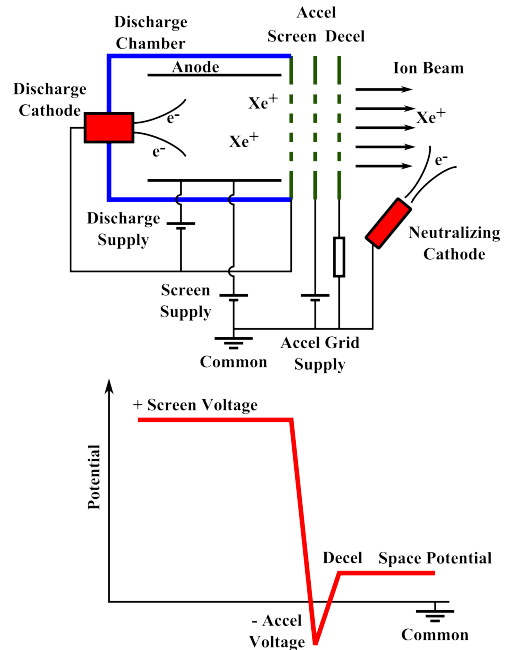
Figure 2.8: Electrical schematic and potential of the plasma in a three gridded ion thruster.

2.3.4 Neutralization

In order to neutralize the ion beam an electron source is needed. Early ion thrusters utilized directly heated tungsten filaments to provide the electrons [2]. This cathode type has, however, a short lifetime of typically several hundreds of hours. The problem can be avoided by the utilization of a hollow cathode. Figure 2.9 shows the cathode used in the beginning of the experiments with the PEGASES thruster. The cathode was designed by the Moscow State Institute of Radio-engineering, Electronics and Automation (MIREA). A wolfram spiral is heating an electron emitting tablet made of LaB_6. Xenon is injected into the cathode and ionized in order to increase the electron flux. The electrons leave the cathode through the orifice in front of the cathode body. The current range of the cathode is between $0.5\,A$ and $8\,A$. The heating current of this cathode is typically between $12-15\,A$ at a voltage of around $10-15\,V$ resulting in a heating power in the region of $120-225\,W$.
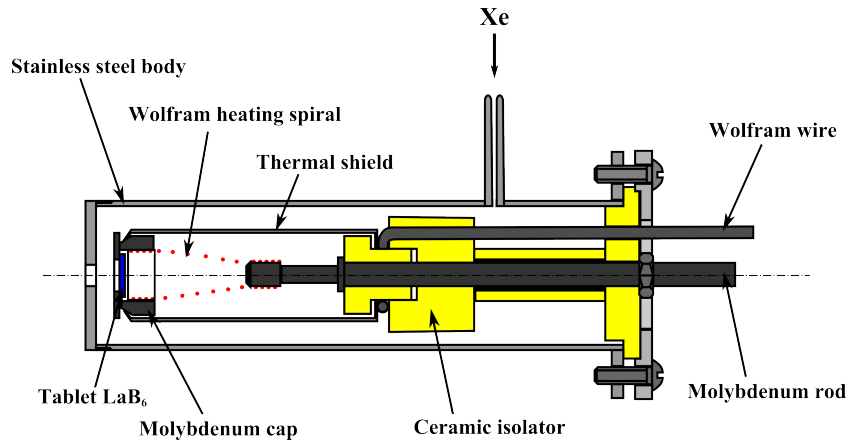
Figure 2.9: Hot cathode used in the beginning of the experiments

2.3.5 Performance

The requirement characteristics for space propulsion systems are quite diverse and it is necessary to find the matching system for each mission. Launchers like the Ariane 5 or the Soyuz need a huge amount of thrust over a short period to be able to reach space. This can not be realized with electric propulsion. But once in space a mission goal might require a large Δv which can not be achieved with chemical propulsion. Some rough numbers are given by Larson and Wetz [8] and are shown in Tab. 2.1 to get an idea of the possible range of thrust and specific impulse. Some numbers of space proven electrostatic ion thrusters have been added. The thrusters which have been in space produce a thrust between 8 mN for the μ10 thruster up to 90 mN for the NSTAR thruster. They have an I_{sp} of $3000 - 3500$ s. Thrusters with higher and lower thrust exist in many labs around the world but as it is very costly to develop them to a level where they can be used to fly in space few are ever flown. A solution to vary the thrust brings the clustering of thrusters. Hayabusa started with a cluster of four μ10 thrusters bringing the nominal thrust up to 24 mN. The Artemis mission used two RIT-10 thrusters with a nominal thrust of 30 mN. The NSTAR on the other hand was used as a single thruster in the Deep Space 1 mission but is built into the Dawn spacecraft in a cluster of three. The clustering brings the advantage of redundancy but usually at the cost of a higher system mass.

The power consumption is another important feature of the electric propulsion system. While with chemical propulsion the thrust period is short (and they usually don not consume a huge amount of electric power) the thrust period of electric thrusters can be months and years. Hence it has to be accounted for in the power calculation of

15

Type	Propellant	Energy	Vacuum I_{sp} (sec)	Thrust Range (N)
Cold Gas	N_2, NH_3, Freon, helium	Pressure	50-75	0.05-200
Electrothermal:				
Resistorjet	N_2, NH_3, N_2H_4, H_2	Resistive heating	150-700	0.005-0.5
Arcjet	NH_3, N_2H_4, H_2	Electric arc heating	450-1500	0.05-5
Electrostatic:				
Ion Thruster	Xe,Cs,Hg	Electrostatic	2000-6000	$5 \cdot 10^{-6}$-0.5
· NSTAR [10]	Xe	"	3200	0.090
· RIT-10 [9]	Xe	"	3460	0.015
· μ10 [4]	Xe	"	3000	0.008
Hall Thruster	Xe	"	1500-2500	$5 \cdot 10^{-6}$-0.1

Table 2.1: Performance characteristics of several space propulsion systems [8]

the spacecraft. The μ10 thruster consumes around 43 W/mN [4] which is relatively high compared to the 30 W/mN of the RIT-10 [9] and the 25 W/mN of the larger NSTAR [10]. As can be seen a larger size of the thruster decreases losses to the walls of the discharge chamber due to an increased volume to surface ratio.

2.4 PEGASES Thruster

2.4.1 Introduction

The PEGASES thruster (acronym for Plasma Propulsion with Electronegative Gases) is a novel design for an ion propulsion system. The PEGASES thruster concept has been created by P. Chabert in the LPP laboratory of the Ecole Polytechnique in Paris in 2005 and since then been patented and researched [11–13]. The concept of this thruster is shown in Fig. 2.10. The plasma is inductively generated by a planar RF coil in the back of the thruster. An electronegative gas such as SF_6 is used as a propellant. The electrons in the plasma are cooled down due to collision within the magnetic field of the barrier. This results in the creation of more negative ions to a point where one can talk of an ion-ion plasma. An ion-ion plasma consists of negative and positive ions and a negligible amount of electrons in such a way that the plasma dynamics are controlled by the ion pairs. The negative and positive ions are then accelerated by a set off alternatively
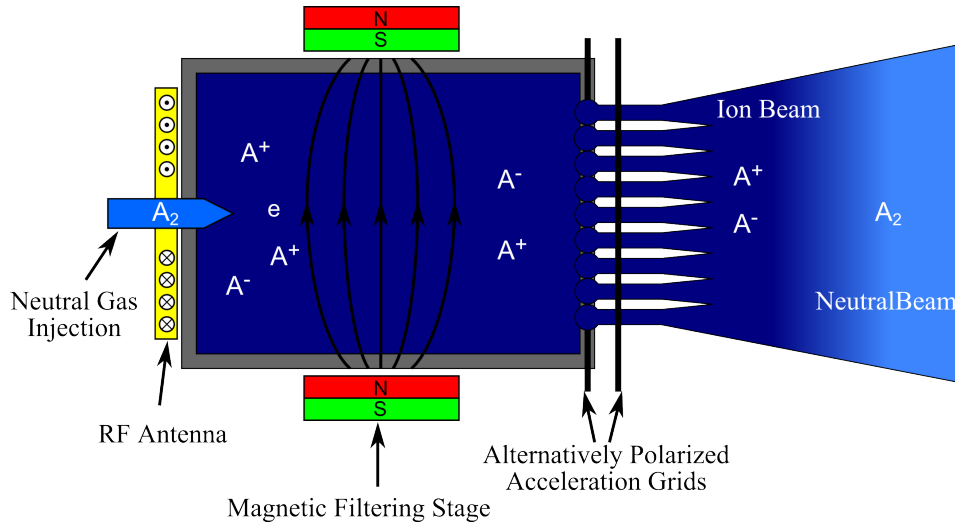
Figure 2.10: The PEGASES thruster concept: RF plasma generation with a planar coil, magnetic filtering to increase the amount of negative ions and the alternatively biased acceleration and recombination of the ions.

biased grids. The recombination outside of the thruster happens between the positive and negative ions which is more efficient than the recombination between positive ions and electrons. This PEGASES concept has no need for a neutralizing cathode which can limit the lifetime of a thruster. Another advantage is that the short recombination length avoids back scattering of charged particles to the spacecraft which can lead to degradation of the solar panels and the optics which are often on board satellites.

A second prototype of the PEGASES thruster is currently mounted at the EPIC test bench of the ICARE institute in Orléans and presented in Fig. 2.11. The thruster operating in xenon and accelerating ions is shown in Fig. 2.12. The picture has been taken from a window located on the side of the test chamber and half the exit plane is shaded by the structure of the test bench.

2.4.2 Second PEGASES Thruster Prototype

The second PEGASES thruster prototype has been used in the frame of this thesis. Our team was not involved in the construction and development of the thruster prototypes which has been done by the LPP (Laboratoire de Physique des Plasmas) of the Ecole Polytechnique in Paris. A detailed description of the first prototype can be found in the thesis manuscript of Gary Leray and Lara Popelier [12, 13].
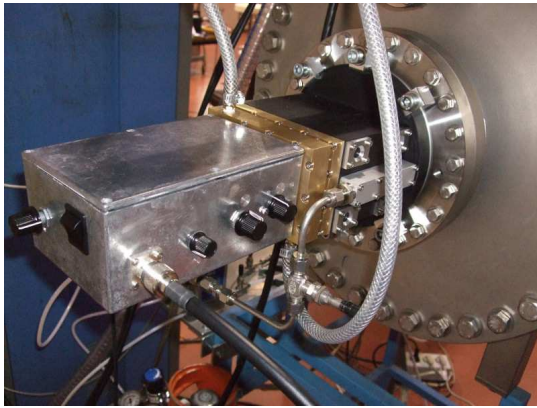
(a)   (b)

Figure 2.11: The second PEGASES thruster prototype mounted to the EPIC vacuum chamber seen from outside (a) and the inside (b).
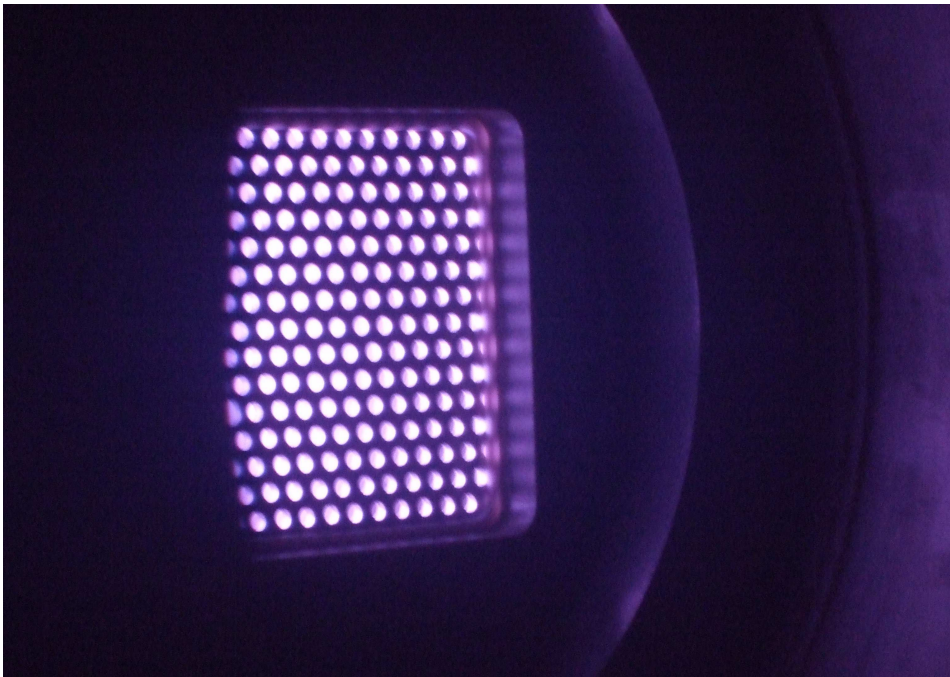
Figure 2.12: The PEGASES thruster firing with a xenon plasma as seen from the side window of the EPIC test chamber.
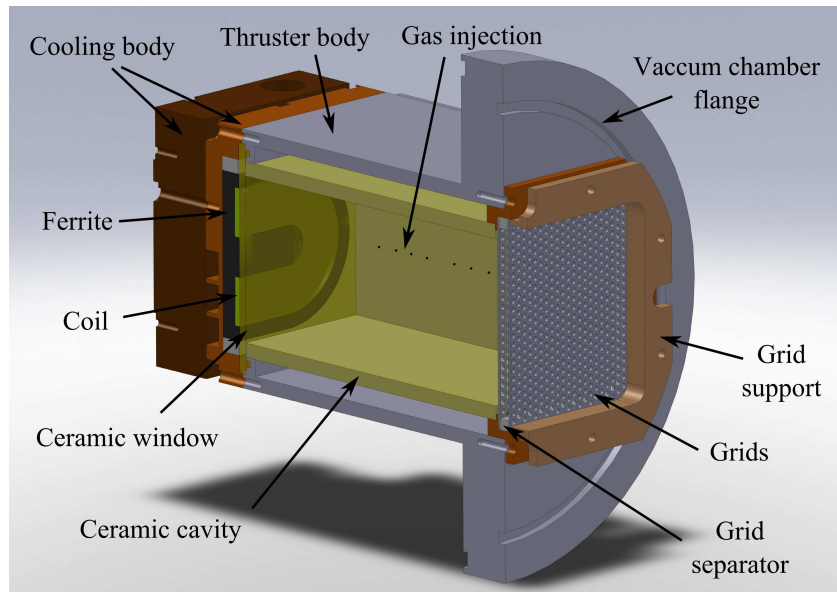
Figure 2.13: The second PEGASES thruster prototype as an assembly drawing made in a CAD system.

The second PEGASES thruster prototype is made out of aluminum and has a DN180LF flange to connect it to a vacuum chamber. A 3D CAD drawing of the second PEGASES thruster prototype is shown in Fig. 2.13. The discharge cavity has a size of $80 \times 120 \times 119$ mm with a volume of roughly 1.1 l. The thruster has a square shape instead of the standard circular form to allow for clustering of multiple thrusters with minimal space loss. The aluminum thruster body is anodized to isolate the discharge chamber from the ground and keep it floating. The anodized layer turned out to be insufficient as an isolator. Arcs formed inside the cavity which broke through the insulation. A cavity made out of four BN-SiO$_2$ ceramic walls was inserted into the thruster to ensure a floating plasma (Fig. 2.14). This reduces the cavity to $58 \times 104 \times 119$ mm and a volume of 0.72 l. A set of grids can be attached to the thruster body with the help of a PEEK (Polyetheretherketone, an organic polymer) support. A RF coil inside a ferromagnetic core is placed at the end of the truster and separated from the plasma by a ceramic window. The coil and and the ferromagnetic core are embedded into a water cooled block of brass to ensure the evacuation of the excess heat produced in the system.
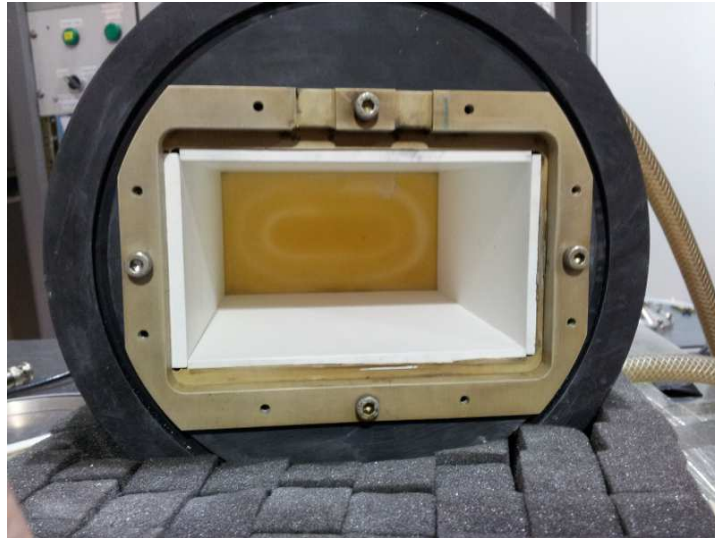
Figure 2.14: PEGASES thruster body with the BN-SiO$_2$ ceramic walls inserted.

2.4.3 Plasma Generation

The second PEGASES prototype [12] uses a seven loop planar coil which is separated from the discharge chamber by an 3 mm thick alumina ceramic window. A 4 MHz RF current is used to drive the coil. The coil wire is made out of stranded silver plated copper with a extruded polytetrafluoroethylene insulation. The wire is intended for use in high temperature environments up to 200 °C and has a low resistance. The coil induces an electromagnetic field which couples inductively to the electrons in the plasma. The electrons create ions due to the collision with the neutral gas atoms. This configuration is also called an ICP (Inductively Coupled Plasma) source.

To increase the power coupling to the plasma the is embedded into a ferromagnetic core[14]. The effect is shown in Fig. 2.15. The RF field is channeled inside the ferromagnetic core and concentrated in the direction of the ceramic window with the discharge chamber and the plasma behind it. This increases the amount of power which can be absorbed by the plasma.

The propellant gas of the PEGASES thruster is injected through 16, 1 mm in diameter, holes which are located on both sides of the thruster on the symmetrical axis (8 holes on right side and 8 holes on the left side). This ensures that the gas is spread evenly in the discharge chamber. The injection of the cold gas within the magnetic barrier helps the formation of negative ions [15–17].

To amplify the RF signal generated by a TTi TG4001 signal generator a RF power
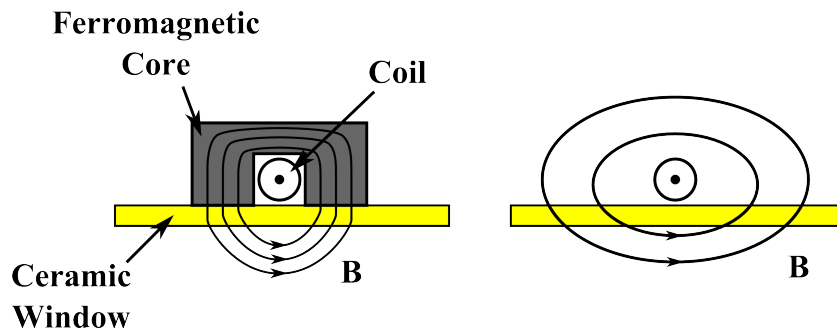
Figure 2.15: Schematic drawing of the magnetic field lines of a RF coil with and without a ferromagnetic core to increase the power coupling.

amplifier E&I A300 has been used. Due to a low reliability of the A300 it later has been replaced by a ADECE 300W Poweramp. Both amplifiers are able to provide 300 W RF power to the plasma. The full power can only be used for a short time as the matching circuit and the thruster body heat up to a critical temperature when a power of more than 200 W is used. A Bird 43 wattmeter has been used to observe and measure the forward and the reflected RF power. The wattmeter is installed between the matchbox and the amplifier.

Matchbox

To transmit the maximum amount of power to the plasma and to avoid power to be reflected into the amplifier, a matching network has to be used with RF circuits. The most common form of impedance matching is the L matching network. In this network one side of the RF coil is grounded and a variable capacitor is installed in parallel to the coil. Another variable capacitor is placed between the amplifier and the coil. By changing the capacitance of both capacitors the impedance of the coil and the capacitors can be matched to the impedance of the amplifier. Such networks are simple and relatively cheap to build but they have the disadvantage that the potential on the coil is not symmetrical and they produce a high voltage on the coil. This type of network with the RF source described has been used in Chapter 5.

For the second prototype of the PEGASES thruster Valery Godyak designed a push-pull matching network with air variable capacitors and a low loss transmission line transformer [13]. In this second version of the matchbox no part of the coil is grounded. Instead the circuit is made so that when one end of the coil is on a high potential the other part is at a low potential. This means the middle of the antenna stays always at

Figure 2.16: Matchbox with a low loss transmission line transformer and air variable capacitors. The PEGASES thruster is attached on the right side.

zero potential and both ends alternate with opposite potential. This design uses the RF coil symmetrical and lowers the peak potential difference with respect to the ground. A reduction of the voltage in the coil lead to a reduction of the capacitive coupling into the plasma. Figure 2.16 shows the matchbox containing the matching network. A more advanced third version of the matchbox is currently in use by the LPP team. On the right side the PEGASES thruster is attached and the wires are leading tho the RF coil which is embedded into a ferromagnetic core and a cooling circuit. The combination of a low frequency RF signal with the specially designed matchbox and the ferromagnetic core creates an efficient ICP source as shall be seen later on. More details to the matchbox can be found in the PhD thesis of Lara Popelier [13].

2.4.4 Magnetic Barrier

The magnetic barrier of the PEGASES thruster at ICARE consist of SmCo permanent magnets (Samarium-cobalt magnet). Compared to Neodymium magnets, the SmCo magnets need to be larger to produce the same magnetic field strength but due to a higher Curie temperature they keep their magnetic properties at higher temperatures. The PEGASES thruster cavity can reach temperatures around 80 °C while in use which is the temperature which should not be exceeded with the available Neodymium magnets. The configuration of the magnetic barrier is shown in Fig. 2.17. The magnets are long and thin to better focus the magnetic field in one region. The field strength can be varied by adding and removing magnets on top of the magnet closest to the PEGASES body. Figure 2.18 shows a front view of the distribution of the magnetic field inside the cavity
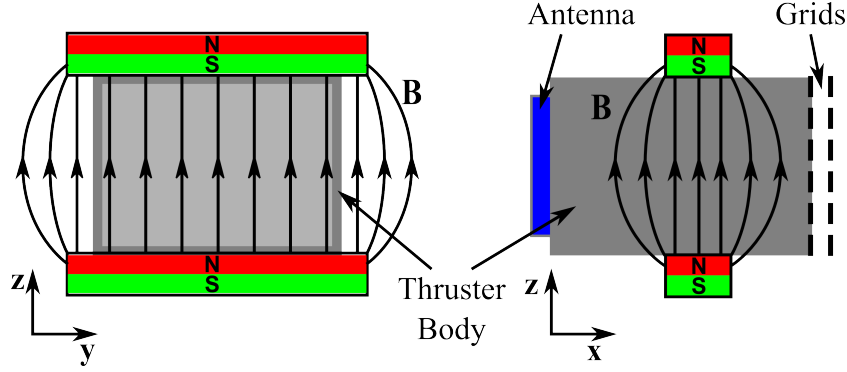
Figure 2.17: Front and side view of the magnetic barrier of the PEGASES thruster.

with a pile of three magnets. The magnetic field was measured and then interpolated for this plot. The field strength along the symmetrical y-axis is 190 G in average for 3 magnets on each side. In the figure the ceramic cavity of the discharge chamber is indicated in black. Configurations can be used where 2 magnets on each side generate an average magnetic field of 109 G or 1 magnet on each side generates a field of 62 G in the middle of the cavity.

The magnetic barrier of the PEGASES thruster is essential for the production of negative ions. The reduction of the temperature of the electrons in the plasma enhances the chance of dissociative attachment when using an electronegative gas like SF_6. The attachment rate increases strongly at electron temperatures around 1 eV [18]. The temperature reduction also reduces the dissociation due to collision with energetic electrons of the already present negative ions [19]. The technique to produce negative ions for the PEGASES thruster has been under investigation by the LPP laboratory of the Ecole Polytechnique in Paris [13, 18–20]. It has been shown that the electron temperature downstream of the magnets is indeed lower and that the negative ion density in this region is high. Further more an acceleration of positive and negative ions has been performed and measured.

In the experiments with the PEGASES thruster as a classical ion engine with xenon, the magnetic barrier has not been used unless otherwise stated. The main goal of the magnetic barrier is the production of negative ions. As the electronegativity of xenon is much lower than that of SF_6, no attempt has been made to produce negative xenon ions and to accelerate them.
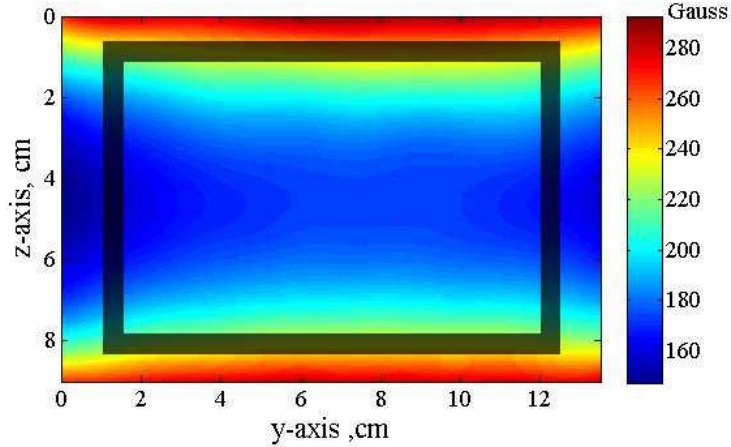
Figure 2.18: The measured magnetic field distribution inside the cavity in the three magnet configuration and 190 G magnetic field along the cavities symmetrical y-axis. The ceramic cavity of the discharge chamber is indicated in black.

2.4.5 Plasma Acceleration

The PEGASES thruster uses, like other ion engines, a set of multi-aperture grids for the electrostatic acceleration of the ions. The difference to the normal ion engines is that the PEGASES thruster accelerates both negative and positive ions which are present in the discharge chamber. To achieve this the grids are alternatively biased.

For the experiments presented in this thesis a set of two planar grids with 2 mm in diameter holes and a transparency of 60 % has been machined. The grid has a thickness of 0.8 mm. Stainless steel was chosen as a material because it is easy to machined. The disadvantage of the material is the vulnerability to erosion. This does not pose a problem in the prototype model of the thruster as the thruster is not operated over a long amount of time. The grid holes for the screen grid and the acceleration grid have the same size. The set of planar grids is shown in Fig. 2.19. The grids are not optimized in shape, meaning that a margin for improvement in the performance level still exists. The main goal of this work was to achieve ion acceleration, measure the plasma properties in the plume and determine the performances in the system. The two grids are separated by a 1 mm spacer made out of Teflon. The latter is simply inserted in between the grids. The disadvantage of this assembly is that after several hours of experiments a conducting layer formed on the surface of the Teflon spacer which favored arcing. This did lead in one case to a sever short circuit which damaged the grid support.

The plasma is elevated by the first grid to a high potential since the cavity of the dis-

24

Figure 2.19: The set of grids used for the experiments made out of stainless steel with a transparency of 60 % and a hole diameter of 2 mm

charge chamber of the PEGASES thruster is floating. This is achieved by the previously mentioned BN-SiO$_2$ ceramic cavity which isolates the plasma from the grounded thruster walls. In the beginning of the experiments the ceramic cavity was not available and a PEEK cavity has been used. This cavity had the advantage that it was easy and quick to produce. The disadvantage was that the cavity deformed under the thermal load of the plasma during the experiments. The total potential of the plasma consist of the grid bias and the plasma potential $((V_b + V_p)$. The second grid is grounded. It would be at spacecraft potential in space. The potential difference between the first and the second grid generates an electrostatic field and accelerate the ions. The expected velocity of the ions can be calculated with,

$$v_i = \sqrt{\frac{2Ze\left(V_b + V_p\right)}{M}},\tag{2.6}$$

where V_b is the bias voltage on the grid, V_p is the plasma potential, Z the charge number and M is the mass of the ion.

Child-Langmuir Sheath

The amount of current an ion thruster can extract and accelerated is called perveance and is limited by the space charge effects and characterized by the Child-Langmuir equation:

$$I = JS = \frac{4\varepsilon_0}{9}\sqrt{\frac{2eZ}{M}}\frac{SV_b^{3/2}}{d^2},\tag{2.7}$$

with the total current I, the ion flux J, the acceleration area S and the potential across

the sheath thickness of d. This equation can be used in to calculate the space-charge-limited ion current of a grid system in an ion thruster where, in an first approximation, d is the gap between the grids [2, p.80]. The maximum perveance P_{max} a thruster can achieve is given by the coefficient in the Child-Langmuir equation:

$$P_{max} \equiv \frac{4\varepsilon_0}{9}\sqrt{\frac{2eZ}{M}}[A/V^{3/2}], \tag{2.8}$$

This gives us a maximum perveance of 4.77×10^{-9} A/V$^{3/2}$ for singly charged xenon ions. For round holes with a diameter D in the grid the maximum perveance is,

$$P_{max} \equiv \frac{\pi\varepsilon_0}{9}\sqrt{\frac{2eZ}{M}}\left(\frac{D^2}{d^2}\right)[A/V^{3/2}]. \tag{2.9}$$

Therefore to maximize the current that can be extracted from a thruster it is important to chose a large hole diameter to grid space ratio. This ratio is limited as the hole diameters of the grid have to be chosen to be in the dimension of the Child-Langmuir length [2, p.190]. The other factor, the grid distance, is limited by the grid voltage. The bias voltage and grid distance have to be chosen, keeping in mind the plasma density, so no arcing can occur in the grids.

Figure 2.20 shows the Child-Langmuir length, calculated from Eq. 2.7 over the ion current for several bias voltages calculated from Eq. 2.7 for xenon. The graph shows that, especially for lower bias voltages in the grids, a high ion current might not be too desirable as the Child-Langmuir length decreases strongly. The ion current can be lowered by decreasing the flow rate and therefore the pressure in the discharge chamber. Another way is to decrease the input power into the thruster but this also decreases the mass utilization of the thruster and is less desirable.

An example for the optimization of the grid system can be found in the Ph.D. thesis of Michaël Irzyk [21].

2.4.6 Neutralization

The PEGASES thruster does not need a neutralization stage. The positive and negative ions leave the thruster in waves and recombine behind the thruster. The short recombination length between positive and negative ions makes this process more efficient than the recombination between positive and negative ions. This is one of the advantages
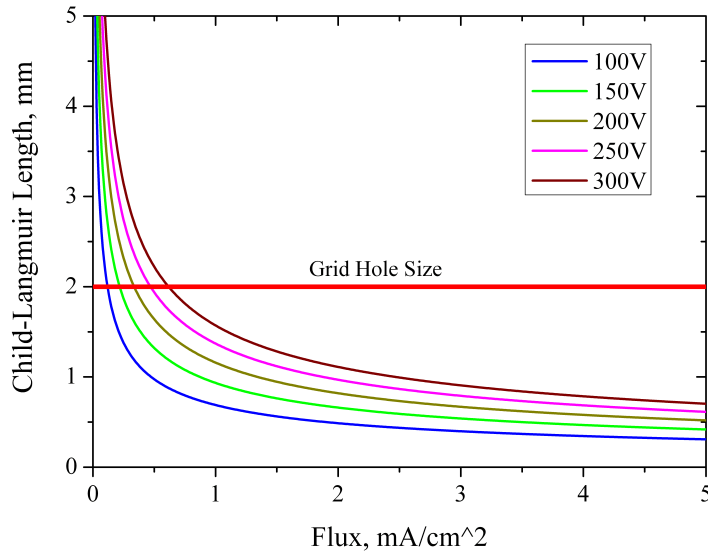
Figure 2.20: The Child-Langmuir length for xenon over the ion current for several bias
voltages.

of the PEGASES thruster as this can avoid the back scattering of charged particles to
the spacecraft. Back scattering can appear when the spacecraft and the plasma plume
are charged differently. The charged particles are accelerated back to the spacecraft and
can degrade the solar panels and the payload which often consists of sensitive optical
material.

Although PEGASES does not need a neutralizing cathode when operated with an elec-
tronegative gas, it needs one when used as a classical ion thruster operated with xenon.
In the beginning of the experiments a hot cathode described in Chap. 2.3.4 has been
used. During the experiments it turned out that the cathode designed for higher cur-
rents around 5 A was not able to provide the required low current. So a heated filament
is used as a neutralizing electron source. The filament consists of a 0.38 mm in diameter
tungsten wire with a length of 20 cm. The wire is bent into a three loop spiral to take
up less space as shown in Fig. 2.21 (a). The heating current of the filament is fixed to
11 A. This requires usually a voltage of around 12 V depending on the grid bias and the
gas flow rate in the source. The heating power supply is floating and its positive side is
connected to a power supply biased to -35 V. This results in the heating filament being
biased to -50 V on one side and -35 V on the other end. This helps the electrons to
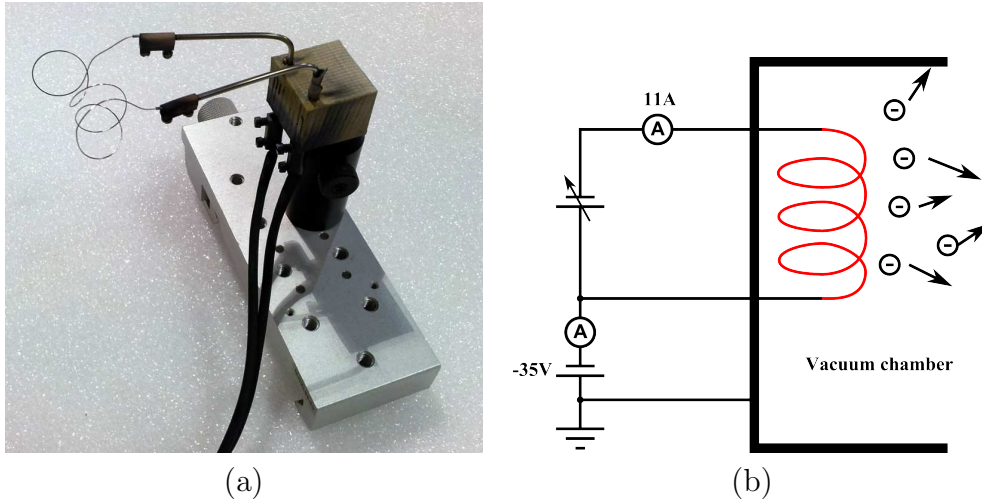
Figure 2.21: (a) The heated filament to provide the neutralizing electrons and (b) the electrical schematics of the heated filament.

escape. To close the electric loop the bias power supply is grounded as are the walls of the vacuum chamber. The current emitted by the heated filament can be read on the current meter of the bias power supply and is typically between 100 mA and 400 mA. The electrical schematics are shown in Fig. 2.21 (b). The electron current emitted by the filament is clearly related to the ion current leaving the grid assembly. This point will be discussed further in Chap. 6.

One disadvantage of the filament is illustrated in Fig 2.22. The filament emits not just electrons but also tungsten atoms and a thin conducting layer is formed on the vacuum chamber, the grids and even the inside of the PEGASES thruster. This coating can lead to short circuits and arcing in the grids. To avoid this it would be advisable to use a cathode within the required current range. A second disadvantage of the filament is the relatively short lifetime. Over time the wire gets thinner as more and more tungsten atoms are emitted. This ends in the wire melting at one point.

2.5 The EPIC Test Bench

The experiments conducted in this thesis have been carried out with the EPIC test bench (acronym for Electric Propulsion Innovative Concepts). A 0.4 m in diameter and 0.75 m long vacuum chamber which is evacuated with a 350 l/s in nitrogen turbomolecular pump connected to a 65 m^3/h primary pump this is the setup which has been used in Chap.5.

Figure 2.22: BN-SiO$_2$ cavity coated with tungsten due to the hot filament neutralizer.

In the last version a 1000 l/s in nitrogen turbomolecular pump has been added to the chamber for the experiments with the PEGASES thruster. The pump can be flushed with nitrogen when operating with reactive gases like SF$_6$.

The chamber has several optical windows, access ports and electrical feedthroughs. It can be equipped with a variety of probes and linear motion stages. A pressure down to 10^{-6} mbar can be reached without any gas flow. The background pressure at a gas flow rates of 20 sccm is typically 10^{-3} mbar depending on the gas. Figure 2.23 shows a schematic drawing of the setup in its final configuration. The gas flow can be regulated by two Aera 7700 gas flow meter calibrated to 20 sccm SF$_6$ and 50 sccm argon. They can be used with other gases by using a conversion factors provided in Appx. A.

A picture of the EPIC test bench with the PEGASES thruster is shown in Fig 2.24. The picture shows the chamber before the 1000 l/s turbomolecular pump and the power supplies for the grid and neutralizing filament were added to the setup.
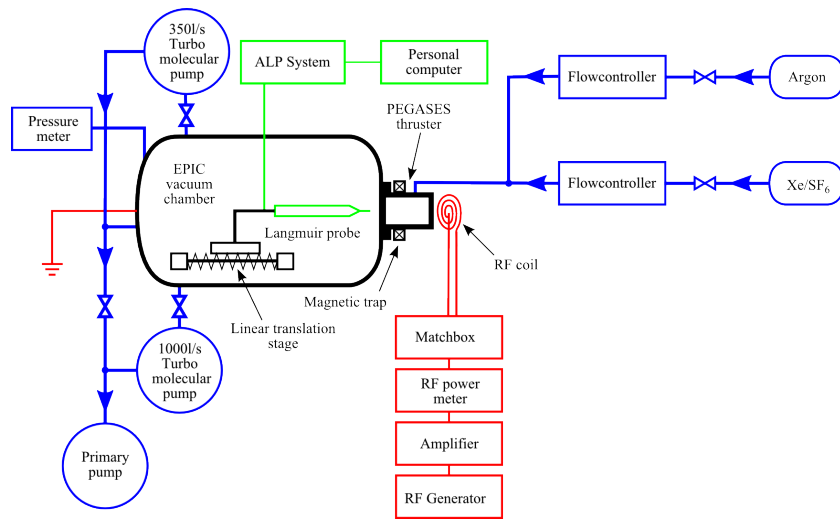
Figure 2.23: Schematic drawing of the setup of the EPIC vacuum chamber with the PEGASES thruster.

Figure 2.24: Picture of the EPIC test bench with the PEGASES thruster mounted and running.

3 Diagnostics

The diagnostics described in this chapter have been used to determine the plasma properties of the various RF discharges examined in this thesis. The probes have mainly been designed and built at the ICARE laboratory. The design of the E×B probe has been an essential part of this thesis and will be described separately in Chap. 4.

3.1 Planar Probe

A planar Faraday probe provides the possibility to measure the ion flux with a high precision. A disadvantage of cylindrical probes, such as the Langmuir probe, is that the collection area strongly depends on the sheath size. If the sheath size is in the region of the diameter of the collecting wire a significant error can be introduced. A planar probe can avoid this problem. A guard ring can be introduced to the probe to increase the precision. This guard ring is around the probe and is biased to the same potential. This allows to have a well defined collection area as displayed in Fig. 3.1. Ions arriving from the side are collected by the guard ring and are not measured. The second advantage is that collecting area of a planar probe is commonly larger than the diameter of a Langmuir probe. This reduces the sheath to probe area ratio and therefore reduces the error. The size of the probe also provides the possibility to collect low currents otherwise not measurable. The size of the planar probe posses a disadvantage as the probe itself can change the plasma locally by draining the charges.

Figure 3.2 shows a 3D CAD drawing of one of the planar probes used within this thesis. This probe has a 15 mm diameter collection area. This area is surrounded by a 10 mm wide guard ring. Both the ring and the collector consist of graphite to reduce emission secondary electrons which can change the measurement outcome. The graphite also reduces the sputtering and helps the probe to withstand ion bombardment. The ring and the collector are separated by a 1 mm gap and are mounted on a PEEK plate which serves as isolator and support.
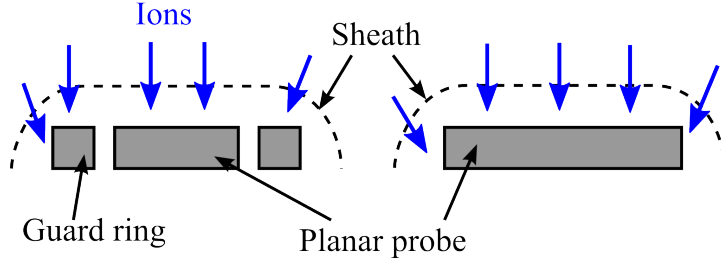
Figure 3.1: A planar probe with a guard ring has a well defined collection area.

The guard ring and the collector are biased to -50 V to reject the electrons. The current of the collector is measured and amplified with a factor ranging from 10 to 90 in steps of ten by our bias source. It is then displayed and measured by an oscilloscope. The voltage U_{sc} measured on the oscilloscope can then be converted to the probe current I_p by,

$$I_p = \frac{0.1A \cdot U_{sc}}{5V \cdot x_g},$$
(3.1)

where x_g is the gain factor.

Figure 3.3 shows a 55 mm planar probe with a guard ring in front of the PEGASES thruster. The probe is of the same design as the smaller 15 mm probe. The measurement circuit available has a current range from 20 μA to 20 mA. The increased collection area of the probe allows for measurements in the far plume of the thruster where the plasma density is lower than inside the cavity or very close to the grids.

3.2 Capacitive Probe

A capacitive probe has been used to determine the RF fluctuations of the potential inside the plasma [22]. The knowledge of RF fluctuations is helpful to classify the character of the discharge. A high level of fluctuation indicates a capacitive coupling of the RF power to the plasma even though an inductive coil is used. The probe consists of a wire which is inserted into a 1 cm in diameter copper cylinder and is insulated by a PEEK cylinder as shown in Fig 3.4. There is no electrical contact between the wire and the cylinder. The cylinder follows the plasma potential. The probe works like a capacitor, when the side in the plasma gets charged negatively the wire inside the probe gets charged positively. Therefore the probe measures the fluctuations in the plasma without draining electrical
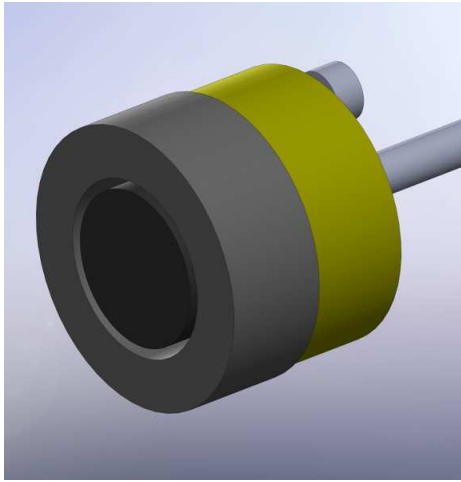
Figure 3.2: CAD drawing of the 15 mm planar probe with a guard ring.
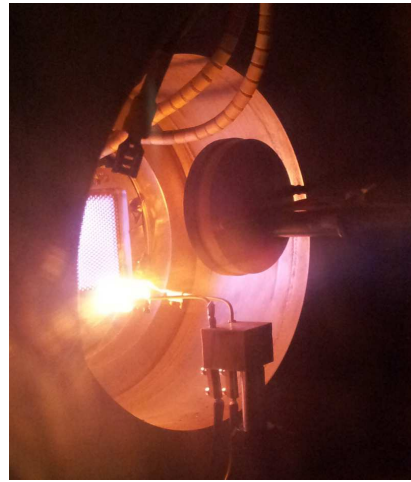
Figure 3.3: Picture of the the 55 mm planar probe with a guard ring in front of the PEGASES thruster. Also visible is the hot wire filament that acts as a neutralizer.

charges and has no direct current component. The probe is directly connected to the $50\,\Omega$ input of an oscilloscope to acquire the potential waveform. A calibration of the system with a frequency generator is necessary to obtain the real value of the fluctuation amplitude at the measurement location. This calibration should be performed before and after the experiment to ensure that the capacitance of the probe has not changed during the experiment. As the PEEK is used close to its thermal limit, a deformation of the insulating layer may occur during the experiments. This would change the factor needed to calculate the plasma potential which has been obtained during the calibration.
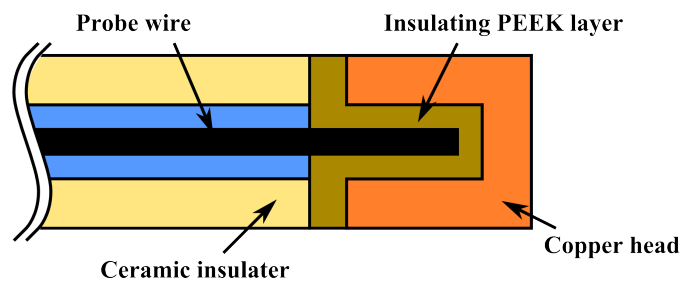
Figure 3.4: Capacitive probe to measure the change in the plasma potential induced by the RF field.
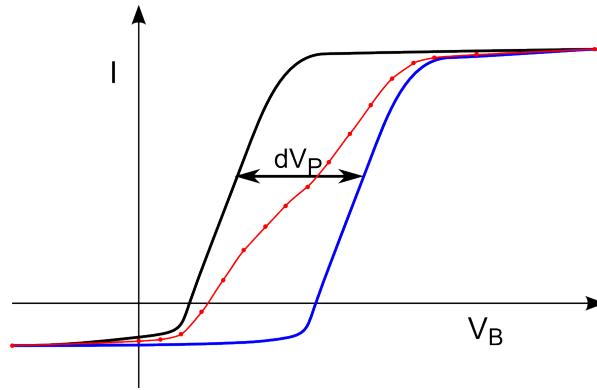
Figure 3.5: The distortion of a Langmuir probe trace due to averaging in an RF plasma. The black and blue curve are the upper and lower limit of the RF fluctuations and the red curve is the resulting average curve.

3.3 Langmuir Probe

3.3.1 Introduction

The Langmuir probe is probably the simplest method to gain a large variety of information over a plasma. A basic Langmuir probe consists simply of a wire which is stuck into a plasma and collects current for a range of bias voltages. The design of the probe however influences the plasma. A variety of theories exist to treat the resulting current voltage characteristics obtained by the Langmuir probe measurements. It is not always easy to find the theory which corresponds best with the conditions found in the plasma. Chen gives a comprehensible overview over the different theory and in which case to use them and also shows how to build a Langmuir probe [23].

A big challenge with Langmuir probe measurements in RF discharges is to overcome the high-frequency fluctuation of the plasma potential which leads to a distortion of the I-V probe curve. This effect is shown in Fig. 3.5. The blue and the black trace symbolizes the upper and the lower limit of the RF fluctuations. The red curve is the average which would be obtained without a compensated probe. To analyze this curve would lead to wrong plasma parameters.

Therefore in Chap. 5 a passively-compensated Langmuir probe has been used to measure the plasma parameters [24]. The probe was built after the design proposed by Chen [23]. The probe has been outfitted with two chokes in series of which the resonance frequency is 13.56 MHz and 27, 12 MHz, respectively. The frequency corresponds to the main
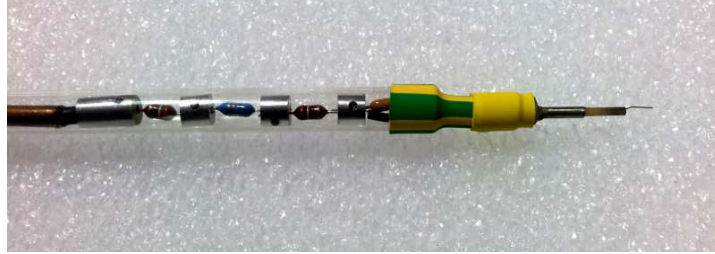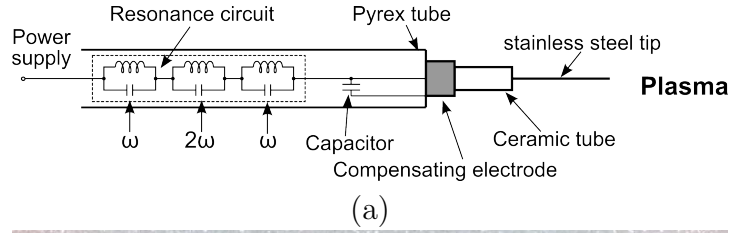
Figure 3.6: (a) shows a sketch of the RF compensated Langmuir probe circuit and (b) a photograph of the compensated Langmuir probe itself used to determine electron parameters in the plasma discharge.

frequency and second harmonic frequency of the RF wave. The chokes isolate the probe tip by blocking high-frequency currents, therefore ensuring the probe follows the sheath potential fluctuations. Moreover, in order to ensure that the probe tip draws enough current to fill the stray capacitances a coupling capacitor connected to an external metal ring was added. This capacitor allows to collect a large amount of charges. The probe tip is a 5 mm in length stainless steel wire with a 0.125 mm diameter. The tip is electrically insulated from the plasma by an alumina cover. An electric scheme and a picture of the probe is shown in Fig. 3.6. The voltage sweep and the resulting probe current measurement were performed using the ALP System^{TM} manufactured by Impedans.

In Chap. 6 an uncompensated probe is used. The RF fluctuations in this case are only in the order of a few volts as will be shown and do not change the measurements significantly. The probes used in this chapter consist of 0.125 mm to 0.25 mm in diameter tungsten or platinum wire. The probe length and diameter have been adjusted to the plasma conditions in order to increase current above the detection limit if the control unit. The platinum wire has been used when a reactive plasma was present. The platinum wire is less sensitive to etching by flour atoms. This increases the lifetime of the probe and ensures a well defined diameter of the probe tip which is important for the calculation of the plasma parameters.

3.3.2 Data Treatment

The acquisition of the data is done by the ALP System^{TM} manufactured by Impedans. The automatic data treatment of the ALP System^{TM} in its early versions is not capable to give a correct plasma potential. For that reason the post-treatment of the data is done using the program of Pavel Kudrna from the Department of Electronics and Vacuum Physics of the Charles University in Prague, Czech Republic. The plasma potential V_P, the electron temperature T_e and the electron density n_e are derived by assuming a Maxwellian distribution and using the standard Langmuir theory. An overview over the different theories, their advantages and disadvantages is given by Chen [23]. The plasma potential, is obtained from the maximum of the first derivative of the probe characteristic. The electron temperature is obtained from the slope of the logarithmic function of the electron current in the transition region (between V_f and V_P). The plasma density is calculated by using the Orbit Motion Limited (OML) model of Mott-Smith and Langmuir [25]. This model predicts a parabolic $I - V$ curve. Plotting the $I^2 - V$ curve then should show a straight line. This was in accordance with our measurements.

3.4 Emissive Probe

An emissive probe has the advantage of being barely sensitive to a magnetic field, contrary to a Langmuir probe. This makes it possible to determine the plasma potential without knowing the exact values of the magnetic field at each measurement point. There are different methods of obtaining the plasma potential with an emissive probe [26]. For the measurements described in Chap. 5 the floating point with large emission method has been chosen. This method allows the direct measurement of the plasma potential with a volt meter once the heating current of the probe has been identified where the emission and the collection of the electrons are balanced.

The tungsten filament of the emissive probe is heated with a DC power supply up to the regime of electron emission. The floating potential of a sufficient emitting hot probe is equal to the plasma potential. The electron current going to the probe is compensated by the emission of electrons due to heating. Therefore the net current of the probe is effectively zero and in theory there is no sheath forming around the probe [27]. A measurement performed to obtain the plasma potential is displayed in Fig. 3.8. In reality the sheath never vanishes completely and the probe voltage has to be corrected with

the electron temperature in order to obtain a more accurate measurement of the plasma potential.

The emitting part of the probe is made out of a 8 mm long loop of 150 μm in diameter, thoriated tungsten wire. The emissivity of thoriated tungsten is higher than that of pure tungsten, this allows for a lower temperature of the filament and increases the limited lifetime of the probe. The ends of the wire are mechanically crimped in copper wires. To do this holes are drilled in the end of the copper wires. The smallest possible diameter for the holes is still too large so the thoriated tungsten wire is inserted into small tubes. After crimping the ensemble is then inserted into two parallel holes of a 100 mm long and 4 mm in diameter alumina tube. The method of construction for this probe is similar to the method of Dannenmayer [28]. Figure 3.7 (a) shows a picture of the emissive probe with and without the alumina tube. The displayed probes have been used till the wire broke. Figure 3.7 (b) shows the emissive probe in a magnetically confined, inductively coupled, RF argon discharge.

In principle an emissive probe can follow high-frequency fluctuations of the discharge. However, due to the capacitive part of the electrical circuit, our probe is limited to frequencies below 100 kHz. The probe has been employed to measure V_p and T_e across the large magnetic field region where the strip forms and develops.

The electron temperature can be estimated from the hot and cold probe potential. In the cold case the potential is the floating one of an unheated probe. In argon at low pressure, T_e is given by [29]:

$$T_e = \frac{V_{\text{hot}} - V_{\text{cold}}}{5.4} \qquad \text{in eV.} \tag{3.2}$$

3.5 RPA

3.5.1 Introduction

The retarding potential analyzer (RPA), also known as retarding field energy analyzer (RFEA), is used to measure the ion energy distribution function (IEDF) in a plasma. A Langmuir probe can not easily provide information of the ion distribution function. At a positive potential, when repelling ions, the Langmuir probe is drawing a high electron current which hides the variations in the ion current. The RPA avoids this problem by

(a)
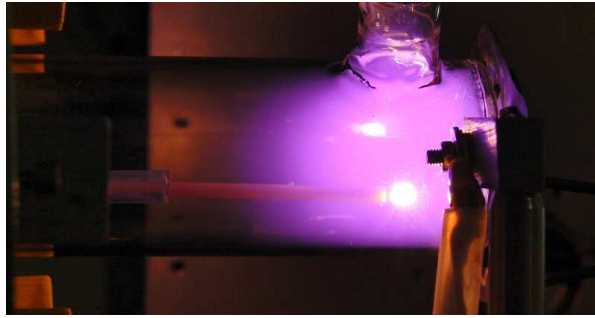
(b)

Figure 3.7: (a) shows a picture of the emissive probe with and without its alumina double bore tube (b) shows a photograph of the emissive probe inside a magnetically confined inductively coupled argon plasma.
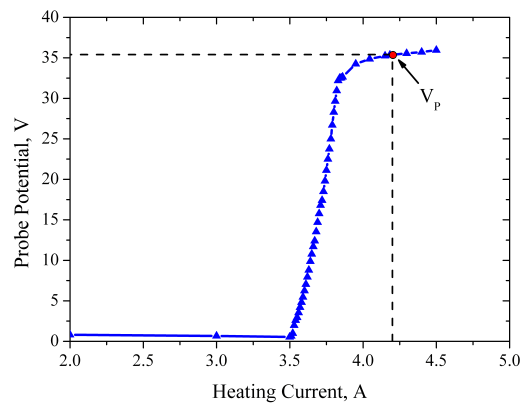
Figure 3.8: Measurement performed with an emissive probe to obtain the plasma potential in an inductively coupled 300 W argon plasma.

blocking the electrons with a negatively biased grid at the entrance of the probe [30, p.94]. A grid inside the probe is biased from a slightly negative value to a positive value where no more ions arrive at the collector. By measuring the collector current as a function of the grid bias an calculating the derivative of this function the IEDF can be obtained. A picture of the RPA used in this thesis is shown in Fig. 3.9.

3.5.2 Measurement

There are different methods to construct a RPA. The probe used in this thesis consists of 4 grids an the bias scheme is shown in in Fig. 3.10. The space between the grids is 1 mm each. The grids are made out of a mesh material with an inside width s_m of 0.38 mm. The grid size has to be chosen accordingly to the Debye length of the plasma as a Debye length smaller than $\lambda_D = s_m/2$ tends to enter the analyzer [31]. The transparency of the mesh material is 70%. Grid No. 4 is the grid separating the probe from the plasma. This creates a sheath and prevents the residual plasma from entering the probe and gives a reference to measure against. Grid No. 3 is biased negatively to repel the electrons which might enter into the probe and only ions will pass this grid. Grid No. 2 is biased grid and ramped from a slightly negative voltage to a potential where the ions are totally deflected. Ions can pass this grid when it is biased with a low voltage and are measured at the collector. With an increasing bias more ions are deflected until the point where the potential of the grid is so high that no more current arrives at the collector. The collector current as a function of the grid bias is shown in Fig. 3.11. Grid No. 1 is located directly in front of the collector and is biased negatively to repel the secondary electrons created from the impact of the ions. The collector is made out of molybdenum to further reduce this effect. The derivative of the obtained trace is the IEDF and is shown in Fig. 3.12.

Figure 3.9: Picture of a RPA with a 10 mm orifice.
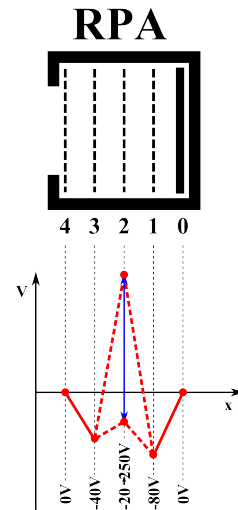
Figure 3.10: The upper sketch shows the geometry of the analyzer of the RPA probe and the lower sketch shows the corresponding potential along the probe axis.
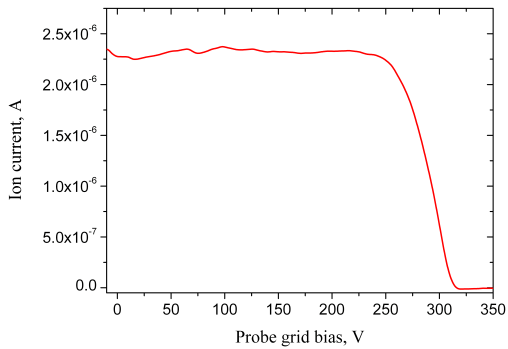
Figure 3.11: Ion current measured over the grid bias with a RPA in a ion thruster with a 5 sccm xenon discharge at 300 V acceleration bias.
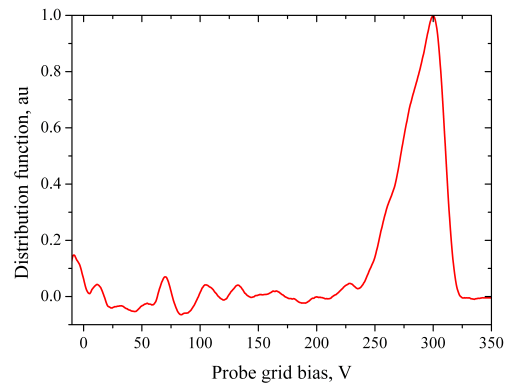
Figure 3.12: IEDF measured with a RPA in a ion thruster with a 5 sccm xenon discharge at 300 V acceleration bias.

3.6 Conclusion

This described set of probe gives enables to analyze a broad range of plasma parameters. The planar probe can be used to measure the ion flux and therefore get information of the plasma density. The capacitive probe can be used to measurement the plasma potential. With this information a differentiation between an capacitive and an inductive discharge can be made. The Langmuir probe is the most classical plasma probe and many theories exist to treat the data obtained from it. A special compensated probe for 13.56 MHz RF plasmas is available to reduce the influence of the fluctuating plasma potential. The Langmuir probe can measure the plasma and the floating potential as well as the electron temperature and density. It is a versatile, well established probe which gives a large amount off information about the plasma conditions. With modifications this probe can measure these parameters in a capacitively coupled RF discharge. The RPA makes it possible to measure the IEDF of a plasma which is especially useful in the plume of electric thrusters.

4 E×B Probe

4.1 Introduction

An E×B probe, also called a Wien filter, is an electromagnetic probe that works as a band-pass filter for ions. It collects and measures ions arriving in a certain velocity range. Ions arriving with a speed outside this range are deflected. Therefore the E×B probe is a diagnostic tool which can be used to measure the velocity distribution function (VDF) of ions in the plume of electric thrusters. E×B probes have been used in the plume of ion thrusters [32] and Hall thrusters [33–38] as well as in negative ion sources for fusion plasmas [39]. Figure 4.1 shows a picture of the probe which has been constructed and build for this thesis.

Electric thrusters usually contain multiply charged ions. In ion and Hall thrusters they are accelerated through a potential drop. They acquire a velocity which is proportional to the square root of their charge according to the energy conservation principle. If the accelerating potential is known, the speed of the ions can be calculated with Eq.2.6. Many studies have been conducted with retarding potential analyzers (RPAs) in the plume of electric thrusters to obtain the energy distribution function [12, 13, 28, 31, 35, 40]. The nature of the RPA, however, makes it impossible to obtain the charge state of the ions. Due to the fact that multiply charged ions are accelerated to a different velocity than singly charged ions, the E×B probe can distinguish between them although the charge number is not included into the governing equation as we will see in the next section. Several species of ions can be present in the plasma of ion thrusters, the cause of this might be the use of a molecular propellant gases like SF_6 or leaks and contamination. Ions of different mass are accelerated to a different velocity. They will therefore show up on the characteristic measured by the E×B probe. In this case the E×B probe works as a mass spectrometer.

As all ions, except the ions produced by charge exchange collisions between the grids,
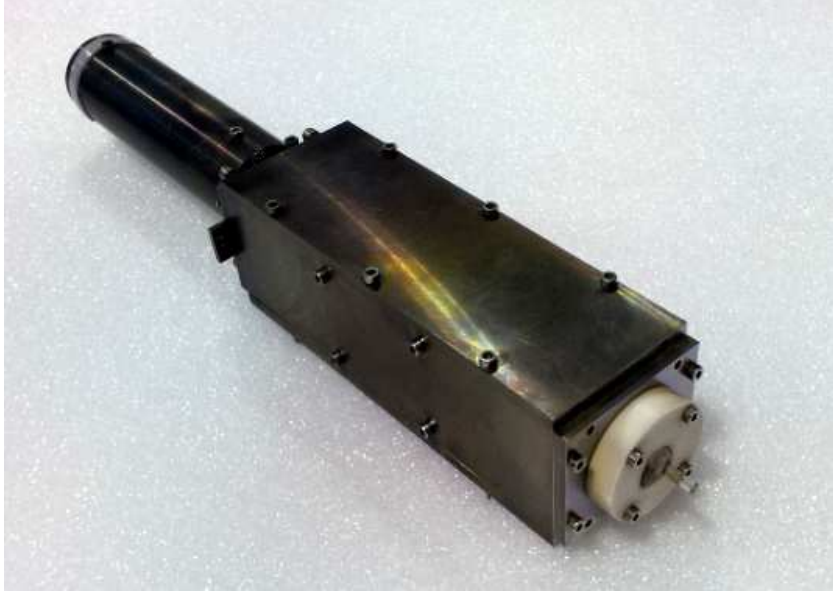
Figure 4.1: Picture of the E×B probe which has been constructed and used in this thesis.

in an ion thruster experience the same acceleration voltage, the ratio between the singly and multiply charged ions can be calculated from the height or area of their respective peak. It is not the case for Hall thrusters as the ions are produced at different positions along the channel. The ions are accelerated with different potentials according to the position of their creation which results in a widening of the ion velocity distribution [33]. This has to be taken into account when calculation the ratio between the ion species.

4.2 Principle

In an E×B probe an electric field ($\vec{E}$) is applied orthogonal to a magnetic field ($\vec{B}$). A particle arriving orthogonal to both fields can only experience the fields undeflected at a certain velocity ($\vec{v}$). This effect is visualized in Fig. 4.2 and described by the Lorenz force,

$$\vec{F} = q \left(\vec{E} + \vec{v} \times \vec{B} \right).$$ (4.1)

With the force set to zero to have an undisturbed trajectory, a straight line, this equation
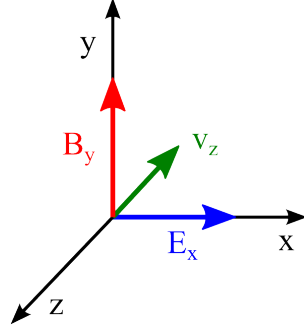
Figure 4.2: Vectors of the velocity, the magnetic and the electric field in an E×B probe.

solves to,

$$\vec{E} = -\vec{v} \times \vec{B} = \vec{B} \times \vec{v}. \tag{4.2}$$

With the electric field orthogonal to the magnetic field according to Fig. 4.2 the equation can be writen as,

$$\begin{pmatrix} E_x \\ 0 \\ 0 \end{pmatrix} = \begin{pmatrix} 0 \\ B_y \\ 0 \end{pmatrix} \times \begin{pmatrix} 0 \\ 0 \\ v_z \end{pmatrix}, \tag{4.3}$$

and solved to:

$$E_x = B_y \cdot v_z \qquad \Rightarrow \qquad v_z = \frac{E_x}{B_y}, \tag{4.4}$$

where v_z is the velocity where the charged particle can cross the magnetic and the electric field without getting deflected.

To be able to scan a range of velocities either the magnetic or the electric field needs to be varied. In this case it was decided to generate the magnetic field with SmCo permanent magnets and vary the electric field which is created by applying opposing bias voltages to two parallel plates inside the probe. With this, Eq. 4.4 can be rewritten as,

$$v_z = \frac{U_b}{Bd}, \tag{4.5}$$
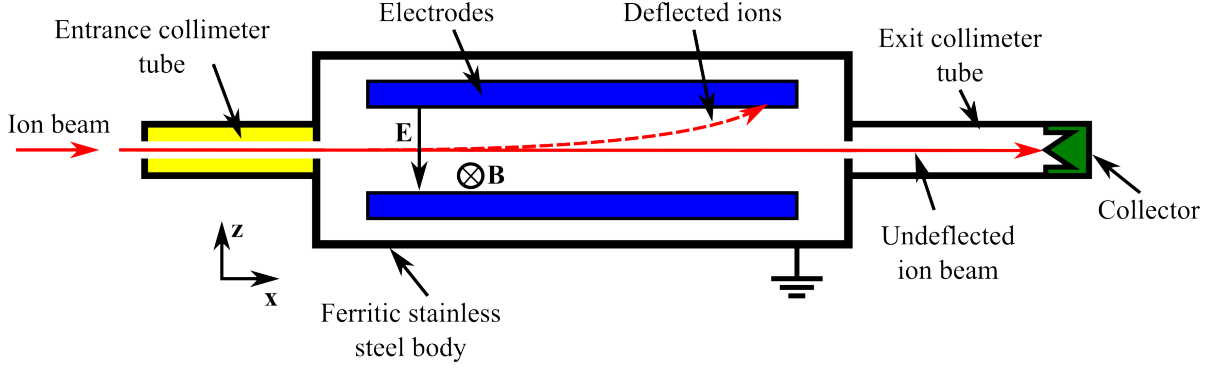
Figure 4.3: Schematic drawing of the E×B probe.

where U_b is the bias voltage of the probe and d is the distance between the electrodes.

Figure 4.3 shows a schematic drawing of the E×B probe designed, built and used in this work. An entrance collimator is used to filter out the ions which are not arriving orthogonal to the magnetic and electric field, i.e. on the axis of the probe. An exit collimator prevents the ions which have been deflected to reach the collector. The current reaching the collector is typically in the region of nano amperes which makes it necessary to use a precise instrument to measure it.

The measurements of the E×B probe can, in theory, be used to determine the ion temperature, T_i. For this to work the velocity distribution function has to be measured with a high resolution. The ion temperature calculates as,

$$T_i = \frac{m_i \sigma^2}{k_B},\qquad(4.6)$$

with the ion mass m_i and the standard deviation σ. In the case of the E×B probe the standard deviation function can be calculated as,

$$\sigma^2 = \frac{\int\limits_{-\infty}^{+\infty} (v - \bar{v})^2\, f\,(v)\, dv}{\int\limits_{-\infty}^{+\infty} f\,(v)\, dv}.\qquad(4.7)$$

This method will overestimate the ion temperature as the signal width in an E×B probe is not only the result of the ion temperature but also a result of several other mechanisms. The E×B probe is a band-filter and the bandwidth (resolution) depends strongly on the entrance and exit collimator. Therefore apparatus function of the probe is not a Dirace

delta function which would make it possible to measured the exact VDF profile. Instead the measured profile is the convolution product between the actual apparatus profile and the ion VDF in the probe direction. In order to estimate the error on the calculated ion temperature a knowledge of the resolution of the probe is essential.

4.3 Numerical Simulations

A numerical model of the E×B probe has been built with the goals:

- to choose the probe dimensions and for a certain velocity range and accuracy.

- to get an idea of the required magnetic and electric field strength.

- to minimize the probe dimensions and weight.

- to determine the influence of the probe materials used in the construction of the probe.

- to numerically model the ion trajectory through the probe and optimize the design with the obtained results.

The numerical model of the E×B probe has been built in COMSOL. The model includes the electric and magnetic field generated by the magnets and the electrodes, as well as the structure and materials of the probe. The computation is performed by using MUMPS (MUltifrontal Massively Parrallel sparse direct Solver) coupled with a Geometric MultiGrid method (GMG). This method allows a faster convergence of the solution, by using different mesh refinement along a V-cycle shape. Between the fine and coarse mesh, Successive OverRelaxation (SOR) iterative methods are used as presmoother and postsmoother. The size of the computational domain is $72 \times 72 \times 260$ mm and the fine mesh contains 190000 elements. The body size of the E×B probe used in the model corresponds with the size of the real probe and is $58 \times 58 \times 180$ mm and is displayed as a wire model in Fig. 4.4.

4.3.1 Magnetic Field

The topology of the magnetic field in the E×B probe is very important to the measurement. The field has to have a strong gradient at the beginning of the test section and has to be constant in magnitude and homogeneous in space inside the test section. This
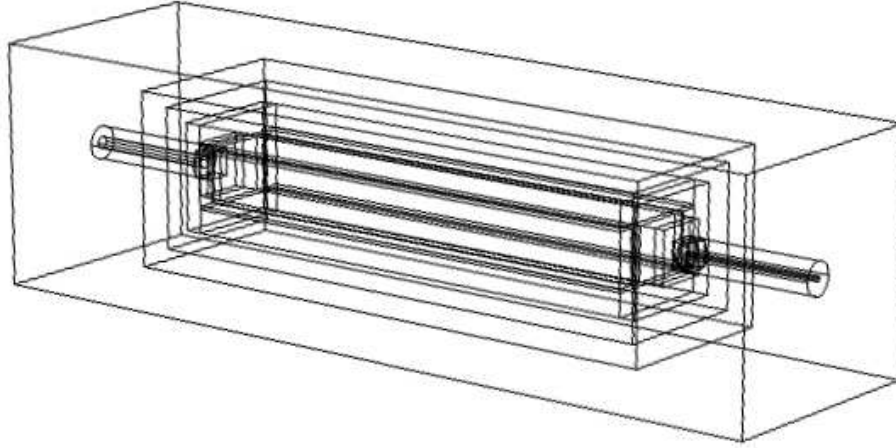
Figure 4.4: 3-D wire model of the simulated E×B probe in COMSOL.

is important because if the magnetic field is not perpendicular to the electric field or if the ratio of the field strengths between the two field changes, the ions crossing the test section of the probe get deflected instead of arriving at the collector. Numerous numerical simulations have been performed to increase the quality of the magnetic field. A 3-D plot of the calculated magnetic field is shown in Fig. 4.5.

Figure 4.6 shows a comparison of the profil of the measured and the simulated magnetic field along the symmetrical x-axis of the probe. The supplier of the permanent magnets was only able to provide a range for the magnetic field strength. The absolute value has been measured in the final position of the magnets within the probe and has been used to correct the value in the simulations. Therefore the valuable information in Fig. 4.6 is the shape of the magnetic field, where the measurements correspond with the simulations. A small dip can be seen in the measured values in the middle of the graph. This is due to the short length of the Gaussmeter probe tip which deforms when inserting the probe tip far into the E×B probe. As the Gaussmeter probe was not long enough to measure across the whole E×B probe the values have been acquired by inserting the Gaussmeter probe from both sides into the E×B probe.

The body of the probe is made out of ferritic stainless steel which conducts magnetic flux. Since the probe is used in plasmas with reactive gases such as SF_6 and oxygen, stainless steel is used to avoid corrosion. This posses a problem as stainless steel is commonly non magnetic and ferritic stainless steel is hard to obtain. The body of the probe is used to shield the magnetic field. This increases the strength of the field and makes it more uniform which is important for the use in an E×B probe. The effect of

47
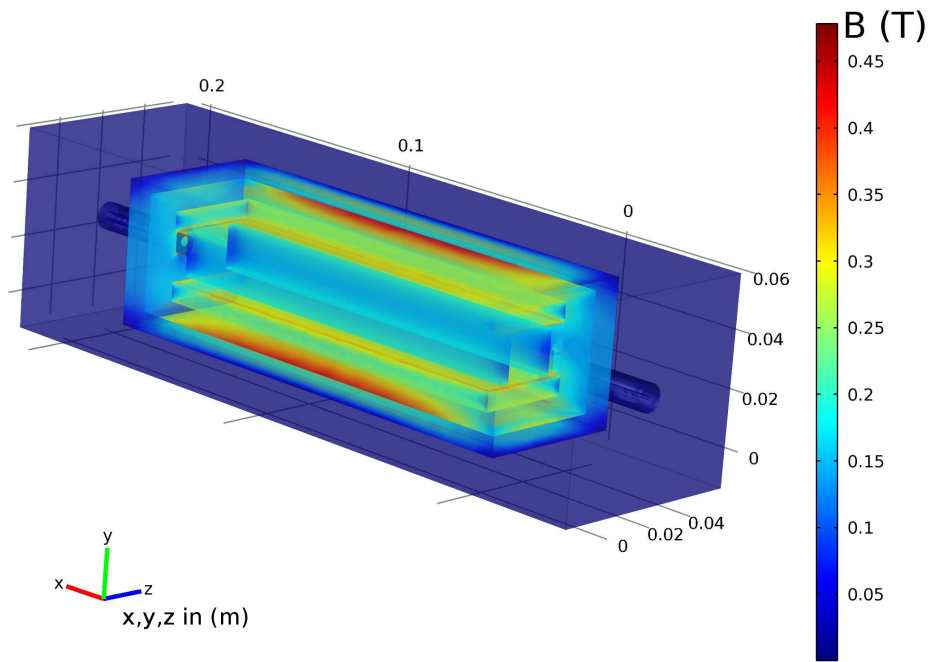
Figure 4.5: 3-D plot of the simulated magnetic field strength for the E×B probe and its surroundings.
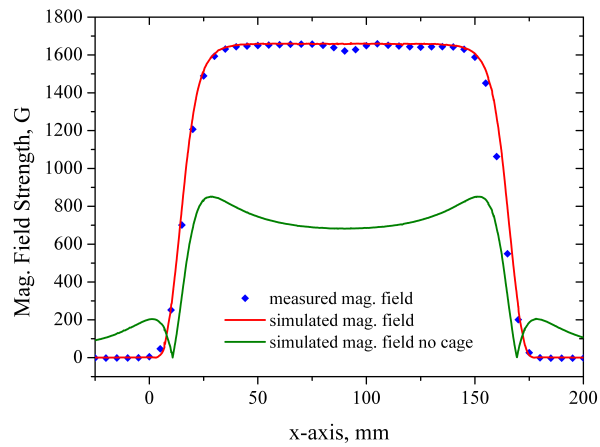
Figure 4.6: Comparison of the measured magnetic field and the simulated magnetic field along the symmetrical x-axis of the probe.
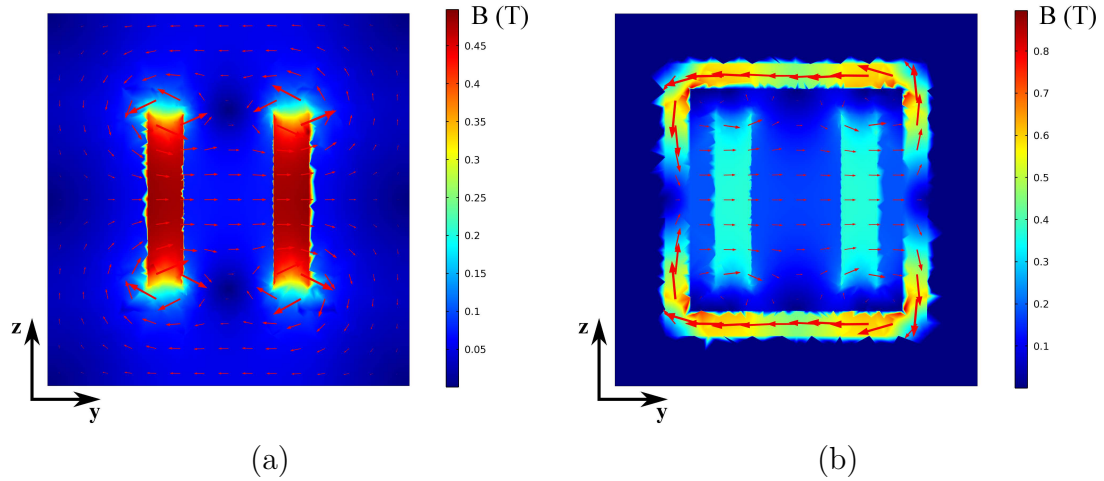
Figure 4.7: Numerical simulations of the magnetic field inside the E×B probe (a) without and (b) with a ferritic shield.

the ferritic cage is displayed in Fig. 4.6. The magnetic field is less strong without the ferritic probe body using the same magnet configuration. The field is also non uniform inside the filter zone between the magnets and shows bumps at the beginning and the end of the probe. This would make a precise measurement with the E×B probe difficult if not impossible. The effect of the confinement of the magnetic field in the yz-plane is shown in Fig. 4.7.

4.3.2 Electric Field

The electric field is created by biasing the two electrodes inside the probe. The strength can easily be calculated by diving the potential difference between the electrodes by the distance. Two different bias schemes exist to bias the electrodes. We talk of a symmetrical bias when one electrode is biased positively and the other electrode is biased negatively with the same value provided by two power supplies. The second possibility is that one electrode is grounded and the other one is biased. This requires only one power supply.

Symmetrical Bias

The simulations for the symmetric bias of the probe in Fig. 4.8 show that the electric field calculated with the electrode bias voltage divided by the distance of the electrodes
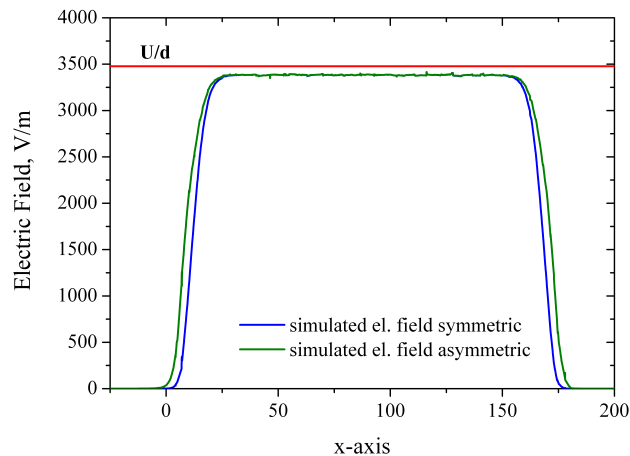
Figure 4.8: The figure shows a comparison of the theoretical value of the electric field and the simulated electric field along the symmetrical x-axis of the probe in the case of the symmetrical and asymmetrical bias.

is roughly 2 % higher than the electric field given by the simulations. The source of the disagreement is unknown and might lie in the code for the numerical simulations. The shape of the electric field along the x-axis is similar to the shape of the magnetic field. This is important as the charged particles can get deflected at the beginning and at the end of the filter zone if the ratio between the electric field and the magnetic field is not similar to the one inside the filter. The numerical simulations of electric field presented in Fig. 4.9 show that the field is as expected symmetric with respect to the zero potential of the surrounding probe body and that an ion can pass the probe undeflected at a certain velocity.

Asymmetrical Bias

The asymmetrical bias has the advantage that only one power supply is necessary as the second electrode is grounded. However it can be seen in Fig. 4.10 that the a strong field is generated between the grounded probe body and the biased electrode. The simulated ion with the same speed as in the case of the symmetrical bias gets now deflected. The simulations reveal that the velocity band in which the ions can pass shifts and can not be estimated anymore with Eq. 4.5. Figure 4.8 shows the generated electric field along the x-axis for both, symmetrical and asymmetrical, bias. The electric field strength between the electrodes does not change. A clear difference can be observed in the beginning and
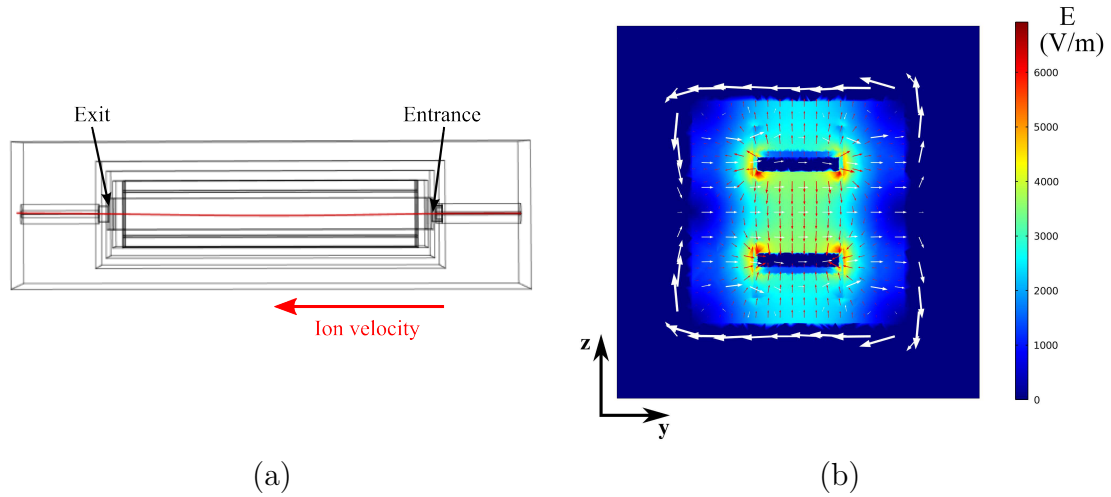
Figure 4.9: Symetrical bias: The path of a singly charged xenon through the E×B probe is shown in (a) and the the electric field in the yz-plane is shown in (b).

at the end of the test section. This is due to the fact that the electric field is stronger between the grounded probe body and the biased electrode. The distance between the biased electrode and the probe body is closer as between the two electrodes. This leads to a deformation in the electric field topology and should be avoided in order to get conclusive results with the E×B probe.

4.3.3 Ion Trajectory Simulations

Simulations have been conducted to trace the particles through the E×B probe with an entrance collimator of 43 mm length and a hole diameter of 1.5 mm plus a exit collimator of 3.6 mm, see Ch. 4.4.1.

To start out an acceleration voltage of 300 V has been assumed. This results for singly charged xenon at ideal acceleration in the grids in a speed of 21 km/s. With the distance of 16 mm between the electrodes and an averaged measured magnetic field of 1656 G a theoretical potential difference of 55.64 V can be calculated. With this potential difference applied to our model particles with a velocity between 21080 m/s and 22340 m/s pass the E×B probe. This is probably due to effects in the beginning and the end of the test section. In these two regions the gradient of the electric field does not correspond to the gradient of the magnetic field and the particles are slightly deflected. This means at a electrode bias voltage of 55.64 V, particles with an average velocity of 21710 m/s (averaged from the velocity range) getting undeflected through the probe. Using Eq. 4.5,

<center>(a)   (b)</center>
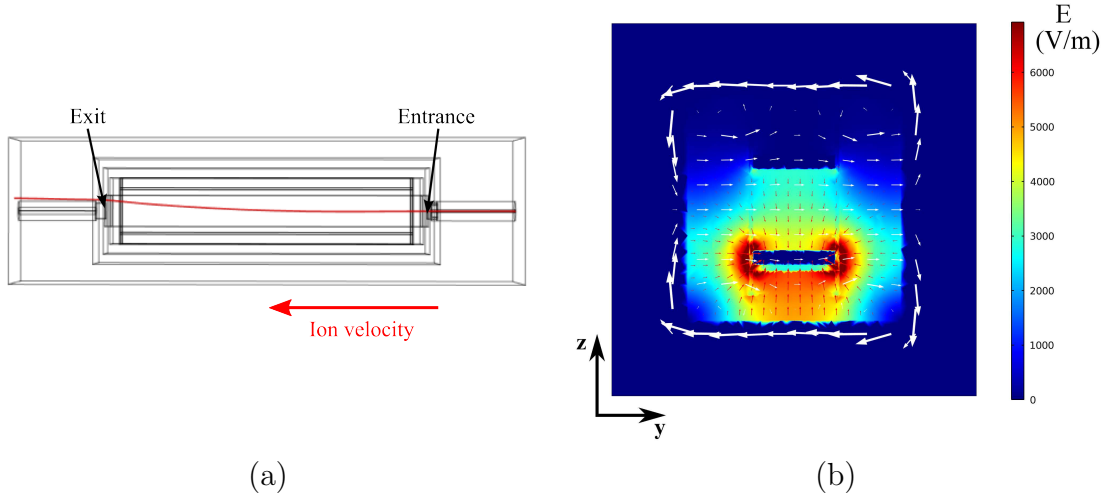
Figure 4.10: Asymmetrical bias: The path of a singly charged xenon through the E×B probe is shown in (a) and the the electric field in the yz-plane is shown in (b).

a theoretical magnetic field strength of 1602 G can be calculated to obtain the correct velocity of the ions. Alternatively the value of 390.19 m/s can be used to convert the probe bias voltage to the speed of the ions which leads to the same result. For these conditions particles which arrive straight on axis can pass the probe within a range of 21710 ± 710 m/s.

The simulations also show that, in this configuration, particles arriving on the xy-plane can only pass if they have an angle smaller than $\pm 1°$ within the speed range of 21710 ± 710 m/s. For the xz-plane the particles are not behaving symmetrically and the minimum and the maximum velocity with which the particles pass at a electrode bias voltage of 55.64 V are given in Tab. 4.1. The table shows that particles with different velocities can pass the E×B prob and that it is advisable to decrease the entrance and exit collimator to the smallest size where a decent signal can be obtained. Although the error induced in this cases seems huge on has to keep in mind that the current for ions entering the probe at a higher angle is weak. The signal strength of the ions entering the probe in dependance of their angle can be approximated, in two dimensions, by calculating the area of two intercepting circles:

$$A = 2r^2 \arccos\left(\frac{d}{2r}\right) - \frac{d}{2}\sqrt{4r^2 - d^2}, \tag{4.8}$$

where A is the area of the overlapping circle, r the radius of the circles and d the

<center>52</center>

Angle (°)	v_{min} (m/s)	v_{max} (m/s)	Δv (m/s)
-2	23700	25600	1900
-1	22350	23600	1250
0	21080	22340	1420
1	20250	21300	1050
2	all particles spiral away		

Table 4.1: Particles passing through the E×B probe with an angular component in the xz-plane for a velocity of 21710 m/s resulting in a bias of 55.64 V.

distance between the centers of the circles. The two intercepting circles represent the projection of the entrance collimator tube when viewed under an angle. The results for this calculation are displayed in Fig. 4.11 where the sine function is considered linear at these low angles. It can be seen that the current is low for the extreme angles where the velocity of the ions which can pass the probe undeflected diverts strongly from the base velocity (at an angle of 0°). Therefore the only ions arriving on axis are considered to calculate the probe resolution which is 6.5 % of the measured ion velocity for the used configuration.

The particle trace simulations can be performed for several conditions but are time consuming as in the current model only one particle can be traced and it has to be verified by eye if the particle arrives at the collector. Therefore simulations have been performed for only one condition to get an idea of the resolution of the probe and the different broadening effects of the signal.

The importance of choosing a magnetic field strength is shown in Fig. 4.12. The ion is deflected at the entrance of the test section even though in theory the particle should pass. This is a result of a too strong magnetic field. The ion Larmor radius described in Eq. 5.1 becomes to small and the ion trajectory inside the probe gets curved and the particle does not arrive at the collector. One has to consider the desired velocity range which was in our case stretches from 10000 m/s to 60000 m/s and chose the magnetic field and the electrode bias range accordingly. The probe use ended up having a theoretical range of up to 110 km/s due to the bias range of the electrodes. The simulations show that particles traveling faster than 70 km/s show an erratic behavior and do not arrive at the collector even though they are in the theoretical measurement range. This is probably due to difference in the gradient of the electric and the magnetic field in the beginning and the end of the probe. This behavior could not be verified as a source providing ions at that speed was not available.
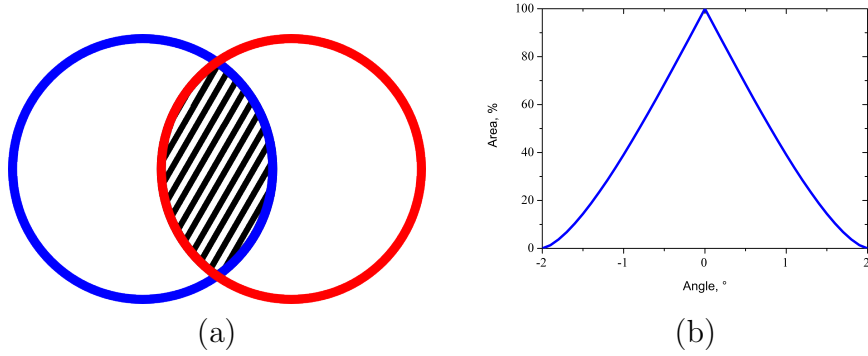
Figure 4.11: The scheme in (a) displays the current which can be approximated as the area of two intercepting circles. Graph (b) shows the current (area) which passes through the entrance collimator at a certain angle.

Table 4.2 shows the calculated theoretical speed for different ion species and gases at several acceleration biases using Eq. 2.6, neglecting plasma potential and potential losses. The table shows some typical acceleration voltages for ion and Hall thruster for which the probe is intended. The speed of the ions lies mainly within the range of the E×B probe built and used in this thesis.

Simulations of the electron trajectory through the probe have been performed. For this an electron with the electron temperature T_e of 5 eV is assumed to enter the probe on axis. Using the root mean square of the total thermal velocity:

$$v_e = \sqrt{\frac{3kT_e}{m_e}}, \tag{4.9}$$

the electron is calculated to have a thermal speed v_e of 6743 m/s. A simulation of the electron path with these parameters is displayed in Fig. 4.13. It can be seen that even the

Ion	Acc. 300 V (m/s)	Acc. 500 V (m/s)	Acc. 1000 V (m/s)
Xe^+	20999	27109	38338
Xe^{2+}	29697	38338	54219
Xe^{3+}	36371	46955	66404
Ar^+	38068	49146	69503
Kr^+	26284	33932	47989
SF_6^+	19909	25703	36349
F^+	55202	71266	100785

Table 4.2: Velocity of different ions for different acceleration biases.
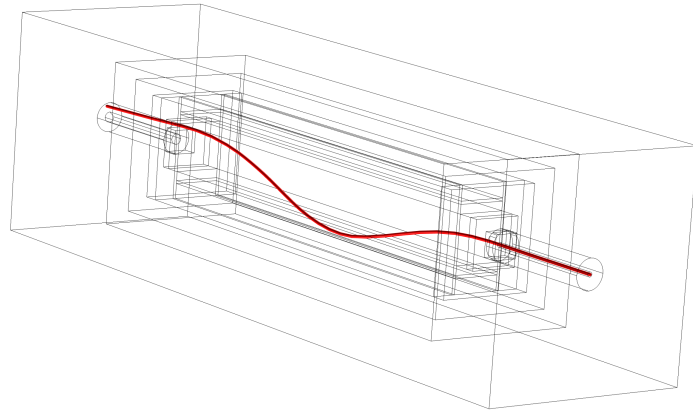
Figure 4.12: Simulation with a strong magnetic field of 3000 G on axis; The particle is deflected.

weak magnetic field present at the entrance collimator is enough to deflect the electron and force it into a spiral trajectory. Even if the electron could enter the test section, the electron Larmor under these conditions is 0.24 µm, calculated using Eq. 5.1, and the electron would end up in a circular motion.
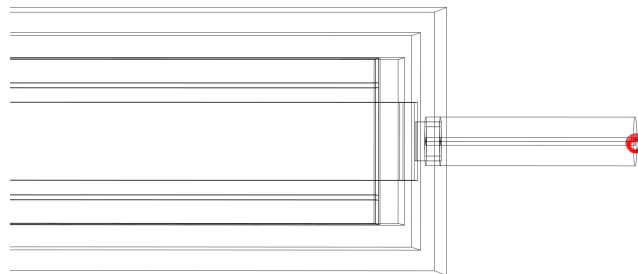
Figure 4.13: Simulation of an electron entering the collimator of the E×B probe with a thermal velocity of 5 eV.
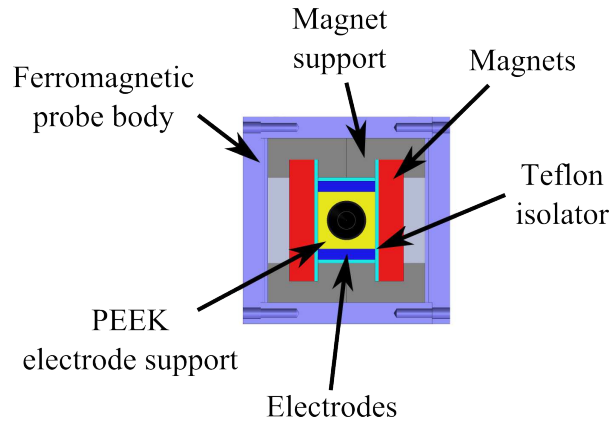
Figure 4.14: Cross-section view of the CAD model of the E×B probe along the y-axis.

4.4 Probe System

4.4.1 Construction of the Probe

To construct the probe preliminary calculations and numerical simulations of the probe architecture have been performed. The test section is 150 mm long and has a 11 mm in diameter hole in the middle to pass the ions. This length has been chosen to allow the ions without the proper speed to be deflected. As magnets in the length of the test section might break easily, instead of two, four SmCo magnets with sizes of $75 \times 34 \times 7$ mm are used to create the magnetic field. The magnets are strong and have to be handled with care to avoid injuries and damage of the magnets them self. To avoid movement and to allow for a risk free assembly the magnets are put into U-shaped rails as shown in Fig. 4.14. A 1 mm thick Teflon layer is placed in front of the magnets to avoid contact with the electrodes and a short circuit. The distance between the electrodes is fixed with two PEEK spacer which have a whole in the middle to pass the ions. The electrodes with the spacer and another Teflon isolation layer can be inserted into the space between the magnets, as shown in Fig. 4.15, and fixed with screws which are also used for the electrical connection of the electrodes. The ferritic body of the probe consists of six parts and is assembled around the test section. The space between the test section and the probe body is purposely kept narrow to concentrate the magnetic field as much as possible and keep the size and weight of the probe small.

The collector consist of a cone inside a tube made out of graphite, as shown in Fig. 4.16. The design aims to reduce the influence secondary electron emission due to sputtering. The collector is electrically isolated from the surrounding tube by a Teflon holder. The
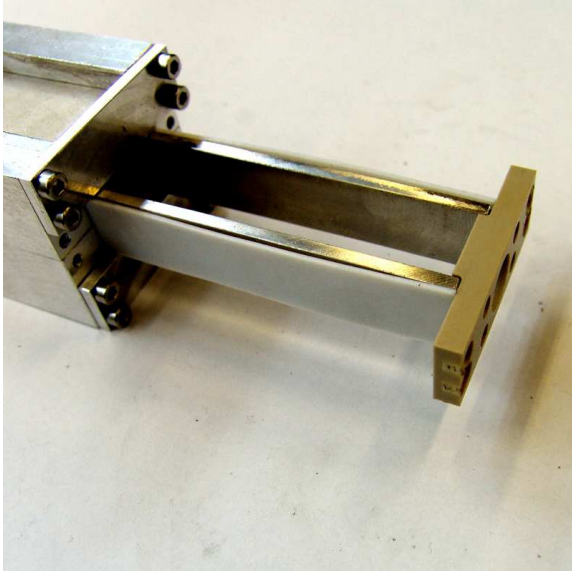
Figure 4.15: Insertion of the electrodes with their holder and Teflon isolator into the block containing the magnets.

Figure 4.16: The collector of the E×B probe consisting of a graphite cone in a tube to reduce the influence of secondary electron emission.

exit collimator tube and collector assembly is roughly 150 mm long so that a differential pumping can be added at a later moment. This might be necessary to achieve a better signal to noise ratio. As a constant stream of ions arrives and the neutral atoms inside the probe have no means to escape except through the entrance collimator, the pressure can build up inside the probe. This can lead to increased collisions between ions and neutral atoms with possible changes in the measurement outcomes.

Collimator

The entrance collimator of the E×B probe in the experiments consist of a 43 mm long glass tube with a hole diameter of 1.5 mm as can be seen in Fig. 4.17. Glass has been chosen as a collimator material as it is easy to work with and tubes of the desired size were readily available. Other materials as ceramics or graphite might also serve as collimator materials. The hole size and length of the glass tube can easily be changed to increase or decrease the resolution of the probe according to the measured plasma.

The exit collimator consists of a plate with a 3.6 mm hole in it to pass the ions. Several plates with different hole sizes are available and can be exchanged to adjust the resolution
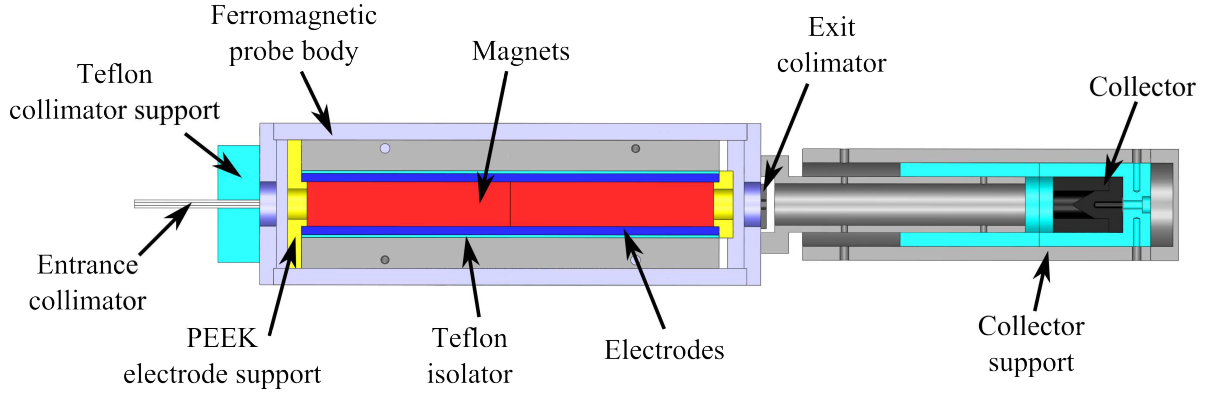
Figure 4.17: Cut through the CAD model of the E×B probe along the x-axis.

and signal strength of the probe. The exit collimator plate is hold in place by several screws which allow to move the hole several millimeters in yz-direction. It is important for the probe to work, that the front and exit collimator are perfectly aligned. To ensure this a laser can be shone through the entrance collimator. The exit collimator plate is then moved into the position where the laser beam can pass. While doing measurements, the surrounding plasma can enter the probe behind the exit collimator plate due to the nature of the adjustment mechanism. This leads to a shift in the measurement if the gap is not closed.

The entrance collimator tube as well as the exit collimator is exchangeable and the signal strength and resolution of the probe can be adjusted. The acceptance angle α of the E×B probe depends on the entrance collimator tube and is displayed in Fig. 4.18. The red lines display the highest angles at which the ions can arrive and still pass the entrance collimator tube which is displayed in blue. The acceptance angle α can be calculated as,

$$\alpha = 2 \arctan \frac{d_c}{l_c}, \qquad (4.10)$$

where d_c is the hole diameter and l_c is the length of the entrance collimator tube. The entrance collimator used in the experiments presented in this thesis has an acceptance angle of 4°.

The length of the entrance collimator strongly influences the acceptance angle of the probe. It can be increased to filter out ions which arrive at a higher angle compared to the E×B probe. This can be used to acquire the divergence angle of the plume of an electric thruster by measuring the angular dependency of the ion current. Although
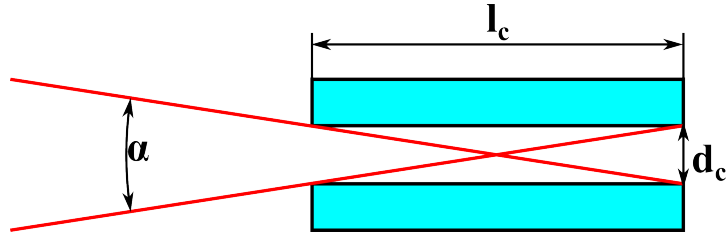
Figure 4.18: Acceptance angle of the E×B probe based on the dimensions of the entrance collimator tube (in blue).

also connected to the acceptance angle, the diameter of the entrance collimator allows to control the signal strength of the E×B probe as the aperture area increases to the power of two with the diameter. If a high angular resolution is required with a high signal strength a long entrance collimator with a large diameter can be chosen.

The material of the entrance collimator might play an important role in the function of the E×B probe. First measurements have been performed with an insulating ceramic tube. The obtained results where unsatisfying but the origin of the problems could not be determined. After changing several parameters including the material of the entrance collimator to a glass tube the quality of the results improved. Charging as well as secondary emission could explain the observed effect. A metal tube could be used as an entrance collimator like in a mass spectrometer to avoid these effects.

The exit collimator has a strong influence on the resolution of the probe. It determines if a particle only lightly deflected by the field can arrive at the collector. The signal strength can easily be increased by choosing a larger diameter for the exit collimator but it comes directly at the cost of resolution.

It is important to keep in mind that all three parameters, the entrance collimator length and diameter and the exit collimator diameter are dependent on each other. A good combination of these parameters has to be found to get good results.

The collector and the electrodes are internally connected to SMA connectors (SubMiniature version A) which are mounted to the body of the probe. With this widely spread standard connector type the E×B probe can easily be installed in a variety of vacuum chambers.

4.4.2 Control Unit and Data Acquisition

The E×B probe system uses a National Instrument USB-6211 data acquisition card to to control and measure a custom build amplifier with two channels which is used to bias the electrodes. The maximum voltage on each channel is ±150 V adding up to a total potential difference of 300 V. Both channels can be controlled independently to obtain asymmetrically biased electrodes.

The ion current accumulated by the collector is measured with a Keithley 6485 Picoammeter. It has a range from 20 fA to 20 mA with a resolution of 10 fA. The up to 1000 readings per second allow for an averaging of the measurements without losing to much time. Special low noise BNC cables should be used with the picoammeter to improve the measurement. While performing measurements in an inductively coupled RF plasma a 100 times higher noise has been observed in comparison to measurements performed within a Hall thruster plume due to the potential fluctuation induced by the RF.

A Labview program has been written to automate the piloting and acquisition of data from the probe. A schematic drawing of the whole system is given in Fig. 4.19. The program allows to adjust the iteration number, the averaging at each point, bias voltage step size and scan range. Most of the measurements presented in Ch. 6 have been performed with a step size of 0.4 V an averaging of 10 values over a range from 0 V to 200 V without iterations. This adds up to 500 measurement steps and takes arround 15 min. The long measurement time is due to the fact that each readout of the picoammeter is already internally averaged and that the Labview program is not written for high frequency data acquisition.

The post-acquisition data treatment is done in Origin 7.5. The files are imported and the measured currents averaged as the Labview program only provides the single measurements. This reduces the noise drastically in the obtained trace. The bias voltage is then converted to the corresponding ion velocity.

4.5 Measurements

4.5.1 Influence of Polarization

The influence of the polarization has been verified in a xenon Hall thruster with a discharge voltage of 250 V. The two measurements methods, symmetrical and asymmetrical
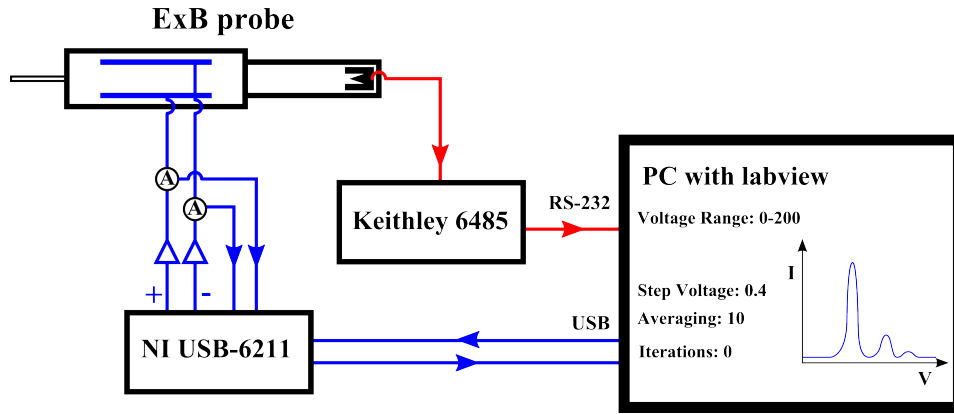
Figure 4.19: Schematic drawing of the E×B probe system with the piloting and data acquisition controled by a Labview program.

bias, are compared to each other in Fig. 4.20. As mentioned before the asymmetric bias of the electrodes changes the electric field in the beginning and at the end of the filter section but does not change the field strength between the magnets and the electrodes. This causes the ions which can pass with a symmetrical bias to be deflected with an asymmetrical bias. If the strength of the electric field is lowered the ions can pass the filter section. The conversion between the voltage bias and the ion velocity is made assuming a symmetrical electric and magnetic field and causes a shift in the peaks which leads to an overestimation in the ion velocity. Figure 4.20 also reveals that the width of the peak increases when using the asymmetric bias. This leads to the assumption that a loss in resolution occurs when using this method.

4.5.2 Measurements in a Hall Thruster

The plume of a Hall thruster is quite different from the one of an ion thruster. The ions are generated in the ring shaped channel of the thruster and are accelerated outward by an electric field. The divergence angle of a Hall thruster is higher than the one of ion thrusters. This leads to ions arriving at a wider angular distribution. This means the alignment of the probe is very important and has a strong influence on the outcome of the measurement. Figure 4.21 shows a measurement with the E×B probe in the far field plume of the PPI Hall thruster (Petit Propulseur Innovant). A low power, permanent magnet, xenon Hall thruster with a discharge voltage of 250 V [41]. The probe is aligned parallel to the symmetrical x-axis of the thruster to point into the ring shaped channel where the ions are created. The figure shows the biggest peak which corresponds to the
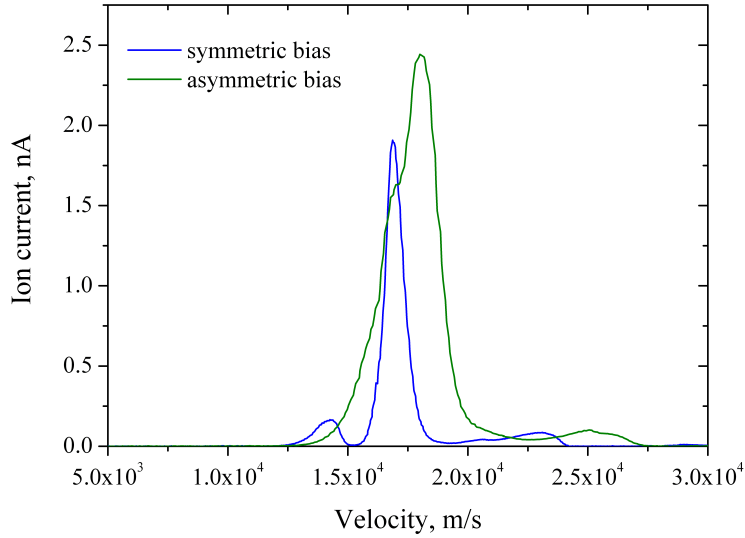
Figure 4.20: Difference between the symmetrical bias and the asymmetrical bias of the E×B probe. The measurements were performed in the far field plume of a Hall thruster with a discharge voltage of 250 V.

Xe^+ ions and two smaller peaks for Xe^{2+} and Xe^{3+} ions. The average speed of the Xe^+ ions is 16888 m/s which corresponds to an acceleration voltage of 194 V. The peaks are separated from the main peak by a factor of roughly $\sqrt{2}$ and $\sqrt{3}$ as expected. The figure shows a peak before the main Xe^+ peak. A peak like this has been observed in most of the measurements of the E×B probe with Hall thrusters and in some measurements with ion thrusters. The cause for this peak is currently unknown. It is likely that this phenomenon is connected to the probe design and function. This penomenon has also been observed by other teams and will be topic of future investigations [42].

4.5.3 Measurements in an Ion Thruster

A measurement of the E×B probe in the PEGASES thruster is presented in Fig. 4.22. In this case the PEGASES thruster was operated in xenon with a grid bias of 288 V. The plasma potential in the ICP discharge is around 20 V in these conditions. It adds to the acceleration potential. The dashed lines mark the expected speed of the ions calculated for an acceleration bias of 308 V. The presented values are averaged 10 times as mentioned before and reveal multiple peaks when zoomed in. Considering all the
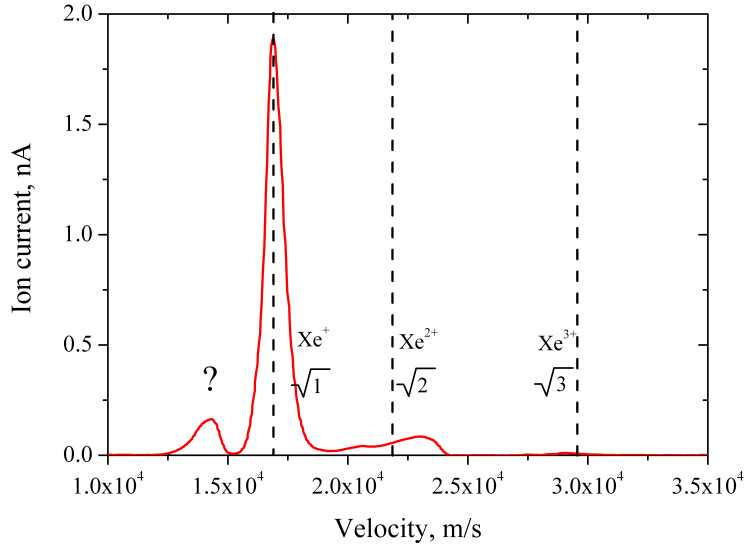
Figure 4.21: Measurements with the E×B probe of the ion velocity in a Hall thruster with a discharge voltage of 250 V.

involved elements which can be present in the plasma due to contamination and leaks and calculating their expected speed, it is likely that Xe^{2+}, Xe^{3+}, O_2^+, N_2^+, H_2O^+, O^+ and O_2^{2+} are present in the plasma and are accelerated. This indicates a leak in the plasma chamber or in the feed line of the gas.

It can be seen that the speed of the ions seem to be higher than value expected from the bias voltage. This effect is not visible in the simulations. The measured ion velocities are given in Tab. 4.3. The theoretical acceleration bias has been calculated with Eq. 2.6. It has to be considered that the plasma potential is not linear along the axis of the thruster. The ion species with a higher charge number might be accelerated with a different plasma potential as they are created further downstream in the source. However it is unlikely to have a 12 V lower plasma potential close to the source than close to the grids. This leads to the conclusion that the values of the electric and magnetic field which have been used to calculated the speed with the probe correspond not with the real values. Therefore a calibration of the probe with a source where the ion speed is well known is necessary to obtain better values. Figure 4.23 demonstrates the necessity of a calibration. Three different conversion factors have been used to calculate the ion velocity and compare them to the expected velocities of the ion species calculated with a bias voltage of 308 V. The conversion factor of 390 m/s has been obtained from the numerical simulations, the
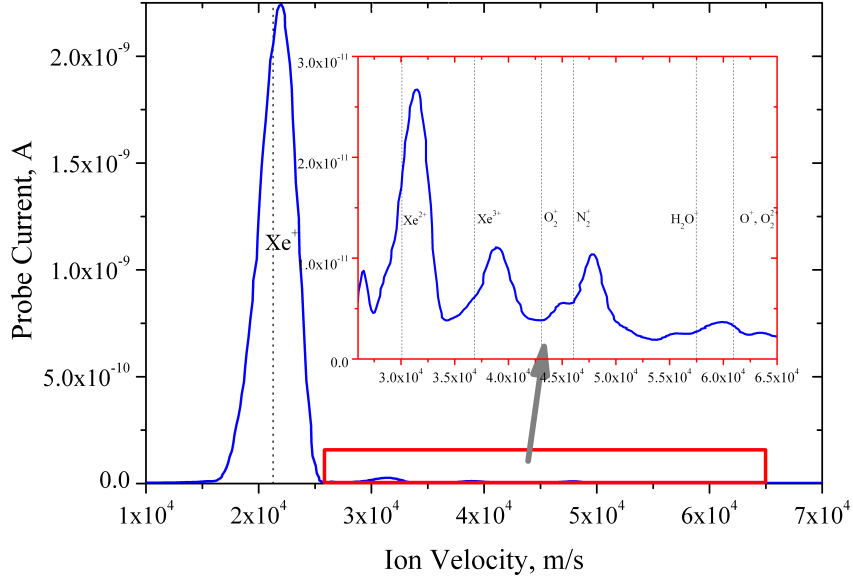
Figure 4.22: Measurement with the E×B probe in the PEGASES thruster at 288 V bias in xenon.

factor 379 m/s is the factor obtained using the averaged measured magnetic field and the electric field calculated with the bias of the electrodes and the factor 363 m/s is one who has been obtained by optically comparing the expected velocities with obtained trace. As the exact accelerating potential is unknown these factors have an uncertainty. The factor obtained through the simulations seems to give unsatisfactory results. The factor obtained by optically comparing the trace with the expected peaks corresponds mostly with the higher peaks but leads to a possible underestimation of the Xe^+ ions. The factor of unit 379m/s is used in the rest of this work as it the most reliable factor so far until a calibration can be made.

Ion	Ion velocity (m/s)	Theo. accel. bias (V)
Xe^+	21997	329
Xe^{2+}	31524	338
Xe^{3+}	38822	341

Table 4.3: Measured peak velocity of the ions with a 288 V acceleration between the grids and their theoretical acceleration bias.
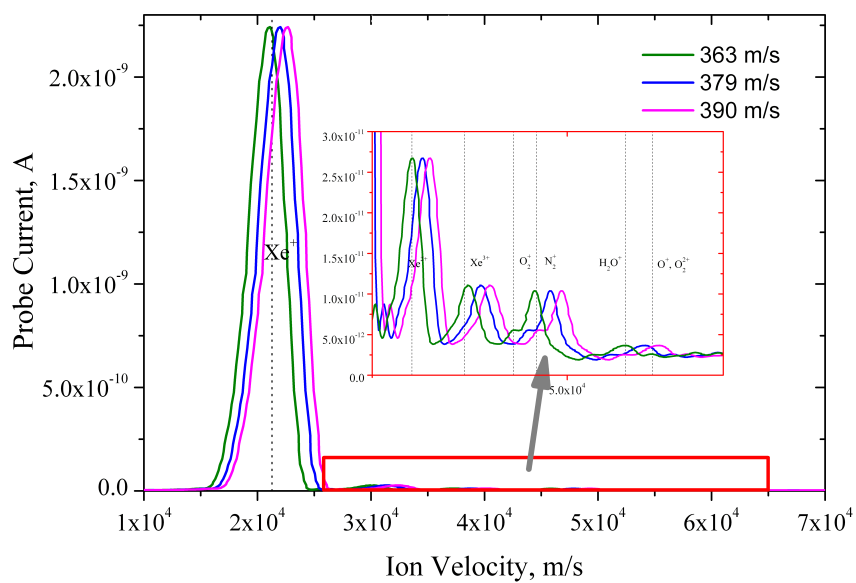
Figure 4.23: Comparison of three conversion factors between the voltage and the ion velocity.

4.6 Conclusion

The E×B probe is a versatile tool in plasma physics which can be used to measure the velocity of ions. If the acceleration potential is fixed and known the velocity of the ions depends on their charge and their mass. Through this, it is possible to distinguish between singly and multiply charged ions and calculate the ratio between them. A trace of the E×B probe also shows the different ions species and can help to identify them. In this case the E×B probe works as a mass spectrometer and reveals the elements and molecules present in the plasma. It remains to be demonstrated if the ion temperature can be measured with an E×B probe with a high resolution.

5 Investigation of the Strip Structure

5.1 Introduction

A magnetic barrier is a crucial element for the generation of negative ions in low-pressure plasma sources running with electronegative gases. Such magnetized sources find technological applications in various fields like material processing for etching of microcircuits [43], controlled nuclear fusion for neutral beam injection [44] and space propulsion with the innovative PEGASES thruster concept [45]. The magnetic field is used to trap electrons and to subsequently cool them down owing to collision events with heavy particles. A low electron temperature leads to a higher electron attachment rate, thus enhancing the production of negative ions [15–17]. The PEGASES thruster concept is one example of negative ion sources that rely on a transverse magnetic field to cool down and filter out electrons in such a way that an electron-free plasma, also called ion-ion plasma, is obtained. More information about the PEGASES thruster can be found in Ch. 2.4.

While studying different magnetic field configurations for the PEGASES thruster trap using a capacitively-coupled RF discharge, we have observed the formation of a stationary two-dimensional pattern in the region of high magnetic field strength, as can be seen in Fig. 5.1. The luminous structure was called a "strip" according to its peculiar shape [46–48]. The strip was always present whatever the operating parameters and gas nature, making us believe it originates in intrinsic properties of a magnetized RF discharge.
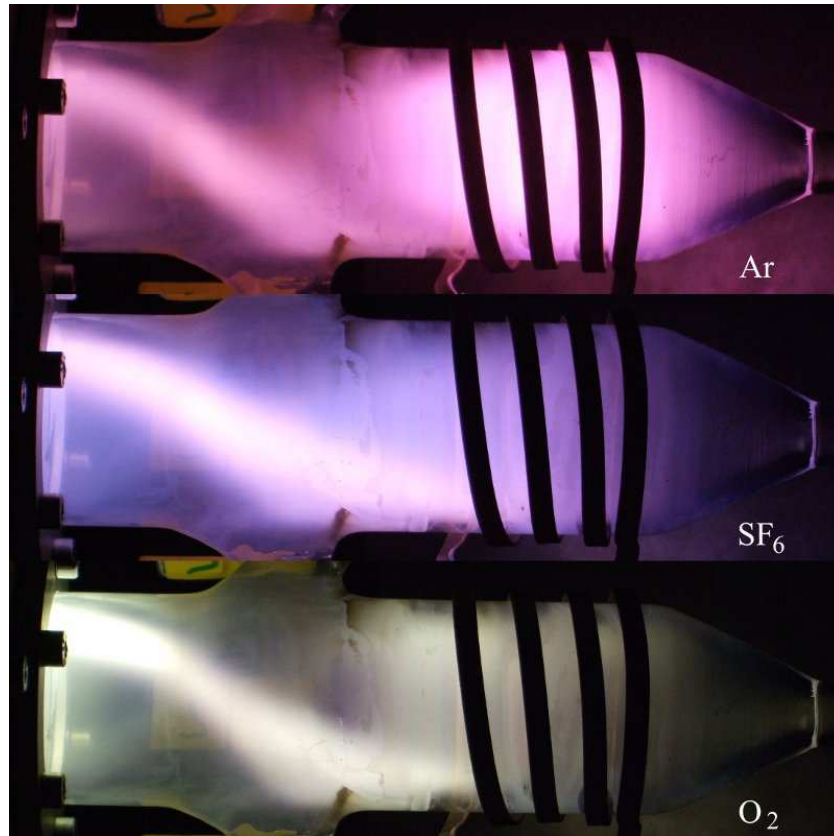
Figure 5.1: Side view of the strip-like structure in a RF discharge created in argon, SF_6, and oxygen (20 sccm, 500 G magnetic field and 250 W input power).

5.2 Experimental Arrangement

5.2.1 RF Discharge

Figure 5.2 shows the three different quartz tubes that have been used during the experiments. The tubes have been altered during the experiment in order to vary the conditions. The tube (a) has been used in the beginning of the experiment and the coil is wrapped three times around the tube. The strip has first been observed in this tube. The tube (b) has been constructed to side inject gas in the zone of the strongest magnetic field. In the case of a electronegative gas this can be used to increase the negative ion production [15–17]. Tube (b) has been used to obtain the pictures shown in Fig. 5.1. The final layout for the experiments is tube (c). This form has been chosen to closer resemble the second PEGASES prototype with a flat coil at the back and provides the possibility to insert a Far aday shield. The flat coil provides the advantage that a

potential difference between the beginning and the end of the coil does not induce a potential difference along the x-axis of the tube due to the RF. Although the plasma potential in the tube and the grounded chamber lead to a potential difference.

The latest plasma source used to investigate the plasma strip formation and properties is outlined in Fig. 5.4. This source has been used to do the majority of the experiments. A three-turn planar spiral coil is operated at 13.56 MHz. The coil is located at the end of a 5 cm in diameter and 20 cm in length quartz tube (shown in Fig. 5.2 (c)) with a flat end to transmit the power into the gas. The tube offers a visual access to the whole plasma discharge. This is essential to optically verifying the presence of the strip and its position . A grounded Faraday shield shown in Fig 5.5, built according to the design by Mahoney to prevent azimuthal RF current to circulate, can be placed in between the coil and the discharge tube [49]. The shield has to be grounded to close the circuit for the capacitive current which does not pass through the plasma and is collected by the shield. Without the shield, the RF power is capacitively coupled to the plasma. When the shield is introduced, the discharge runs in inductive mode. The spacing between the coil and the plasma is more important with the Faraday shield as the skin depth of an inductive discharge is small. The Faraday shield and the coil have to be placed as close as possible to the plasma without creating a short circuit between the Faraday shield and coil.

The gas is injected through a feed line which is mounted on the side of the discharge tube. The amount of gas deposited in the discharge can be regulated by a flow controller. Two flow controllers are used so it is possible to mix two gases together.

Figure 5.3 shows the setup of the strip experiment mounted on the epic test bench. The Faraday shield is inserted between the spiral coil and the discharge tube to block the capacitive part of the discharge. The magnetic field confines the plasma to the end of the tube. The coil which is wrapped around the tube has been used for another experiment an was not in use at the point where the picture was taken. The L-type RF matchbox can be seen in the background and is connected to the RF coil via big copper wire to lower the resistance of the line.

Two RF power supplies were available for these studies. A RF generator operating at a fixed frequency of 13.56 MHz was able to deliver power between 5 W and 1000 W. The RF frequency 13.56 MHz is an open frequency and widely used in industrial applications. This results in the equipment like the amplifier being cheaper. A variable frequency amplifier was used to produce RF power with a maximum output of 200 W. The amplifier
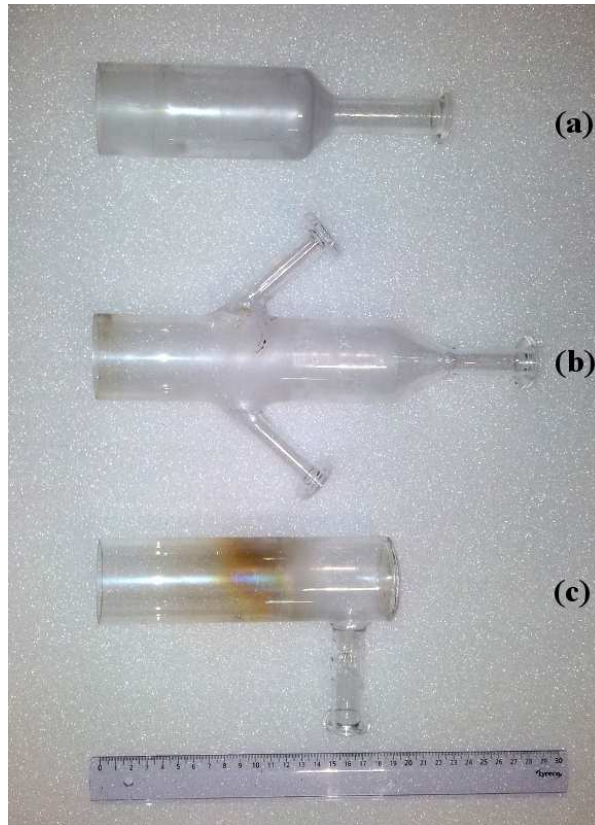
Figure 5.2: The three different quartz tubes that have been used during the experiments.

was driven by a sine wave function generator. The influence of the RF frequency on the strip has been verified with the variable amplifier. The rest of the experiments have been performed at 13.56 MHz. This was necessary as the Langmuir probe has to be adapted to each frequencies and chokes with the same resonance frequency have to be found.

To minimize the reflected RF power, a L-type matchbox was placed in between the coil and the power supply. As mentioned in Chap. 2.4.3 the L-type matching circuit has the disadvantage that one side of the coil is always grounded and the resulting potential difference is not symmetrical. The fraction of reflected power after matching the circuit was typically below 15 %. This is important as the reflected power can damage the components of the RF circuit and especially the RF amplifier or the RF generator. As the RF wattmeter in the RF amplifier was not reliable a Bird 43 wattmeter has been used to observe and measure the forward and the reflected RF power.

A magnetic field perpendicular to the direction of the plasma flow was created by placing several stacks of permanent neodymium magnets on either sides of the discharge tube. Magnets made from neodymium are the strongest commercially available magnets at the

70
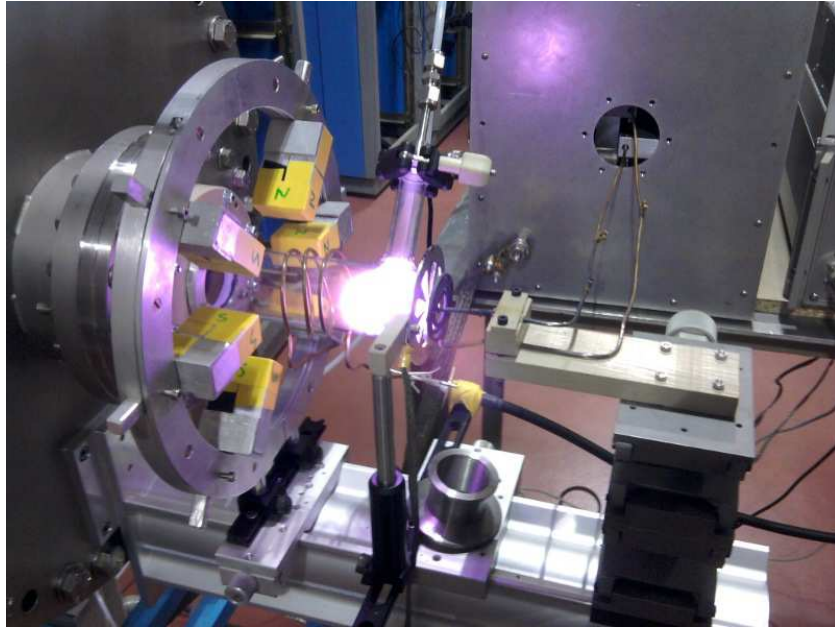
Figure 5.3: The picture shows the EPIC test bench with the strip experiment mounted.
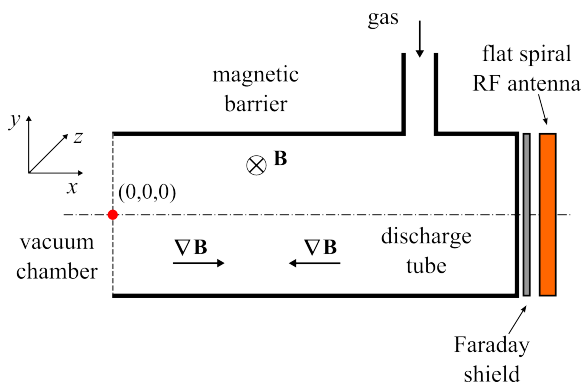
Figure 5.4: Layout of the RF discharge assembly for experiments with a magnetic barrier (**B** goes into the page at the cross). This magnetic configuration corresponds to the picture in Fig. 5.4.
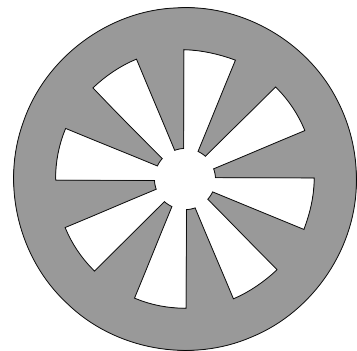
Figure 5.5: Faraday shield to prevent a capacitive coupling to the plasma.
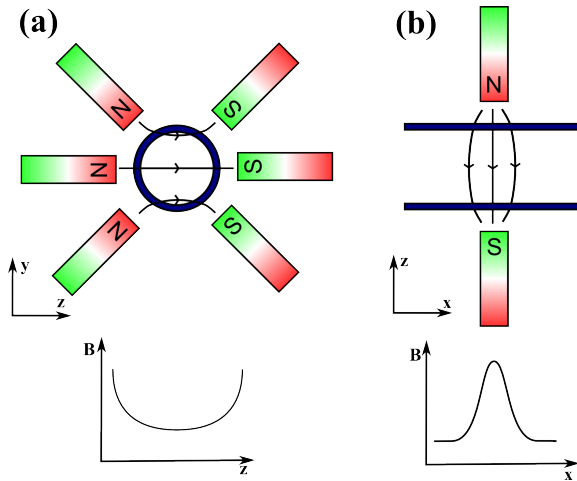
Figure 5.6: The magnetic trap used in the experiments with the strip.
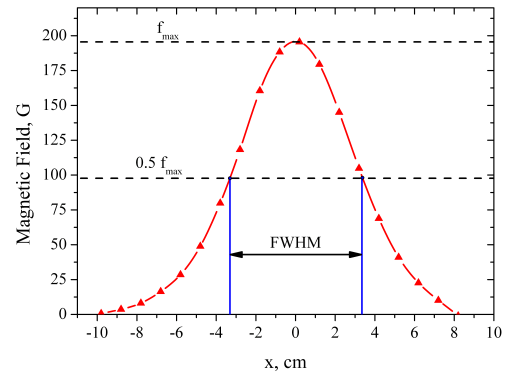
Figure 5.7: A measured magnetic field strength configuration and its FWHM along the x-axis for the experiments with the strip configuration.

moment. This allows for the creation of strong magnetic fields without using too much space. The magnets used in the experiments are $15 \times 15 \times 3$ mm and have a magnetic remanence of 13200 G to 13700 G. The magnets are usually stacked in piles of 20. A schematic drawing of the configuration of the magnetic trap and the field it generates is shown in Fig 5.6. The placement of the magnets creates a magnetic field which is mostly parallel to the z-axis inside the discharge tube. Figure 5.7 shows a magnetic field configuration with a maximum of 200 G. Measurements and simulations of the axial distribution of the field show that it is Gaussian with a full width at half maximum (FWHM) between 3 cm and 7 cm. The field strength is changed by varying the number of magnets, the number of stacks or the gap between the stacks and the tube. The maximum field intensity that has been used in the experiments is 1200 G in the center of the tube. In experiments corresponding to Fig. 5.4 the magnetic south pole was placed behind the tube.

5.3 Plasma Characteristics with the Strip

5.3.1 Capacitive Discharge

As mentioned before, the strip structure with its S-type shape has been observed, when a magnetic field is added, over a broad range of parameters with the discharge operated in capacitive mode, i.e. without the Faraday screen [47]. The first observation was made in SF_6, a strongly electronegative gas used for the PEGASES prototype [45]. Since the strip is also observed when running the RF discharge with Ar, Xe, He, O_2 and N_2, see Fig. 5.1. It can be concluded that the strip formation is not connected with the nature (atomic versus molecular), mass and electronegativity of the gas. The gas flow rate has been varied between 1 and 120 sccm in Ar, thus varying the pressure between 10^{-4} mbar and 10^{-1} mbar. The change in the pressure does not have an observable influence on the strip formation. The frequency has been tuned from 10 MHz to 60 MHz. This was the range which was achievable with our combination of the matchbox and the RF power amplifier at the time. With the acquisition of a RF generator at the fixed frequency of 13.56 MHz a variation of the transmitted power between 10 W and 600 W was possible. The RF generator is able to supply a power of up to 1000 W but at 600 W the coil started glowing red and the thermal load was so high that a further increase of the power was not possible. Modifying the discharge parameters did not influence the formation of the strip although the strip was brighter at higher power.

When a transverse magnetic field is added to the RF discharge, whatever its magnitude between 50 G and 1200 G, a luminous strip forms. At low field strength, only electrons are magnetized. At large strength, ions and electrons can be considered magnetized as the ion Larmor radius becomes significantly smaller than the geometric properties of the discharge tube. A small increment in the inclination of the strip was observed while increasing the strength of the magnetic field. The inflection point of the strip along the tube axis is always slightly downstream the maximum of the field. The direction of the strip changes when the direction of the magnetic field is reversed. According to the drawing in Fig. 5.4, the strip is oriented upwards, respectively downward, when **B** goes into the page, respectively comes out of the page.

The Larmor radius, r_g also otherwise known as the gyroradius can be calculated as

$$r_g = \frac{mv_\perp}{|q|\,B},$$
(5.1)
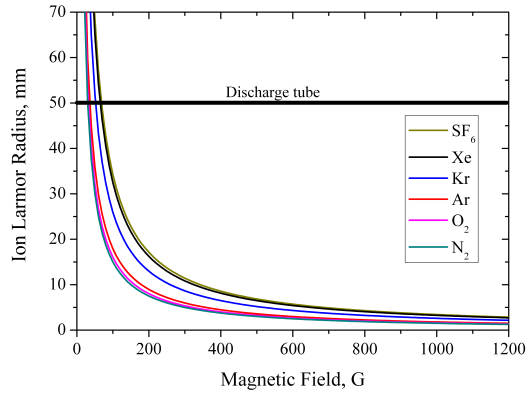
Figure 5.8: Ion Larmor radius for several singly charged ions calculated for the thermal velocity at 300 K.

where m is the mass of the particle, $v_\perp$ is the velocity component which is perpendicular to the magnetic field B and q is the charge of the particle. The ion Larmor radius for several singly charged ions with a thermal velocity of 300 K is shown inf Fig. 5.8. It can be seen that only for strong magnetic fields the ion Larmor radius becomes significantly smaller than the geometric properties of the discharge tube. That means the strip properties are governed by the electrons as they are always magnetized. For example the electron Larmor radius in a 500 G field for an electron at 5 eV is 0.18 mm.

Measurements of the electron properties were carried out with a compensated Langmuir probe (described in Chap. 3.3) at the exit of the discharge tube with argon as the working gas, see Fig. 5.9. For this measurement the probe was placed on a linear displacement stage in order to measure the electron temperature (T_e) and the electron density (n_e) along the y-axis of the tube. In the case of the magnetic field the probe moves into the luminous region of the strip. In the figure the strip ends on the positive radial position side. Without a magnetic field, there is no visible structure in the plasma. The radial distribution of the electron density and the electron temperature is symmetrical about the tube axis as expected. When a transverse magnetic field is added, radial profiles are no longer symmetrical. The electron density is much higher in the region where the strip exits the tube. In like manner the electron temperature is larger inside the strip. The thickness of the strip can be deduced from the radial profile of the electron temperature. It is around 1 cm, in agreement with visual inspection. Note that Fig.5.9 reveals the efficient cooling of an electron fluid across a magnetic barrier. The electron temperature in the region outside the strip is significantly lower than in the case without
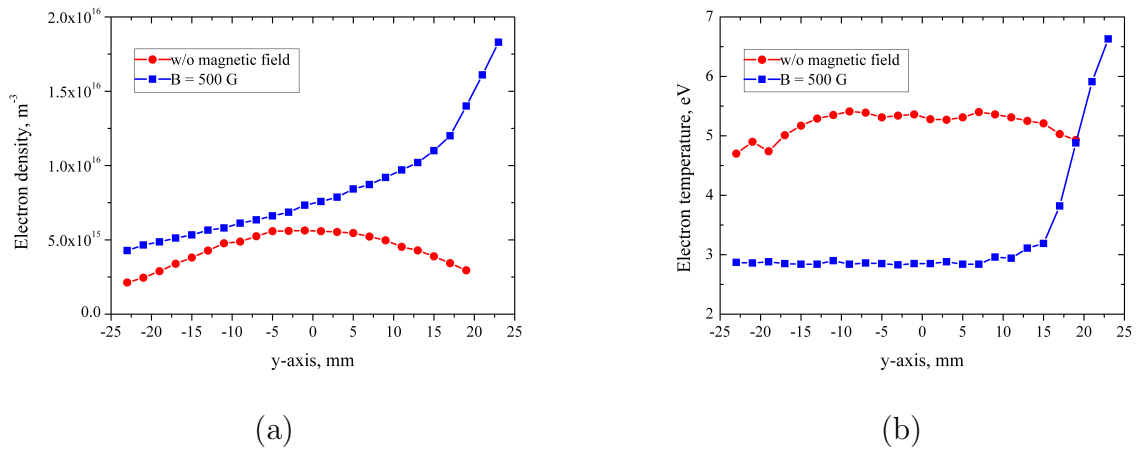
Figure 5.9: Graph (a) shows the distribution of the plasma density and (b) the electron temperature along the y-axis at the tube outlet with magnetic field and strip formation and without magnetic field (Argon, 150 W).

the magnetic field whilst having roughly the same electron density. This is the desired effect of the magnetic barrier.

The ion current was also measured inside and outside the strip with the RF discharge operated with argon. Two 8 mm planar probes were placed on either sides of the discharge tube in such a way one probe sees the strip while the other one sees the plasma bulk. In Fig. 5.10 an upward (in flow direction) strip is displayed. The results are displayed in Tab. 5.1. The ion current is larger by a factor of about 3 inside the strip. When reversing the direction of the magnetic field, the strip horizontally flips but the ion current inside the filament stays unchanged.
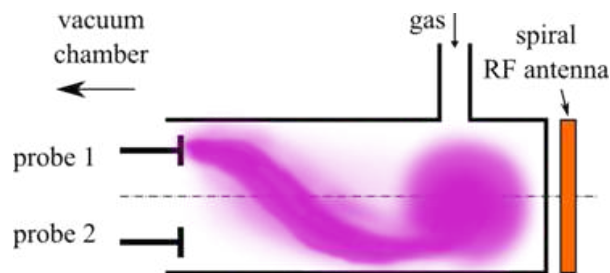
Figure 5.10: Setup of the measurements of the ion current in and outside the strip measured with two planar probes.

75

	Upward strip (A)	Downward strip (A)
Top probe	1.91×10^{-4}	8.48×10^{-5}
Bottom probe	7.7×10^{-5}	2×10^{-4}

Table 5.1: Ion current in and outside the strip measured with two planar probes for the two strip directions (Argon, 150 W).

5.3.2 Inductive Discharge

A way of reducing the capacitive coupling of the RF power is to place a grounded Faraday shield in between the coil and the plasma, see Fig. 5.4 [22]. The shield localizes the electrostatic field between the coil without disturbing the induced electromagnetic field that drives the plasma. Note that the plasma does no ignite itself anymore when the shield is used, a clear proof of a good inductive coupling as it is usually the capacitive part of the discharge that ignites the plasma. It is necessary to ignite the plasma without the Faraday shield. After the plasma is stable and matched the Faraday shield can be insert slowly as not to extinguish the plasma. While inserting the shield the impedance of the network changes and has to be accounted for in the matchbox. Special care has to be taken to avoid a short circuit between the coil and the grounded Faraday shield.

A capacitive probe was used to measure the RF potential fluctuations with and without the shield in an argon plasma with and without a 500 G magnetic field [22]. This measurement is displayed in Fig. 5.11. Inserting a shield has a great influence on the oscillation of the potential in the plasma. For instance at 4 cm downstream of the strongest magnetic field the peak-to-peak voltage amplitude drops from 190 V without, to 45 V with a shield in the case of the magnetic barrier. The lower fluctuation level indicates that in this case the power coupling has changed from a capacitive mode to an inductive mode. The graph also shows, that the magnetic field limits the fluctuation in the plasma potential. In both cases with the magnetic barrier the fluctuations are lower than in their corresponding counterpart without the magnetic field.

When placing the magnets around the discharge tube in capacitive mode, a strip was formed whatever the operating conditions. Figure 5.12 illustrates the difference observed by the naked eyes between a capacitive and an inductive discharge. With the Faraday shield in inductive mode the strong luminous strip disappears. The plasma is confined to the region close to the coil and can not be observed anymore behind the magnetic barrier.

Measurements have also been carried out with an emissive probe along the axis of the
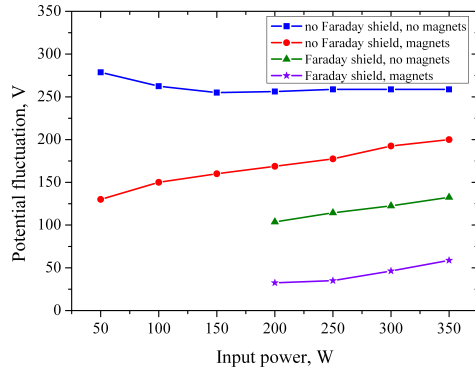
Figure 5.11: Measurements of the peak to peak potential fluctuation with the capacitive probe in a 20 sccm argon discharge at 410^{-3} mbar 4 cm downstream of the strongest magnetic field.
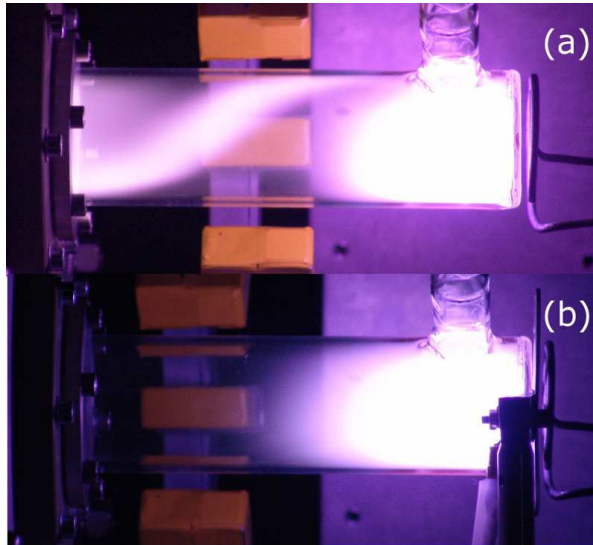
Figure 5.12: Picture of the RF plasma discharge with 20 sccm argon, 300 W input power, at a background pressure around 10^{-3} mbar and 500 G magnetic field (a) without and (b) with a Faraday shield. The magnetic field points towards the reader.

discharge tube for the four possible operating conditions, namely: with and without the magnetic field and with and without a Faraday screen. As previously mentioned, the emissive probe can give conclusive measurements of the plasma potential and the electron temperature within and across a magnetic field. Results of the measurements are presented in Fig. 5.13. The x-axis position 0 mm refers to the tube outlet where the tube ends into the vacuum chamber. The peak of the magnetic field distribution is located at 80 mm. The plasma potential development along the x-axis is displayed in Fig. 5.13 (a). The plasma potential is here assumed to correspond to the potential of the hot emitting probe [50]. The heating current was fixed to 4.3 A where the emission of electrons due to the heating in the probe is in balance with the electrons collected from the surrounding plasma.

The plasma potential is lower in inductive mode (with the Faraday shield). Without the magnetic field and the Faraday shield, the plasma potential decreases when moving away from the region wherein energy is deposited, i.e. the back section of the tube on the right side of the graph where the RF coil is located. With the magnetic barrier and the Faraday shield, the plasma potential is lower along the whole length of the tube and it seems not to undergo any significant change of the axial coordinate. The most interesting profile is however obtained in capacitive regime without the Faraday shield in the case of the strip. The plasma potential starts out low and then jumps suddenly when the probes goes throughout the strong magnetic field region, i.e. when the probe crosses the strip, see Fig. 5.1 and 5.4. When the probe moves outside the strip, the plasma potential drops but is still higher than the potential at the source. This might be due to the probe still being close to the strip even on axis.

The electron temperature T_e was also inferred from the emissive probe data. The electron temperature can be calculated from the hot and cold probe potential. In the later case the potential is the floating one. The electron temperature is then calculated using Eq. 3.2.

In Fig. 5.13 (b), the cooling of the electron fluid due to the magnetic barrier is visible for the two discharge regimes. The rapid increase in the electron temperature is a signature for the existence of the strip in capacitive mode. As previously explained, the strip is a region of large electron temperature. In the case of the strip (blue curve) the electron temperature is divided in three regions. The first region close to the source on the right side has an electron temperature of around $8 - 9$ eV. This is where the plasma is initially generated. The electron temperature is higher than in all the other cases as the
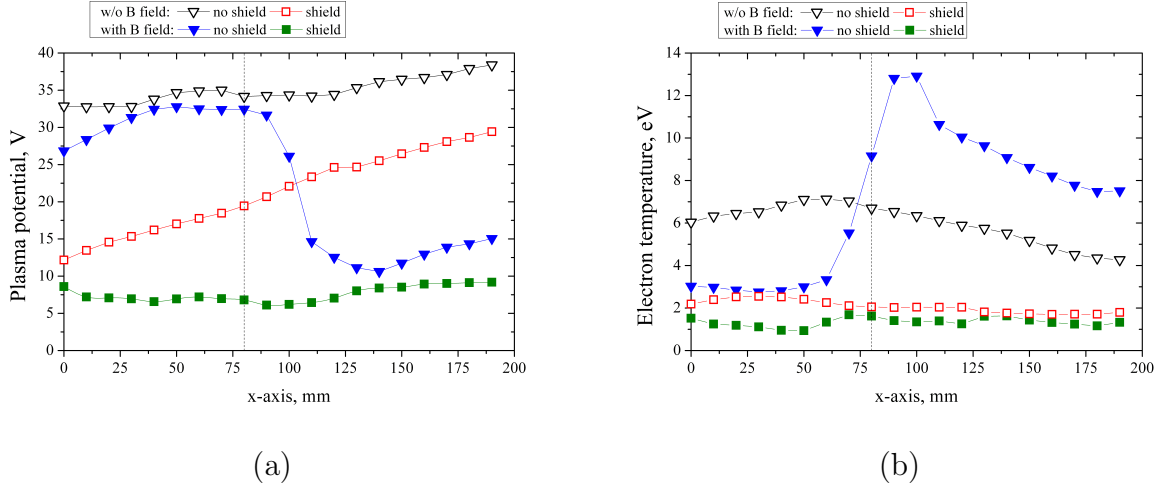
Figure 5.13: (a) Plasma potential and (b) electron temperature distribution along the discharge tube x-axis for 4 operating conditions. The position 0 mm refers to the tube exit. The dashed line indicates the magnetic field peak.

plasma is confined to that region. When the probe moves to the left and starts entering the strip the electron temperature increases. This strengthens the assumption that the strip consists of hot electrons. Moving out of that region the electron temperature drops below its original value. It seems that the electrons are effectively cooled down by the magnetic barrier. This was the original idea of the magnetic field. The rest of the measurements in Fig 5.13 (b) behave like expected. In the case of no magnetic field and no shield the discharge is dominated by a capacitive coupling as previously mentioned. This leads to an elevated temperature compared to the discharges where a Faraday shield is present and this component is eliminated. For the two cases with the Faraday shield the electron temperature starts out low at around 2 eV compared to the other cases. A slight difference can only be observed downstream of the magnetic field where the electron temperature seems to be lower in the case of the shield and the magnetic barrier. This is probably due to the cooling effect of the magnetic field.

5.4 Origin of the Strip

One way to understand the mechanism at the origin of the strip formation is to consider the equation of motion for the electron fluid in a magnetized plasma [51, p. 147]. For simplicity we do not take ions into account. Let us assume steady state so that the convective derivative terms can be removed. Besides, the pressure p_e is also assumed to
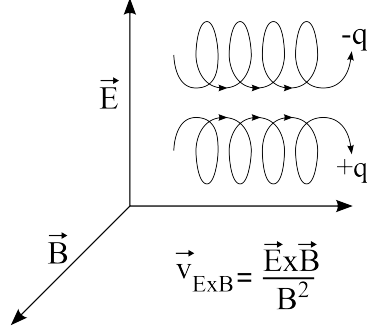
Figure 5.14: Visualization of the E×B drift.

be isotropic. The electron fluid equation of motion then reduces to:

$$en_e(\mathbf{E} + \mathbf{v}_e \times \mathbf{B}) + \nabla p_e = 0, \tag{5.2}$$

where e is the elementary charge. Taking the cross-product of Eq. 5.2 with $\mathbf{B}/B^2$ and rearranging the terms, one obtains an expression for the electron drift velocity across the magnetic field. The drift velocity can be divided into two components: the $\mathbf{E} \times \mathbf{B}$ drift $\mathbf{v}_{\mathbf{E} \times \mathbf{B}}$ and the diamagnetic drift $\mathbf{v}_{\text{dia}}$. They read:

$$\mathbf{v}_{\mathbf{E} \times \mathbf{B}} = \frac{\mathbf{E} \times \mathbf{B}}{B^2} \qquad \text{and} \qquad \mathbf{v}_{\text{dia}} = \frac{\nabla p_e \times \mathbf{B}}{en_e B^2}. \tag{5.3}$$

The electron drift current can then be written as:

$$\mathbf{j}_e = -en_e(\mathbf{v}_{\mathbf{E} \times \mathbf{B}} + \mathbf{v}_{\text{dia}}). \tag{5.4}$$

A reasonable approximation in the case of our magnetized RF discharge is to consider the three vectors $\mathbf{E}$, $\mathbf{B}$ and ∇p_e have only one component, namely: E_x, B_z and $\frac{\partial p_e}{\partial x}$ according to the coordinate system in Fig. 5.4. Therefore the electron current becomes:

$$j_{e,y} = en_e \frac{E_x}{B_z} + \frac{\frac{\partial p_e}{\partial x}}{B_z}. \tag{5.5}$$

This equation indicates the drift current is transverse to both the $\mathbf{E}$ and the $\mathbf{B}$ field. Figure 5.14 visualizes the E×B part of the drift motion. This is in agreement with the strip direction in Fig. 5.1 as well as in Fig. 5.12.

The direction of the drift can be visualized with the help of the right hand rule shown in Fig 5.15. Due to the plasma potential and the grounded chamber the electric field

points in the direction of the flow. The magnetic field shown in the picture points out of the plane. The $\mathbf{E} \times \mathbf{B}$ drift gives us an upward drift motion. Equation 5.4 states that the current direction for electrons is opposing the drift direction this results in the electrons being forced to the bottom of the tube. As the ions in this case are not fully magnetized, they can cross the magnetic barrier without experiencing a strong deflection and are driven by the pressure gradient due to the gas injection at the back. An ambipolar field of course exists to maintain the quasi neutrality of the whole plasma. As a consequence the ion density is stronger in the strip in agreement with the measurements presented in Fig. 5.9 and Tab. 5.1.

The strip therefore originates in the transverse drift of the electron fluid that is intercepted by the dielectric walls of the discharge tube. In other words the drift does not form a closed loop in this situation, contrary to what is realized in e.g. Hall thrusters [52]. This picture is supported by recent computer simulations carried out by Hagelaar and Oudini [53]. An interesting part of their works is the modeling and simulation of the low-pressure RF ITER negative ion source. With its magnetic filter, this source has a configuration similar to our inductive RF discharge. Numerical outcomes indicate the electron flux creates a strip-like structure in the high magnetic field region because the electron drift is confined by the chamber walls. Ion transport is included into the model. However, as ions are weakly magnetized in comparison with electrons, they do not contribute significantly to the formation of the strip.

The strip, with its typical S shape, therefore appears to be a general phenomenon that occurs in RF discharges with a transverse magnetic field for which the geometrical configuration does no permit the electron drift to close up. The strip is especially visible for a capacitively coupled RF discharge because of the existence of a strong electric field. In that case the appearance of the strip is mainly due to the electron $\mathbf{E} \times \mathbf{B}$ drift, wherein the electric field results from the capacitive coupling between the high-voltage part of the coil and the grounded walls of the vacuum chamber. In inductive mode, the electric field is linked to the ambipolar diffusion and pressure effects dominate [53].

5.5 Conclusion

In low-pressure discharges, the strip structure corresponds to an open drift of magnetized electrons that interacts with the reactor walls. In capacitive mode, the strip lights-up due to collisions between the hot electrons and the gas particles. Light is emitted when
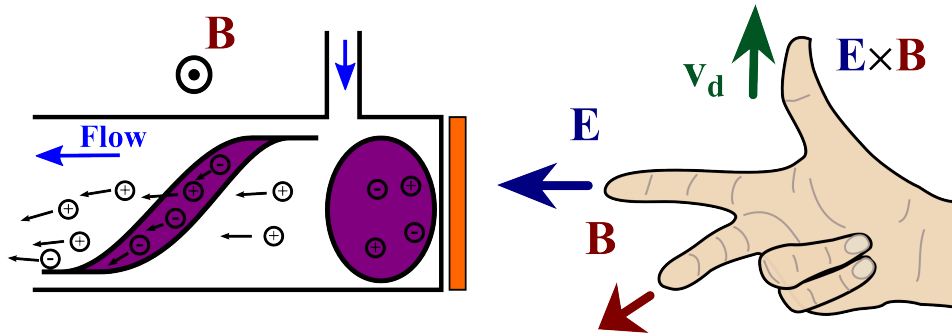
Figure 5.15: Visualization of the strip with E×B drift and the right hand rule.

atoms deexcite. Electrons are not hot enough in inductive mode to create a large amount of visible radiations. The origin of the hot electrons, however, remains an open question. They could be heated locally in the strip but the mechanism at work has to be identified. Or they are just hot electrons from the upstream region crossing the magnetic barrier. Although it is always present, the strip intensity depends upon the discharge features in terms of field strength and gradients. The strip is of course a path for electrons, as well as energy, to escape the magnetic barrier. Moreover, the interaction between the strip and walls creates losses. As a consequence, the strip not only leads to an inhomogeneous and asymmetrical plasma, which can affect ion extraction and acceleration processes, but it also reduces the efficiency of the source, e.g. in terms of negative ion yield, since the magnetic confinement becomes less efficient.

The strip in an inductively coupled plasma source is weak or non existent. Most likely the plasma is homogenous in the region where the ions are extracted and where the grids are placed in a thruster. The consequence for the PEGASES thruster is that the strip is only weak in certain conditions and can be avoided by carefully choosing the discharge conditions. The latest measurements performed in the PEGASES thruster with a magnetic field without grids in a xenon plasma have revealed an asymmetrical structure similar to the strip in a low density plasma under certain conditions. This however has to be further investigated.

6 PEGASES Thruster

6.1 PEGASES in Classical Mode with Xe

The PEGASES thruster is not only a source to create a strongly negative ion plasma or even an ion-ion plasma, it can also be used as a classical ion thruster. This means that a plasma is created and only the positive ions are extracted and accelerated making it necessary to neutralize the plasma behind the acceleration stage like in other ion thrusters. The performances of the PEGASES thruster have been investigated mainly in xenon in order to compare the obtained results with other ion thrusters.

6.1.1 Power transfer efficiency

The power transfer efficiency (PTE) shows how much of the power put into the system actually ends up in the plasma. It can be calculated as,

$$\eta = \frac{P_d}{P_{tr}},\tag{6.1}$$

where P_{tr} is the power provided by the power supply and P_d is the discharge power into the plasma. P_d can be calculated by measuring the power P_0 and the coil current I_{RMS0} of the coil-matchbox system when the plasma is turned off and then measuring these values when the plasma is ignited (P,I_{RMS}). Therefore P_d reads

$$P_d = P_{tr} - P_0 \frac{I_{RMS}^2}{I_{RMS0}^2}.\tag{6.2}$$

Figure 6.1 shows the PTE for Xenon for different thruster operating conditions. For higher flow rates the power deposition into the thruster is more efficient as the electron-neutral collision frequency becomes larger [54]. The PTE increases with the flow rate. For 150 sccm an PTE of 87 % can be reached. Most of the following experiments have
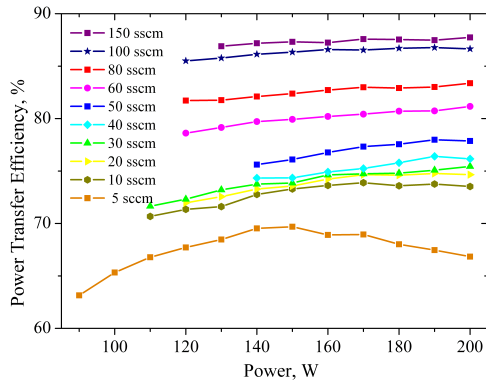
Figure 6.1: The power transfer efficiency for the PEGASES thruster in xenon.
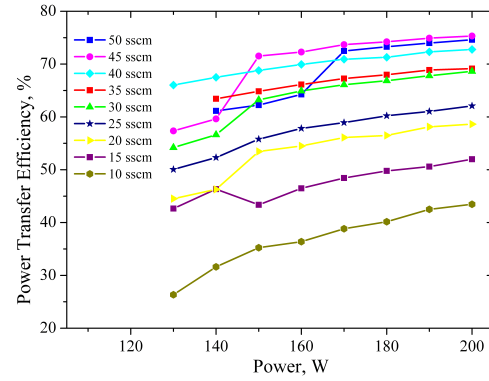
Figure 6.2: The power transfer efficiency for the PEGASES thruster in argon.

been done at lower flow rates of around 5 sccm where the PTE decreases to around 67 %. The PTE values for argon are displayed in Fig. 6.2 for comparisons. It can be seen that the efficiency is lower in argon due to the higher ionization energy of argon atoms. Argon has an ionization energy of 1520.6 kJ/mol compared to an ionization energy of 1170.4 kJ/mol for xenon. The matchbox and coil system is designed to be flexible in order to adapt to the changing parameters which occur in the starting phase of experiments. The efficiency can be improved by simplifying the matching network. This would reduce the resistance of this network by using fewer electrical components and shorten the wire length by packing the components closer together. This increases the efficiency of the thruster by reducing the loss in the matchbox.

Measurements of the fluctuation of the plasma potential show that the coupling of the PEGASES thruster is purely inductive due to a good coupling efficiency with the ferrite and a low RF frequency. Figure 6.3 shows a measurement performed with a capacitive probe in a 20 sccm xenon plasma, 180 W input power and 160 mm away from the ceramic window. The fluctuations at this point are around 2 V peak to peak and in the order of the electron temperature. This means an uncompensated Langmuir probe can be used.

6.1.2 Plasma Parameters in the Cavity

The plasma has been characterized inside the open cavity(no grids) with the help of a Langmuir probe. The measurements have been performed on a linear displacement stage
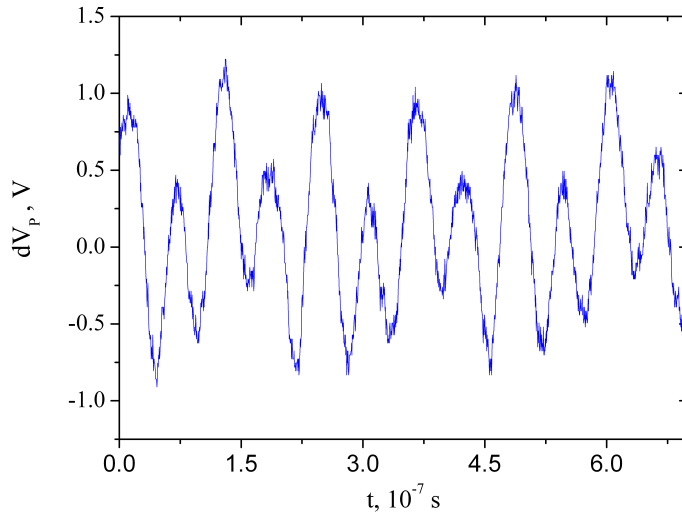
Figure 6.3: Fluctuation of the plasma potential measured in the open cavity of the PE-
GASES thruster with a capacitive probe in a 20 sccm xenon plasma, 180 W
input power and 160 mm away from the ceramic window.

which allows a displacement of the probe along the x-axis of the thruster. The position
x=0 mm is the plane where the grids are usually mounted and the position x=119 mm
is where the ceramic window separates the coil from the plasma. Figure 6.4 shows the
results of these measurements for different conditions. It can be seen that the plasma
potential as well as the electron density reaches its peak around 15 mm away from the
ceramic window and then loses in strength. This is due to the collision less skin depth
which can be calculated with,

$$\delta = \sqrt{\frac{m_e}{e^2 \mu_0 n_e}},$$ (6.3)

and is around 10 mm in our case. The energy is deposited within this region around the
antenna. Together with the energy loss to the wall this results in the highest electron
density and plasma potential at around 15 mm distance to the ceramic window. The
plasma potential and the electron temperature are lower for the higher flow rates as
more energy is lost to the walls due to a larger diffusion rate. The electron density on
the other hand increases with the flow rate. The input power has no strong influence
on the plasma potential and the electron temperature. The electron density increases
slightly with the input power. Part (c) of Fig. 6.4 shows a plot of $\ln(n_e)$ over V_p/T_e for

85

the obtained values. The linearity in the measurements shows that the plasma follows the Boltzmann law,

$$n_e = n_{e,0} exp \left(-\frac{eV_p}{kT_e} \right). \tag{6.4}$$

That means there is a balance between the electron pressure and the internal electric field [43].

Figure 6.5 shows the plasma potential and the electron temperature measured 2 mm upstream of the screen grids in a closed cavity with the grid assembly. The plasma potential and the electron temperature are decreasing with an increasing flow rate. This is to be expected since a higher flow rate means automatically a higher pressure in the cavity. This increases the diffusion to the walls for ions and electrons and also decreases the mean free path. This results in more losses. Measurements of the ion flux were performed with a planar probe rather than with a Langmuir probe. The advantages of a planar probe over a Langmuir probe are described in Ch. 3.1. In this measurement a 15 mm in diameter graphite planar probe equipped with a guard ring has been used. The probe was biased to -50 V. The measurements have been performed without a bias and the grid was grounded instead. The probe has been inserted through a hole cut into a grid and is roughly 2 mm upstream of the screen grid. This has been done to simulate similar pressure conditions as in experiments with a set of biased grids. The results are shown in Fig. 6.6. The ion current increases with a higher flow rates as the PTE does. The ion current in front of the extraction grid increases with the pressure inside the discharge chamber. It can be seen that the influence of the flow rate is not as strong as one would expect when looking at the PTE presented in Fig. 6.1. One factor is the increased loss of energy as a result of the increased pressure in this cases. The input power has also a strong influence on the ion flux. As expected, the ion flux increases as more RF power is deposited in the discharge chamber.

An ion mass flow rate can easily be calculated for the measured current density. In the calculation we assume an homogeneous acceleration profile with an rectangular shape and singly charged ions only. This is a first order approximation, which gives an upper limit for the ion mass flow rate. The latter is given by,

$$\dot{m}_i = \frac{jSM_{Xe}}{e}, \tag{6.5}$$

where S is the acceleration area based on the cavity size after inserting the ceramic
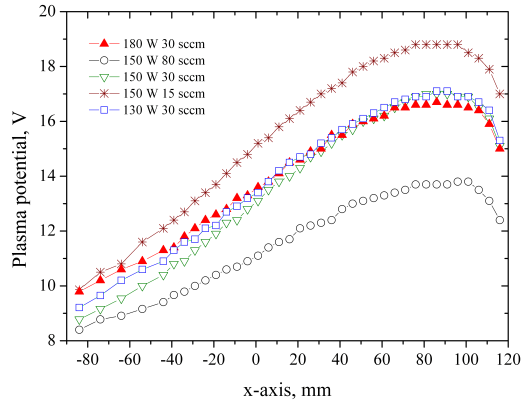
(a)
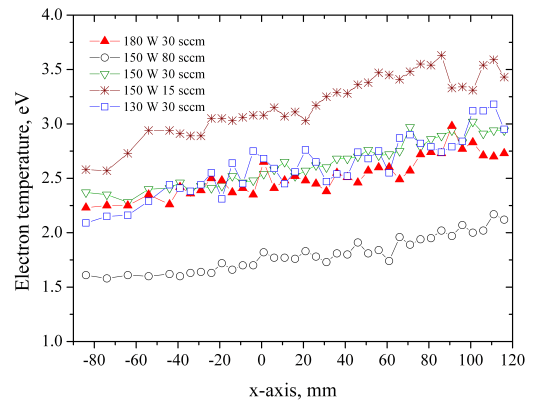
(b)
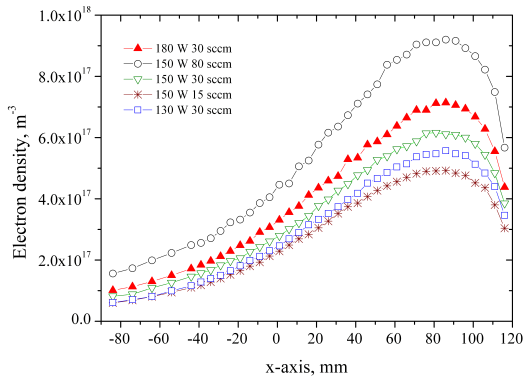
(c)
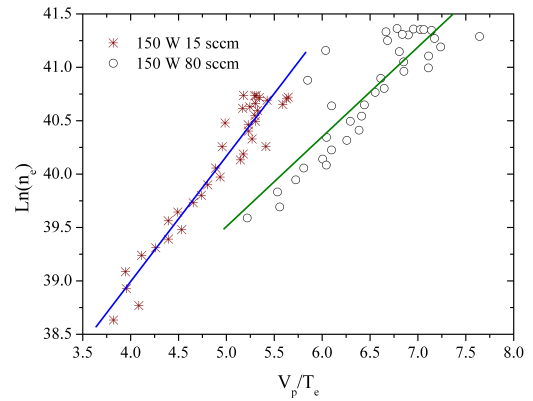
(d)

Figure 6.4: Plasma parameters in the open cavity of the PEGASES thruster in xenon: (a) the plasma potentiel, (b) the electron temperature, (c) the electron density and (d) the Boltzmann relation.
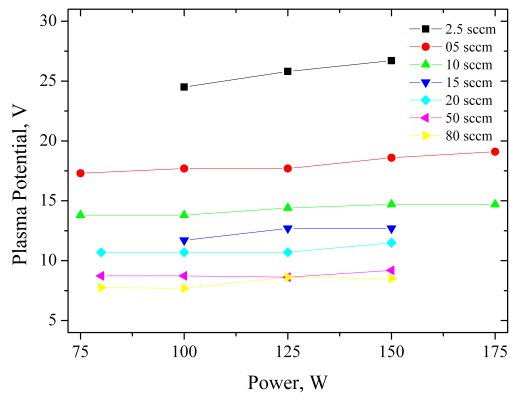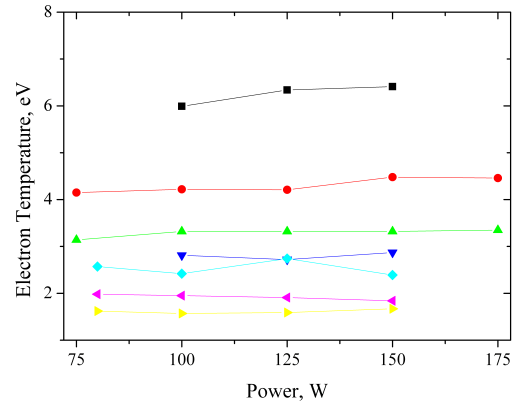
Figure 6.5: Plasma potential and electron temperature in the PEGASES thruster for a xenon discharge 2 mm upstream of the screen grids measured with a Langmuir probe.

isolator ($5.8\,\mathrm{cm} \times 10.4\,\mathrm{cm} = 60.32\,\mathrm{cm}^2$).

The neutral mass flow rate is given by the flow controller. It can be converted from sccm to mg/s for xenon with,

$$1 sccm(Xe) = 0.0983009 \left[\frac{mg}{s} \right]. \tag{6.6}$$

The mass utilization is defined as,

$$\eta_{Mass} = \frac{\dot{m}_i}{\dot{m}}, \tag{6.7}$$

and shows the fraction of the injected gas that is ionized.

Figure 6.7 shows the mass utilization for different flow rates and power. At lower flow rates the plasma is highly ionized and the ionization increases with the power as expected. For higher flow rates only a fraction of the atoms get ionized. This leads to a decrease in the mass utilization rate. It can be seen that the mass utilization rate also depends on the RF power deposited into the plasma. The highest mass utilization rate has been observed for a flow rate of 5 sccm xenon and an input power of 150 W. In this case the mass utilization is around 90 % and gets close to the mass utilization in other RF thrusters like the RIT-15 [55] and the RIT XT [6] which reach a mass utilization
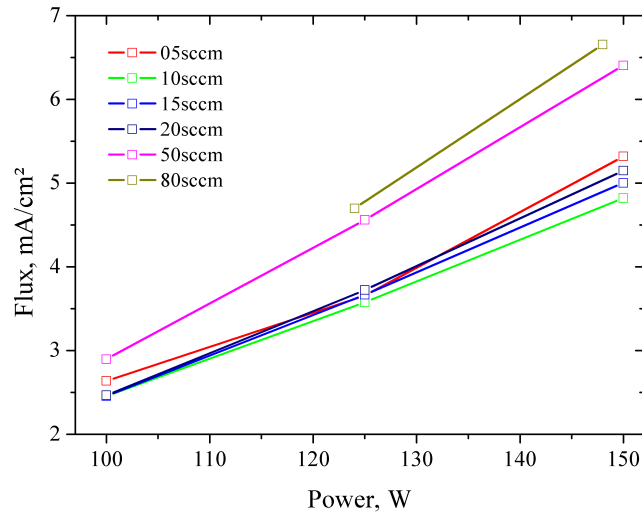
Figure 6.6: Ion current density measured with a planar probe with a guard ring at the position of the grids.

rate of up to 96 % in certain conditions.

The trend of the mass utilization and the PTE correspond with the findings in the article of Chabert [54] where he creates a global model of a gridded ion thruster powered by RF. This model predicts a rapid decrease of the mass utilization rate with the gas flow rate. This corresponds with the measurements presented in Fig. 6.7. The model also predicts that the PTE increases significantly with the gas flow rate. This confirms the measurements displayed in Fig. 6.1. This means a trade-off between a high mass utilization and a high PTE has to be found.

6.1.3 Acceleration in Xe

Figure 6.8 shows a schematic drawing of the PEGASES thruster working in xenon. The propellant gas is injected from the side of the thruster and gets ionized by the inductive current induced by the electric field generated by the RF current flowing through the coil. The first grid in flow direction, the screen grid, is biased and lifts the plasma to a high potential. This is possible because the cavity is isolated by walls made of BN-SiO$_2$ and is therefore floating. The acceleration grid is grounded. The positive ions are accelerated due to the electric field between the screen and the acceleration grid. In order to neutralize the ions and keep the plasma in quasi neutrality, a hot wire
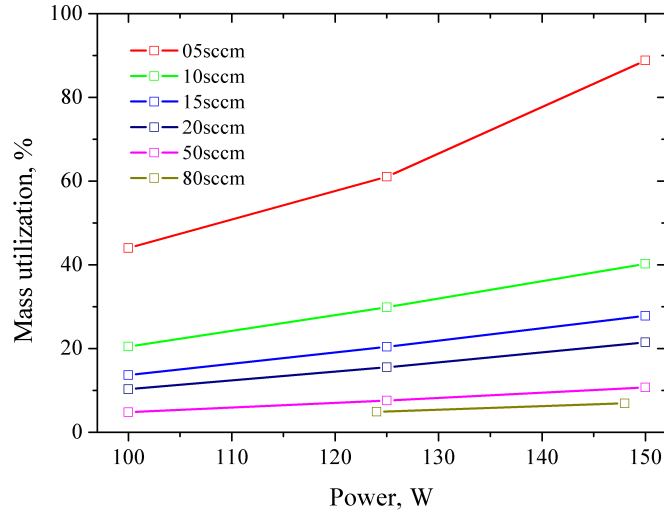
Figure 6.7: Mass utilization of the PEGASES thruster in xenon for different flow rates and power.

neutralizer located behind the acceleration grid provides the necessary electrons. The hot wire neutralizer consists of a 20 cm long tungsten wire with a diameter of 0.38 mm. The wire is placed in the beam and heated with a current of 11 A until the wire glows red an emits electrons.

A measurement of the plasma potential with a Langmuir probe inside the cavity for a varying screen grid bias is shown in Fig. 6.9. The measurement has been performed in a 5 sccm xenon plasma at 150 W. The trace shows that the plasma potential follows the grid potential and is elevated by the value of the plasma potential measured at 0 V bias. The plasma potential can be calculated with,

$$V_p = V_b + \eta \frac{kT_e}{e}, \tag{6.8}$$

where η is 5.8 for xenon. The green line in the graph represents the potential calculated for an electron temperature of 3 eV.

Figure 6.10 demonstrates that a neutralizer is necessary in order to achieve acceleration. The measurement has been performed in a 5 sccm xenon plasma with a power input of 100 W. The background pressure was $9 \cdot 10^{-4}$ mbar in nitrogen. Part (a) of the figure shows the ion flux measured with a 55 mm in diamenter planar probe 100 mm downstream of the grids. Part (b) of the figure shows the plasma potential measured
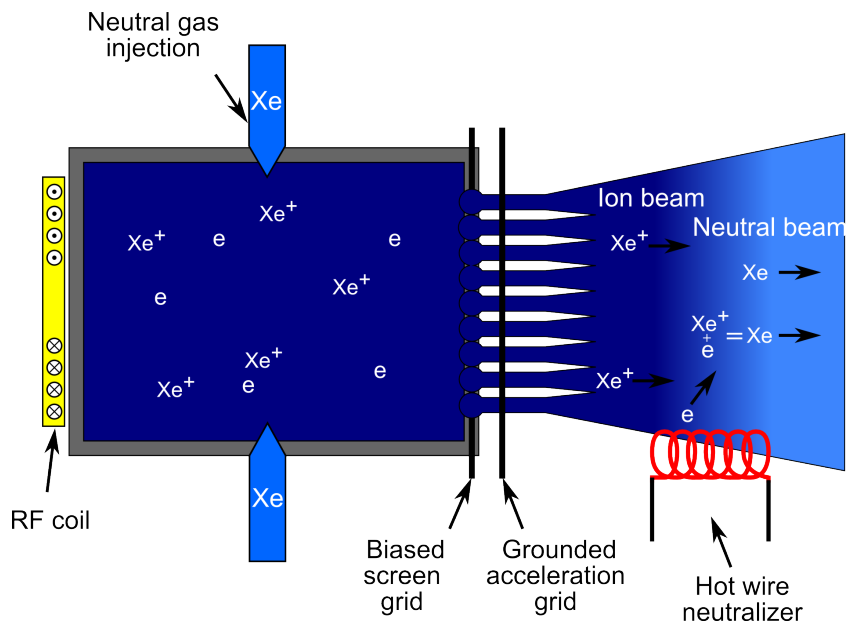
Figure 6.8: Sketch of the PEGASES thruster functioning in xenon.
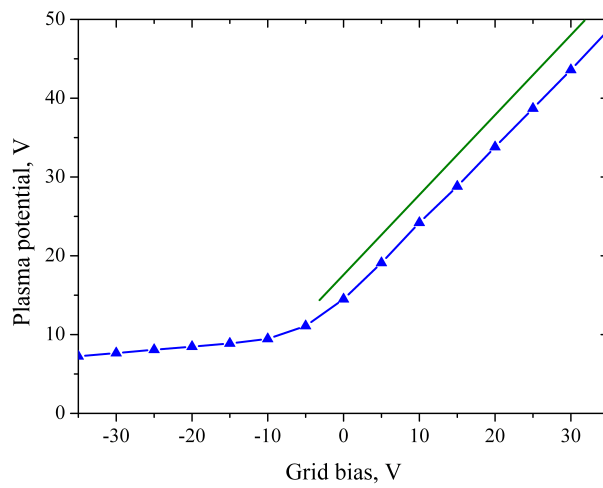
Figure 6.9: Measurement of the plasma potential inside the cavity over the screen grid bias in 5 sccm xenon (green line for Te=3 eV).

with a Langmuir probe at the same position. It can be observed that for both cases, with and without neutralizer at low voltage up to around 30 V, the plasma leaks through the grids. The ion flux decreases as the bias of the screen grid is increased. At around 25 V the current measured in the case with the neutralizer starts to increase again. The plasma potential stays roughly the same for this condition which lead to the conclusion that part of the plasma is accelerated. The measured ion flux is dependent on the ion velocity and the ion density. It seems that the obtained curve follows the square root of two for a constant ion density until a grid bias of $200 - 250\,\mathrm{V}$. Above that value the measured ion flux seems to follow the Child-Langmuir law (green curve), given by Eq. 2.7.

The ion flux stays well bellow the maximum limit given by the Child-Langmuir law which would be, as an example, $2.47\,\mathrm{mA/cm^2}$ for a grid bias of 300 V at the grid spacing of 1 mm. This indicates that all of the plasma is blocked by the grids at this bias potential and ions are accelerated through the grids. In the case without the neutralizer, the ion flux measured with the probe decreases beyond the screen grid bias of 25 V and reaches its minimum at around 50 V. Then the current starts to increase again but not with the same slope as the curve with the neutralizer. At the same time the plasma potential measured behind the grids follows the potential of the screen grid. This indicates that the plasma just leaks through the grids and is not accelerated. This leads to the conclusion that the neutralizer is necessary to ensure the quasi neutrality of the plasma which, if not given, prevents the acceleration of the plasma. This is due to the fact that unneutralized ions create an electric field which is opposed to the electric field in the grids and are decelerated. In a vacuum chamber the ions can get neutralized at the chamber walls but in space they would be accelerated back to the increasingly negatively charged space craft [56].

Figure 6.11 shows the ion flux measured with a 55 mm in diameter planar probe and the plasma potential measured with a Langmuir probe 100 mm downstream of the grids with the neutralizing filament for various gas flow rates. The input power for all measurements has been kept at 100 W. The screen grid bias has been ramped from 0 V to 300 V for several flow rates. The background pressure varied with the flow rate from $3 \cdot 10^{-4}$ mbar to $2 \cdot 10^{-3}$ mbar in nitrogen. It can be seen that the measured ion flux and the plasma potential follow the same trend as described for Fig. 6.10 and are in accordance with the Child-Langmuir law. The figure also shows that the ion flux measured by the probe is higher in the case of the lower flow rates. At first glance this seems to contradict the outcome of the measurements presented in Fig. 6.6 where the ion flux inside the
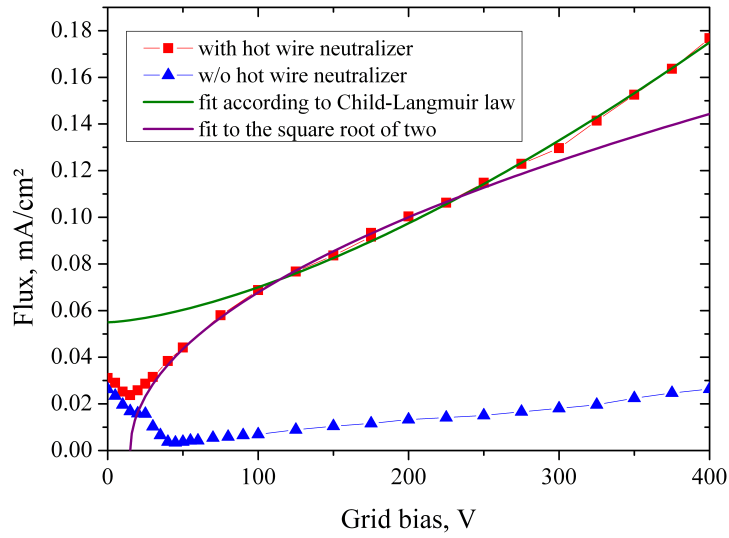
(a)
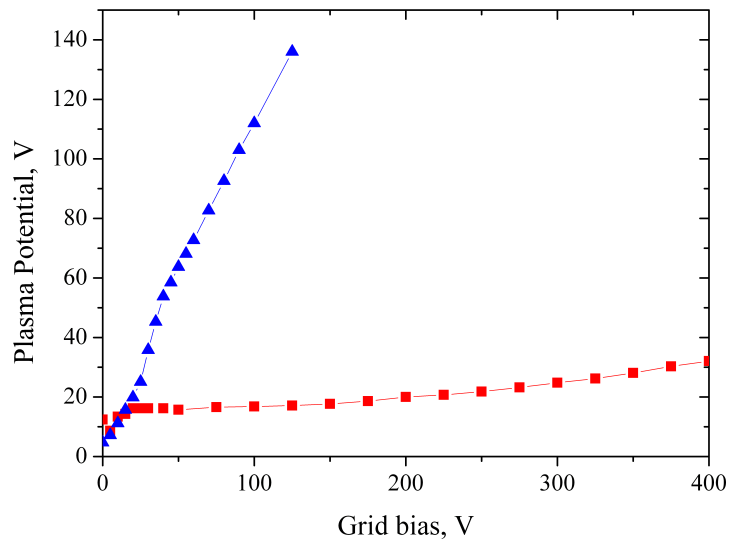
(b)

Figure 6.10: Comparison of the (a) flux measured with a planar probe and (b) the plasma potential measured with a Langmuir probe between operation with a hot wire neutralizer and without. Measured in xenon at a 5 sccm flow rate and 100 W input power in the beam 100 mm downstream of the grids.
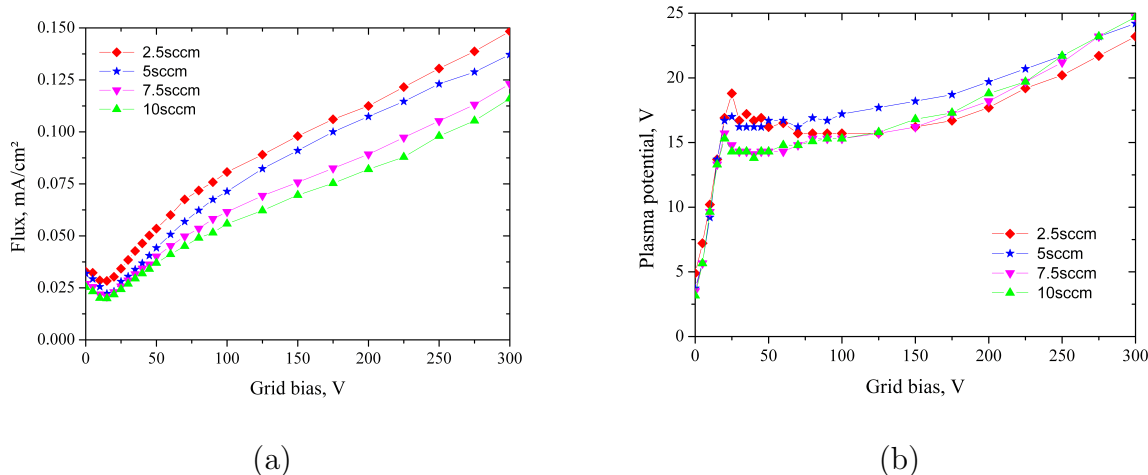
Figure 6.11: The (a) flux measured with a planar probe and (b) the plasma potential measured with a Langmuir probe for different flow rates at 100 W input power. Measured in the beam 100 mm downstream of the grids.

discharge chamber, in front of the grids, increases with a higher flow rate. One would expect a more efficient acceleration for these cases. A possible explanation is a grid design problem as the grid geometry is not optimized. Another explanation is charge exchange collisions of the fast ions with slow neutral atoms. At 100 V the cross section of Xe^+ ions is $6 \cdot 10^{-19}$ m^2 with the resulting mean free path of 14 cm for a pressure of $5 \cdot 10^{-4}$ mbar. This is a conservative estimate and the mean free path is probably even smaller. The charge exchange collisions reduce the measured ion flux.

To investigate the influence of the distance on the ion flux, a 55 mm in diamenter planar probe has been mounted in the plume of a 5 sccm xenon plasma with a discharge power of 100 W and a screen grid bias of 300 V. The pressure in the chamber was $3 \cdot 10^{-4}$ mbar in nitrogen in this experiment. The results of this measurement are presented in Fig. 6.12. The position $x = 0$ mm corresponds to the exit of the acceleration grid. It can be seen that the measured ion flux decreases with the distance from the grid. The decrease in the signal appears to be linear. If the loss of signal strength is connected to the divergence of the plasma beam the measurement should decay with $1/x^2$ if started from a point source. This reinforces the assumption that the observed effect is not only due to the beam divergence. For instance charge exchange collisions in the plume might play a role. As the collection area of the probe is roughly a third of the grid area a strong averaging

94
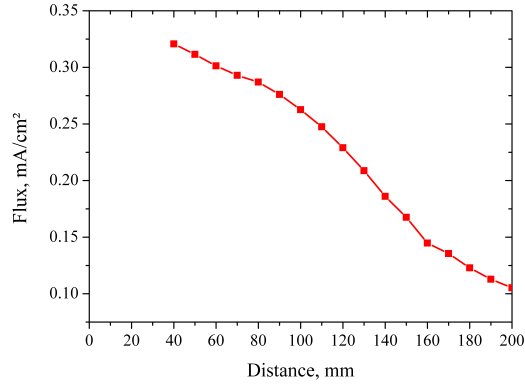
Figure 6.12: Measurement with a 55 mm planar probe in the plume of a 5 sccm xenon plasma with a discharge power of 100 W along the x-axis and a screen grid bias of 300 V.

effect occurs.

6.1.4 Current Balance

In order to understand the stream movement of electrons and ions inside the PEGASES thruster and in the plume it is important to look at the current balance of the system. Table 6.1 shows the current balance for the PEGASES thruster in a 5 sccm xenon discharge at an input power of 100 W for two different acceleration biases at the screen grid. The screen grid elevates the plasma to a high potential and collects electrons. Ions which pass through the screen grid are accelerated between the screen grid and the acceleration grid, which is usually grounded. A small amount of ions is accelerated onto the acceleration grid due to imperfect ion optics. The electron current emitted by the filament is higher than the current collected by the first grid. This is due to losses to the wall of our chamber. The charge conservation demands that:

$$\sum I_x = I_S + I_A + I_F + I_W = 0, \tag{6.9}$$

where I_S is the current of the screen grid, I_A is the current of the acceleration grid, I_F is the current of the neutralizing filament and I_W is the charge lost to the wall.

For an acceleration bias of 300 V, a grid gap of 1 mm, xenon as a propellant and a grid size of 60 cm^2(with the cavity) the Child-Langmuir limit calculates to 144 mA.

Accel. bias V_b	Screen grid I_S	Accel. grid I_A	Neutr. filament I_F
200V	-181 mA	9 mA	286 mA
300V	-212 mA	8 mA	315 mA

Table 6.1: Current balance for a 5 sccm xenon discharge at 100 W input power.

The electron current collected by the screen grid should in theory be the same as the ion current accelerated through the grids as the discharge cavity of the thruster is electrically insulated, floating and the plasma needs to be quasi neutral. The 212 mA given in Tab. 6.1 for the screen grid current is above the maximum theoretical value of 144 mA. This implies that electrons are arriving from somewhere else and add to the measured electron current on the screen grid. A possible source for the electrons is the neutralizing filament. To prove this assumption an experiment has been performed where the screen grid bias is fixed at 300 V and the acceleration grid is biased and ramped from 0 V to -100 V in order to block the electrons from reaching the screen grid. The schematic of this experiment is sketched in Fig. 6.13. The neutralizing filament is biased at -35 V to increase the extraction of the electrons. With the bias of -18 V, which is used to heath the filament, the electrons can have a potential of -35 V to -53 V. The currents measured at the different locations are presented in Fig. 6.14. The currents of the filament and the acceleration grid stay roughly the same over the whole bias range even though the effective acceleration bias increases from 300 V to 400 V. The electron current collected by the screen grid however decreases strongly while the bias gets more negative and saturates at around -50 mA. The electrons coming from the filament get deflected by the acceleration grid and can not reach the screen grid anymore. The remaining current on the screen grid seems to be the electron current collected by the screen grid from the side of the plasma source and should therefore correspond to the ion current accelerated between the grids. It is well below the theoretical limit given by the Child-Langmuir law. The current collected by the acceleration grid seems to be a pure ion current which is generated by an unfocused beam. This means the current which is accelerated and passes both grids is in this case the electron current measured at the screen grid plus the ion current measured at the acceleration grid and calculates to around 20 mA in this case. This shows that the ion optics used in the experiment are far from optimized.

An ion flux of 0.137 mA/cm^2 has been measured at 100 mm distance for a flow rate of 5 sccm and 300 V, presented in Fig. 6.11. Taking this flux and multiplying it by the grid size of 60.9 cm^2 one obtains a current of 8.3 mA. The current is a factor of 2.4 lower than
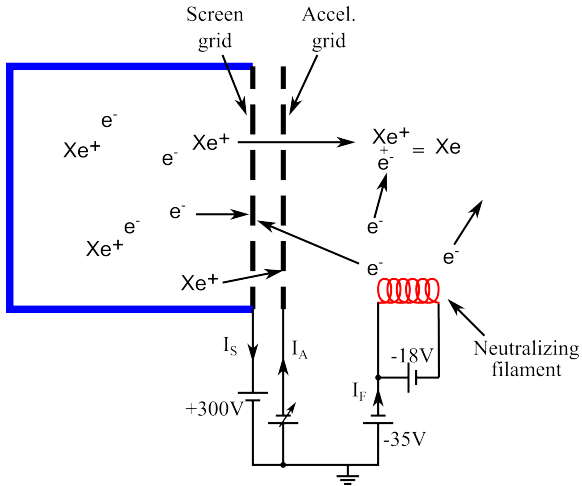
Figure 6.13: Schematic drawing of the experiment to determine the electron current flowing from the neutralizing filament to the screen grid.
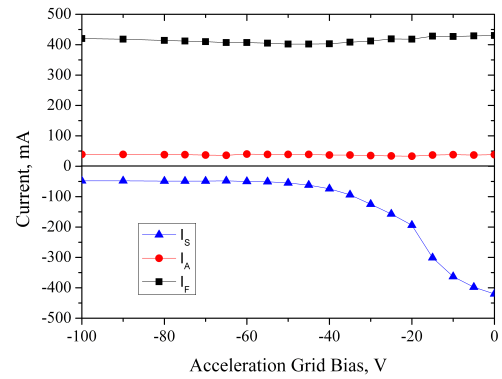
Figure 6.14: The currents measured the screen and acceleration grid as well as the electron current emitted by the filament for different acceleration grid biases.

the one measured at the grids which might be explained with a loss due to divergence of the beam and charge exchange collisions.

The results of the experiment lead to the conclusion that a negative acceleration grid bias should be used to block the electrons from crossing the acceleration grid and getting collected from the screen grid. Alternatively a third slightly positive biased grid can be used. This permits to bias the screen grid strongly positive and the acceleration grid negative (which in this case blocks the electrons). The large bias difference increases the maximum extractable current imposed by the Child-Langmuir law. The last grid is then used to decelerate the ions again and recuperate energy from them. The positive bias of the last grid also avoids erosion through ion bombardment of the grids as previously mentioned in Ch. 2.3.3.

6.1.5 E×B Probe Velocity Measurements

Measurements with an E×B probe have been performed to obtain the velocity distribution function (VDF) of the ions in the plume of the PEGASES thruster. Figure 6.15 shows an E×B measurement in a 5 sccm, 100 W xenon discharge with an applied acceleration grid bias of 288 V. The dotted lines represent the expected velocities of the

97

ion species which can be calculated with Eq. 2.6. Measurements show that the ions are usually faster than the calculated speed. One possible source for the discrepancy is the plasma potential. The ions get accelerated between the plasma and the screen grid in the discharge chamber as the plasma is at a higher potential than the screen grid. Measurements with a Langmuir probe presented in Fig. 6.5 show a plasma potential of roughly 20 V for the discharge conditions shown in Fig. 6.15. Therefore the calculation of the expected velocities have been done with 308 V. The remaining observed discrepancies in velocities are most probable due to calibration errors with the E×B probe as discussed in Ch. 4.5.3. Figure 6.15 shows peaks for Xe^+, Xe^{2+} and Xe^{3+} as expected. The Xe^{2+} ions account for 0.51 % and the Xe^{3+} for 0.17 % of the xenon ions measured. The numbers have been obtained by integrating the area under the peaks and set them into relation with the main peak. This is low compared to 11 % for Xe^{2+} and 1 % for Xe^{3+} obtained in a Hall thruster at a discharge voltage of 300 V [34]. Furthermore peaks which are most likely O_2^+ and N_2^+ can be observed. This is probably due to a small leak in the thruster or the gas feed line where air can enter into the discharge chamber. Due to observations of the pressure it can be estimated that the leak is a fracture of a sccm and will not change the measurements drastically. The expected velocities for H_2O^+, O^+, O_2^{2+} and N^+ have been marked in Fig. 6.15. Peaks in the measurements can be observed which might correspond to these ions but the noise level is to high to make certain claims. With a higher averaging and an improved signal strength these species could probably be identified.

Measurements with the E×B probe have been performed over a wide range of parameters. Figure 6.16 shows the VDF for (a) 2.5 sccm and (b) 5 sccm for different acceleration grid biases at a input power of 100 W. The pressure inside the vacuum chamber was $3 \cdot 10^{-4}$ mbar in the case of the 2.5 sccm flow rate and $7 \cdot 10^{-4}$ mbar for the 5 sccm flow rate (pressure measured in nitrogen). As previously mentioned the measured velocities are usually a bit higher than the calculated velocities. The dotted lines are based on the screen grid bias in the following figures. The velocities follow the bias as expected and the signal strength increases with the bias. The lower limit of the measurements has been given by a low signal strength for grid biases of less than 136 V. The signal for the low biases of 136 V and 186 V show a strong discrepancy with the expected velocity and a peak before the main Xe$^+$ peak which can not be explained at the moment. The signal strength for the biases of 235 V, 284 V and 333 V seem to be where a full acceleration of the ions is achieved and the signals resemble each other. The upper limit has been given by arcing between the grids. The arcing depends on different factors such as the
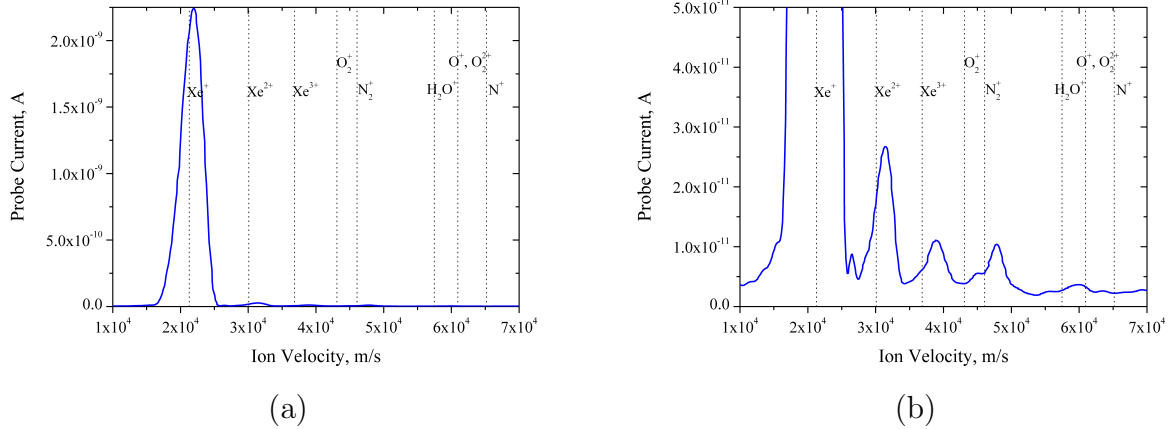
Figure 6.15: Measurement with the E×B probe at 288 V acceleration grid bias in a 5 sccm xenon discharge at 100 W. The whole VDF is shown in (a) and (b) shows the same measurement where the first peak is cut of to better visualize the succeeding peaks.

pressure in the chamber and is favored by deposition of conducting metals on the grid separator.

Figure 6.17 shows the VDF for several input powers for two grid biases, (a) 186 V and (b) 284 V at a pressure of $7 \cdot 10^{-4}$ mbar at a 5 sccm flow rate. The grid bias of 186 V reveals again a peak before the main Xe^+ peak. The measurements show for both acceleration voltages that the signal is lower for the 80 W power input. For the powers exceeding 100 W no clear difference is observable. In theory the measured ion current should increase with the power as the ion flux inside the cavity increases, see Fig. 6.6. This effect might lie hidden within the error margin of the probe as the variation in the signal is only around 15 % for the input powers above 100 W.

In order to investigate the influence of the pressure on the acceleration of the ions the E×B probe has been placed in the plume of the PEGASES thruster and the flow rate has been varied between 2.5 sccm and 10 sccm with the pressure ranging from $3 \cdot 10^{-4}$ mbar and $1.5 \cdot 10^{-3}$ mbar. Figure 6.18 shows the VDF for a grid bias of (a) 186 V and (b) 284 V and an input power of 100 W. It can be seen that the signal strength increases with decreasing flow rates. The flux in these regions (shown in Fig 6.6) is roughly constant for the presented flow rates. This leads to the assumption that decrease of the signal is due to an increased pressure downstream of the grids in the plume of the thruster. This points to charge exchange collisions as an origin. An increase in the velocity has been observed for the lower flow rates. This is in accordance with the measurements of the
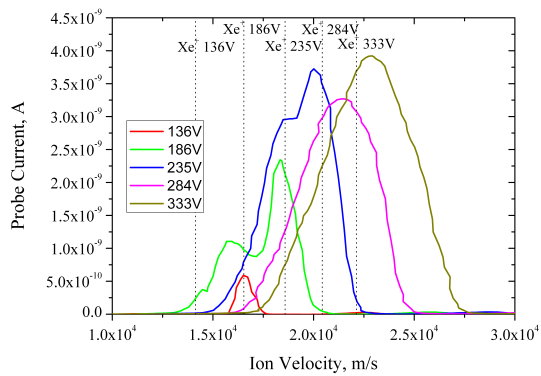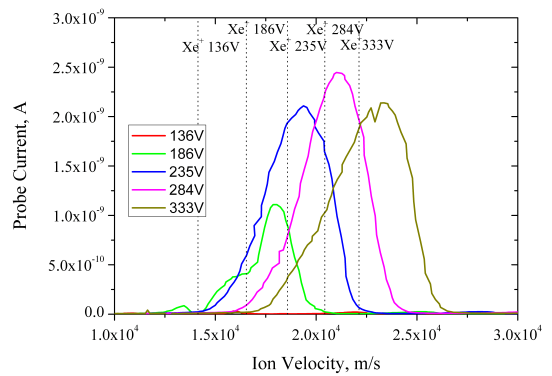
(a)   (b)

Figure 6.16: Velocity profile measured with an E×B probe for different acceleration bias on the grid. The profiles were measured at 100 W input power and (a) 2.5 sccm and (b) 5 sccm flow rate
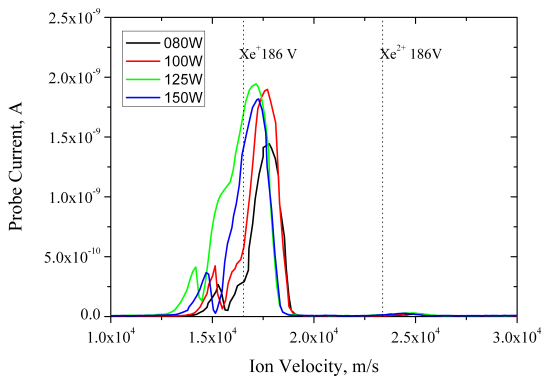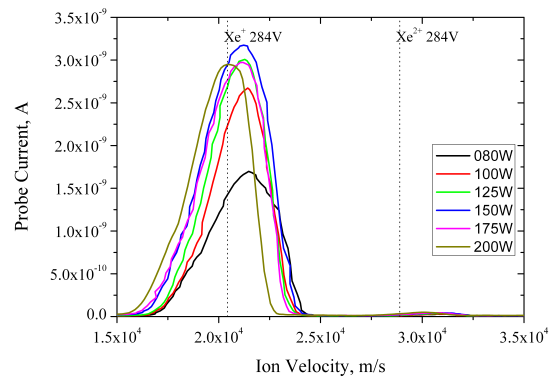
(a)   (b)

Figure 6.17: Velocity profile measured with an E×B probe for several input power. The profiles were measured at a flow rate of 5 sccm and (a) 186 V and (b) 284 V grid bias
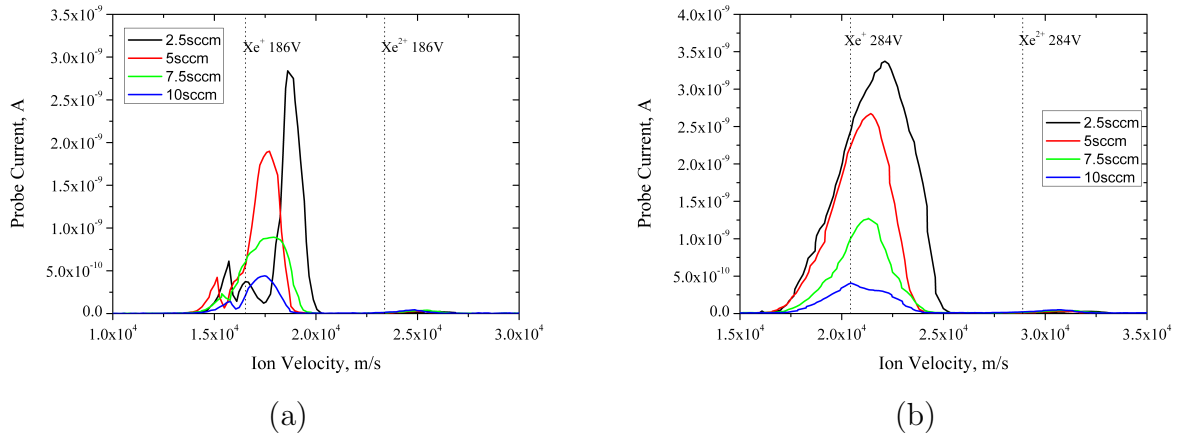
Figure 6.18: Velocity profile measured with an E×B probe for several flow rates. The profiles were measured at 100 W input power and (a) 186 V and (b) 284 V grid bias

plasma potential in Fig. 6.5 which are higher for lower flows and the assumption that the ions are already accelerated in the sheath before the first grid.

The E×B has been mounted on a rotary platform to investigate the angular dependency of the ions in the thruster plume. The rotation axis was orthogonal to the xy plane. As the rotary platform could not be operated from outside the chamber the vacuum chamber had to be pressurized between the different angular measurements. The center of the E×B probe was mounted 305 mm away from the acceleration grids as in the previously presented experiments. Rotation around this point leads to the E×B probe pointing at different points on the grid. Figure 6.19 illustrates the experimental setup.

The results of this experiment are presented in Fig. 6.20. The measurements have been
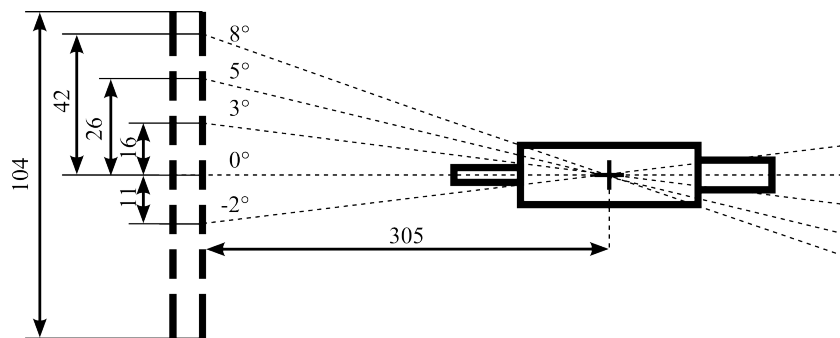
Figure 6.19: Schematic drawing of the angular measurements performed with the E×B probe.
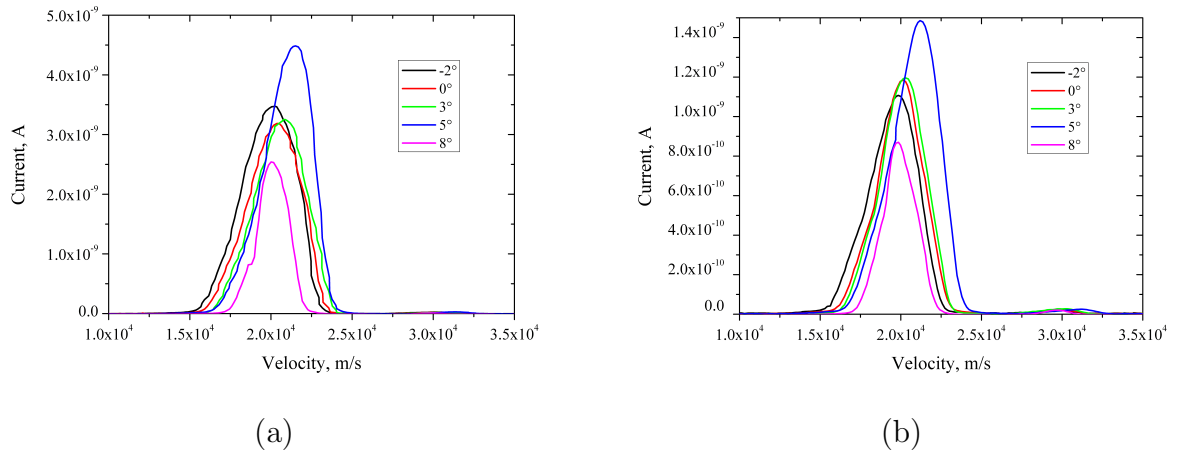
Figure 6.20: Velocity profile measured with an E×B probe for several angles. The profiles were measured at 100 W input power and 260 V grid bias with flow rates of (a) 2.5 sccm and (b) 5 sccm.

performed with 100 W input power and 260 V screen grid bias for flow rates of 2.5 sccm with a pressure of $3 \cdot 10^{-4}$ mbar and a 5 sccm flow rate with a pressure of $8 \cdot 10^{-4}$ mbar. The measurements show no strong dependence of the angle on the signal strength or the velocity. The measurements of 5° degree show a slightly higher velocity and a higher signal and the measurements with the 8° angle show a reduced signal strength. The small observed variations follow no trend and might be due to the fact that the measurements had to be spread out over several days and the same plasma conditions are hard to reproduce. The results of the measurements lead to the assumption that the probed section of the grid can be considered a uniform source with an divergence angle of at least 8°.

In order to evaluate the behavior of the PEGASES thruster and the E×B probe in different conditions experiments in argon have been performed. The ionization energy of argon is higher than the one for xenon. Stable discharge conditions where only possible for an input power of 150 W. The pressure inside the vacuum chamber was $3 \cdot 10^{-4}$ mbar for the 10 sccm flow rate and $2 \cdot 10^{-4}$ mbar for the 5 sccm flow rate. The results of the measurement are presented in Fig. 6.21. The expected velocity is based on the acceleration bias on the screen grid as the plasma potential inside the cavity has not been measured for argon. It can be seen that the same behavior can be observed as in the measurements with xenon. The signal strength increases for the lower flow rates. The ion velocity is also higher in the case for the 5 sccm flow rate. Table 6.2

Accel. bias V_b	Flow rate $sccm$	Ion velocity m/s	Theor. accel. bias V
175V	5	33418	231
175V	10	31438	205
275V	10	39050	316

Table 6.2: Measured velocities with the E×B probe in a 150 W argon discharge and the theoretical acceleration bias.

shows the velocity at the peak of the signal and a conversion of the velocity back to the acceleration voltage with Eq. 2.6. It can be seen that the applied acceleration bias and the theoretical acceleration bias have a difference of 56 V. This is quite extensive as being the sole result of the plasma potential and the calibration of the E×B probe probably factors in as well as possible alignment problems. For the higher flow rates the difference is lower as expected as the plasma potential at higher flow rates are usually lower for the same conditions.

The E×B probe has been placed on a linear drive inside the vacuum chamber to investigate the plasma plume over the distance. The center of the E×B probe had a distance of 305 mm to the acceleration grid in all the previous experiments. With the linear drive, the center of the probe can be displaced between 430 mm and 680 mm. The measurements have been conducted in a 5 sccm xenon plasma at a pressure of $7 \cdot 10^{-4}$ mbar with an input power of 100 W and a grid bias of 160 V and 260 V. The measurements, presented in Fig. 6.22, show the main Xe^+ peak only when the probe is close to the grid for a screen grid bias of 160 V. The small peak which has been observed before, shows also up and is less influenced but changes slightly the velocity with increasing distances. For the measurements with the 260 V bias we can see that the signal of the main xenon peak reduces with the distance. With increasing distance the single large peak develops into two peaks. The first peak resembles the small unexplained peek which also shows up in the other measurements. This peak seems to be hidden in the main peak when the signal is higher. The decrease in the signal inside the plume has been observed in the measurements with the planar probe (Fig. 6.12). This points again to charge exchange collision and beam divergence as an origin of this behavior.

6.1.6 RPA Measurements

Measurements with the RPA have been performed in the PEGASES thruster in order to obtain the ion energy distribution function (IEDF) inside the plume. The RPA probe
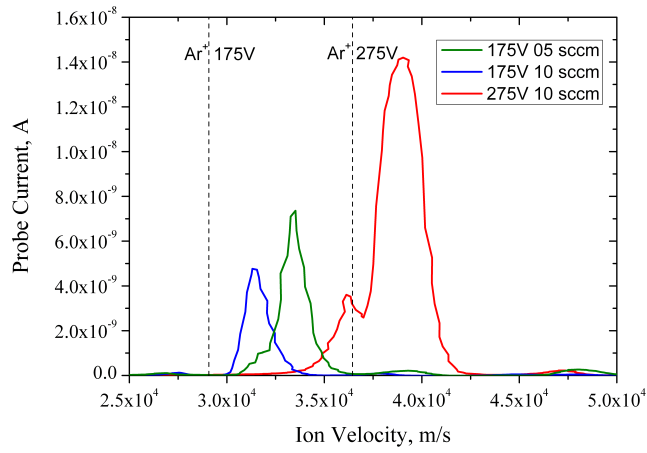
Figure 6.21: Measurements with the E×B probe in argon for different conditions.

(a)   (b)
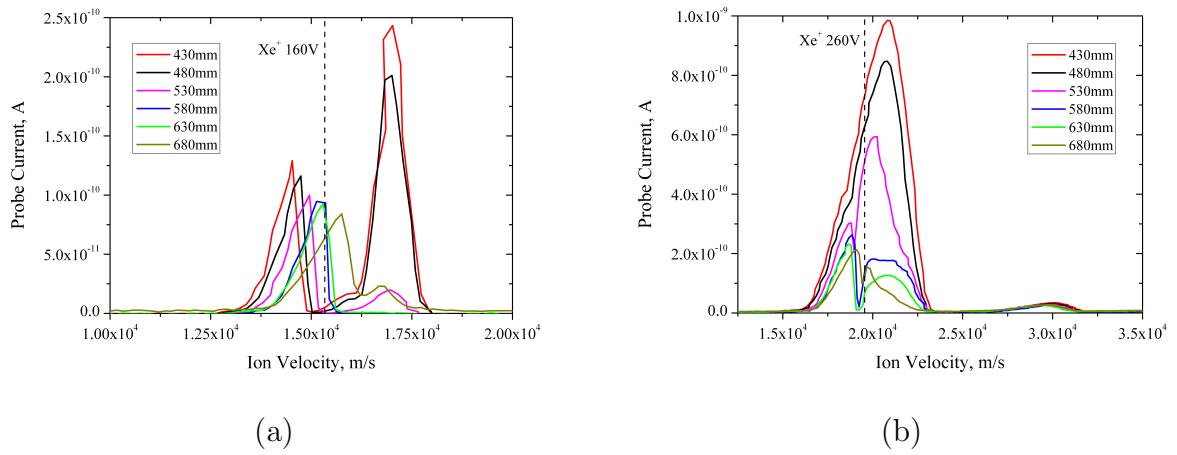
Figure 6.22: Velocity profile measured with an E×B probe for varying distances. The profiles were measured at 100 W input power and 5 sccm xenon flow rate for a grid bias of (a) 160 V and (b) 260 V.
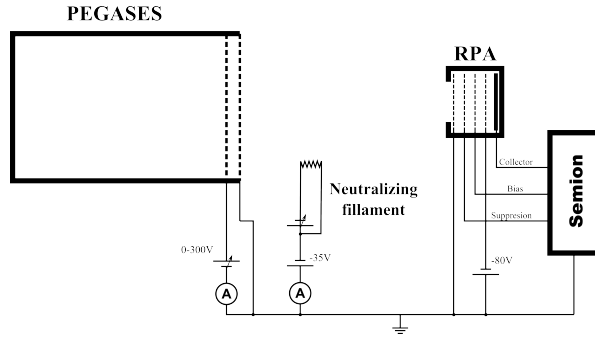
Figure 6.23: Sketch of the installation of the RPA probe in front of PEGASES thruster.

has been placed on a linear drive to measure at 5 different locations along the axis. A sketch of the installation of the probe is given in Fig. 6.23. The measurements have been performed in a 100 W xenon discharge with a flow rate of 2.5 sccm and 5 sccm for the two acceleration biases of 188 V and 285V. The measurements have been performed with similar parameters as the E×B probe. This makes the results comparable.

The measurements for a xenon flow rate of 2.5 sccm are presented in Fig. 6.24. The measured pressure inside the vacuum chamber was in this case $2.5 \cdot 10^{-4}$ mbar. The measurements show that the ions in the case of the 188 V bias in part (a) of the figure have an average energy between 201 V and 204 V. This effect corresponds with the assumption that the plasma potential which is in these conditions around 20 V contributes to the acceleration of the plasma. As the entrance grid of the RPA (namely grind No.4) is grounded the measurement is not dependent on the plasma potential in the plume. The average ion energy for the measurement presented in part (b) with an acceleration grid bias of 285 V is between 295 V and 300 V. A similar behavior can be observed for the measurements performed with a flow rate of 5 sccm xenon at a pressure of $5 \cdot 10^{-4}$ mbar. In the case with the 188 V acceleration bias in part (a) of the figure the ions have an energy between 194 V and 199 V and in part (b) for an acceleration bias off 285 V between 289 V and 300 V.

It can be seen that the ion current, which is the area under the curve reduces in all cases with the distance. This effect corresponds with the measurements performed with the E×B probe in Fig. 6.22. As previously mentioned it is probably due to charge exchange collisions and divergence of the plume.

The results of the measurements, shown in Fig. 6.25 (b), with the RPA can be compared to the results of the measurements with the E×B probe in Fig. 6.15. The comparison shows that there is a gap between the two results of around 30 V between the calculated

(a)   (b)
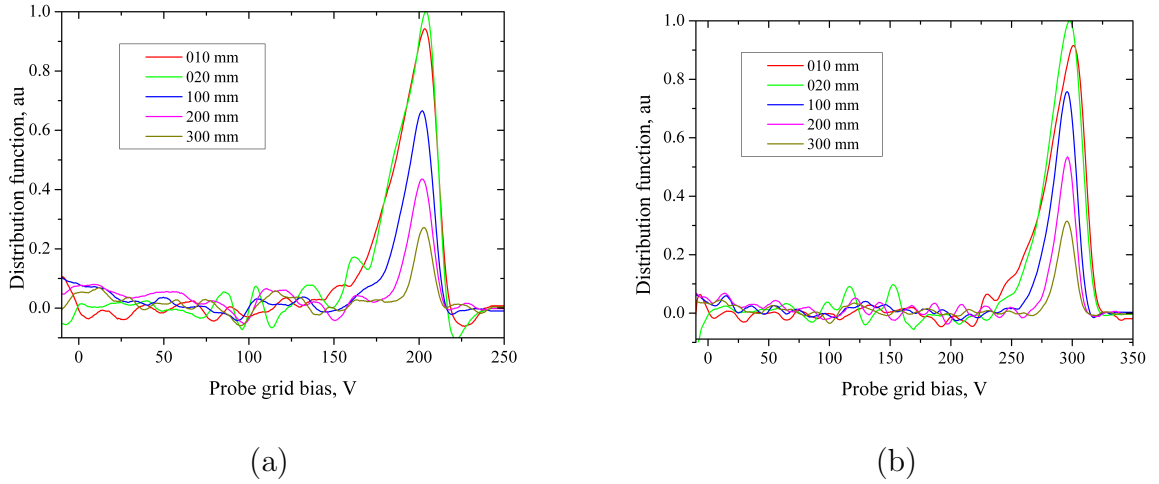
Figure 6.24: Measurement with the RPA in the PEGAES thruster in a 100 W xenon discharge with a flow rate of 2.5 sccm for an acceleration bias of (a) 188 V and (b) 285 V.

acceleration voltage, based on the velocity measured with the E×B probe, and the ion energy measured with the RPA. The measurements of the E×B probe overestimate the ion velocity as mentioned in Ch. 4.5.3. A Laser Induced Fluorescence (LIF) measurement [57] has been used to calculate another conversion factor of 367 m/s for the E×B probe. With this factor the calculated velocity peak for Xe$^+$ decreases from 21966 m/s to 21282 m/s and the calculated acceleration based on the velocity decreases from 328 V to 308 V. This leaves still a gap of around 10 V between the measurements with the E×B probe and the RPA which can not be explained at this moment.

In theory the RPA probe measurements should show the residual plasma in the present in the vacuum chamber. A theoretical obtained curve to show the presence of residual plasma is shown in Fig. 6.26. None of the performed measurements showed any peaks which corresponds to the expected signal. To measure the ion energy of this plasma the RPA would have to be adjusted. The waves in the signal which can be observed between the zero potential and the ion energy peak are induced by a second order polynomial smoothing which is necessary to perform the derivation of the current trace. Therefore they have to be considered as noise and should not be confused as a signal.

106
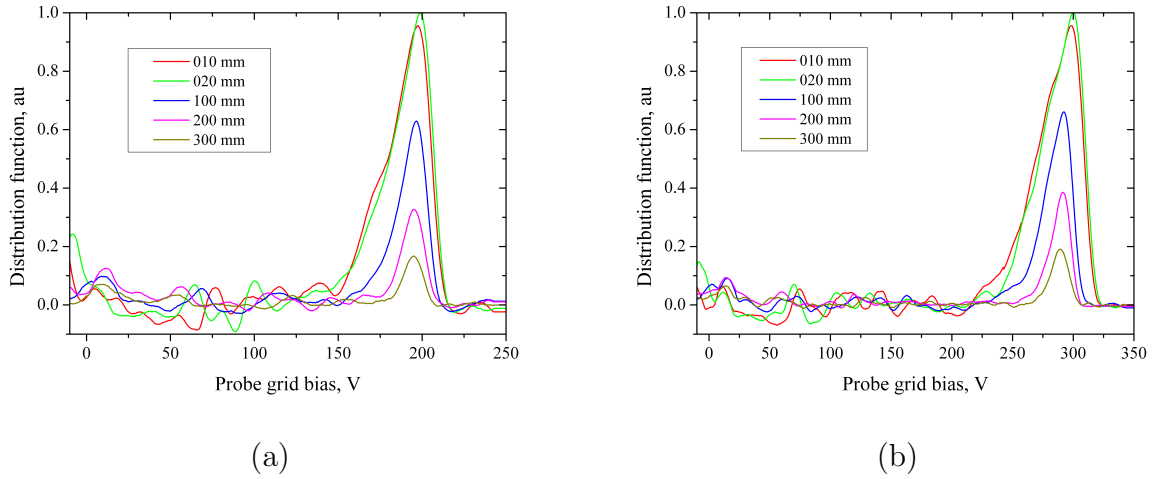
Figure 6.25: Measurement with the RPA in the PEGAES thruster in a 100 W xenon discharge with a flow rate of 5 sccm for an acceleration bias of (a) 188 V and (b) 285 V.

6.1.7 Thrust Estimates

Combining the measurements of the ion flux and the measurements of the ion velocity, the expected thrust T can be estimated with simply calculating,

$$T = \dot{m}_i v_i. \tag{6.10}$$

This calculation is based on a rectangular ion flux profile.

Figure 6.27 shows the minimum and the maximum thrust for in a 5 sccm xenon plasma with an ion velocity of 21000 m/s which corresponds to an acceleration bias of 300 V including the plasma potential. The numbers for the maximum thrust are based on the
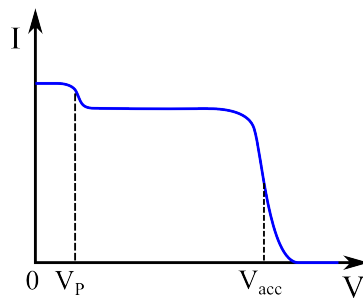
Figure 6.26: Theoretical measurement with the RPA which shows the presence of residual plasma.
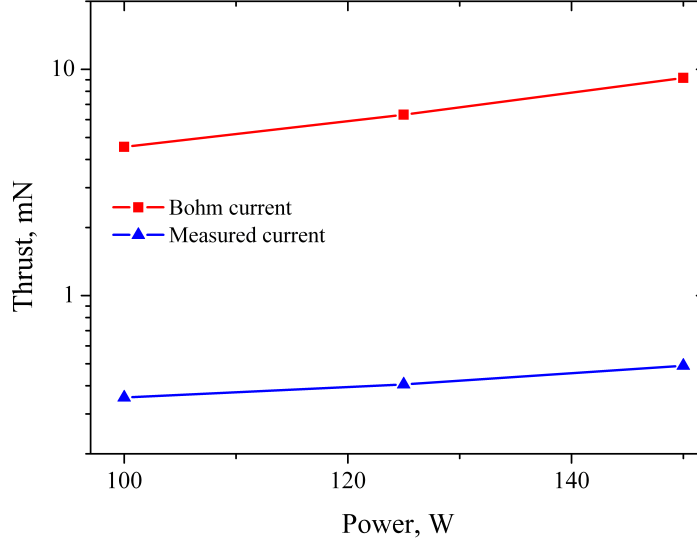
Figure 6.27: Minimum and maximum thrust estimation for the PEGASES thruster operating in xenon at 300 V acceleration bias.

measurements of the ion flux just ahead of the grid presented in Fig. 6.6 (i.e. Bohm flux). The numbers of the minimum thrust are based on the ion flux measured 100 mm behind the acceleration grid with a 55 mm in diameter planar probe using a factor of 1.5 for beam divergence and charge exchange collisions.

In order to estimate how much of the energy put into the thruster is converted into thrust the total efficiency of the thruster can be calculated as,

$$\eta_T = \frac{T^2}{2\dot{m}P_{in}}, \tag{6.11}$$

where the total power P_{in} consists of the input power P_{tr} to generate the plasma the acceleration power P_{acc} and the cathode heating power P_c. The power needed for the acceleration is roughly 15 W when the electron current coming from the neutralizing filament is blocked (as shown in Fig. 6.14). The heating power required by the neutralizing filament is 130 W. The calculated numbers are presented in Fig. 6.28. The numbers for the thrust are the ones presented and described in Fig. 6.27. The power consumed by the neutralizing filament is high compared to the discharge power. The emitted electron current is higher than necessary and could probably be reduced. The use of a cold cath-
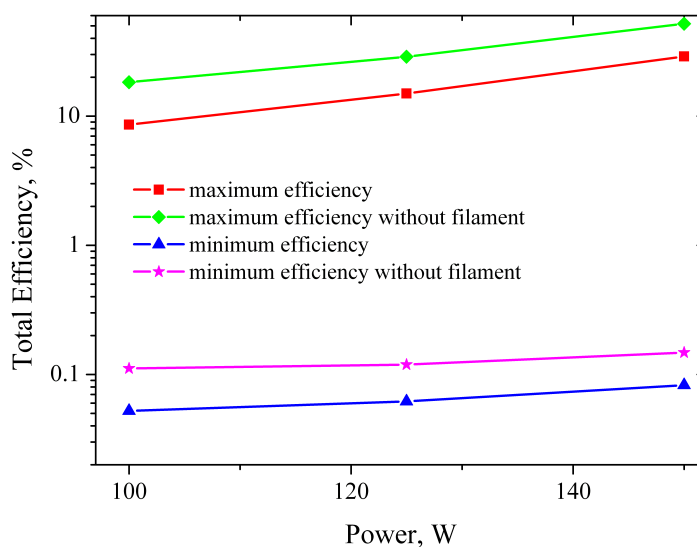
Figure 6.28: Thrust efficiency for the PEGASES thruster operating in xenon with a 300 V acceleration grid bias.

ode would further decrease the power consumption. The total efficiency has therefore also been calculated without the power consumption of the filament. It can be seen that at the current ion flux the efficiency is poor compared to the possible maximum efficiency and the ion flux in the plume has to be drastically increased to obtain good numbers.

At the moment, even if it is possible to increase the ion current in the plume to where it gets close to the Bohm current, the thruster compares poor to thrusters like the RIT15 which has a total efficiency of 67 % [55]. To reach these kind of numbers the not just the acceleration hast to be improved but also the ion production.

6.2 Plasma Drift in the PEGASES Thruster

After installing an optical window on axis for laser detachment experiments, which allows a frontal view of the discharge chamber, and performing alignment experiments without the grids present an asymmetrical structure has been observed inside the PEGASES thruster cavity. The strip has first been observed in a Xe-SF$_6$ mixture but has since been confirmed for Xe and Ar discharges. Figure 6.29 (a) and (b) shows a picture

109

of the asymmetrical structure in the discharge chamber for a 200 W discharge with at 10 sccm SF_6. The pictures in part (b) and (c) have been taken in a 150 W, 5 sccm xenon discharge. The direction of the magnetic field has been changed between the pictures and the field displayed in (e) corresponds to the pictures in part (a) and (c). The field displayed in (f) corresponds with the pictures in part (b) and (d). The magnetic field strength in the pictures was the 190 G configuration described in Ch. 2.4.4. The structure has been observed in the three magnetic field layouts with magnetic fields of 190 G, 109 G and 62 G in the middle of the cavity. The magnets were positioned at x=35 mm (upstream of the grids between the grids and the coil). A variation of the power from 180 W to 225 W and flow rates from 5 sccm to 19 sccm in SF_6 did not eliminate the structure. In contrast Fig. 6.31 shows a picture taken in the same conditions in xenon without a magnetic field. This leads to the assumption that the observed luminous structure is not an effect of possible asymmetries in the thruster, the discharge cavity or the RF coil.

Pictures of the asymmetrical structure for different field strengths are shown in Fig. 6.30. The pictures have been taken in a 5 sccm, 150 W xenon discharge. The structure is barely visible at a field strength of 62 G and the visibility increases with the field strength. The luminosity of the plasma is the strongest in the case of the 190 G field.

An uncompensated Langmuir probe has been installed on two linear displacement drives to further investigate the drift effect. The linear drives allow the probe to be displaced along the xy-plane of the thruster. The measurements have been performed on the symmetrical axis in z direction. Figure 6.33 shows interpolated data taken at 100 points inside the cavity. It shows a view from the top where the RF coil is at the upper part and the lower part opens into the vacuum chamber. The magnets are placed horizontally at 3.5 cm. The applied magnetic field has a peak value of 190 G along the x-axis on the symmetrical axes of the thruster shown in Fig. 6.32. In part (a), (c) and (e) the magnetic north pole is located on top of the cavity and the magnetic field lines go into the graph. In part (b), (d) and (f) the magnets are inverted, the magnetic north pole is located bellow the picture and the magnetic field lines come out of the picture. The measurements have been performed in a 125 W, 5 sccm xenon discharge at the pressure off $2 \cdot 10^{-3}$ mbar.

The measurements presented in Fig. 6.33 reveal that the observed luminous structure origins in the back corner of the cavity close to the antenna and seems to be confined by the magnetic field. Unlike the strip described in Ch. 5 it seems that there is no structure

(a)

(b)

(c)

(d)

(e)

(f)
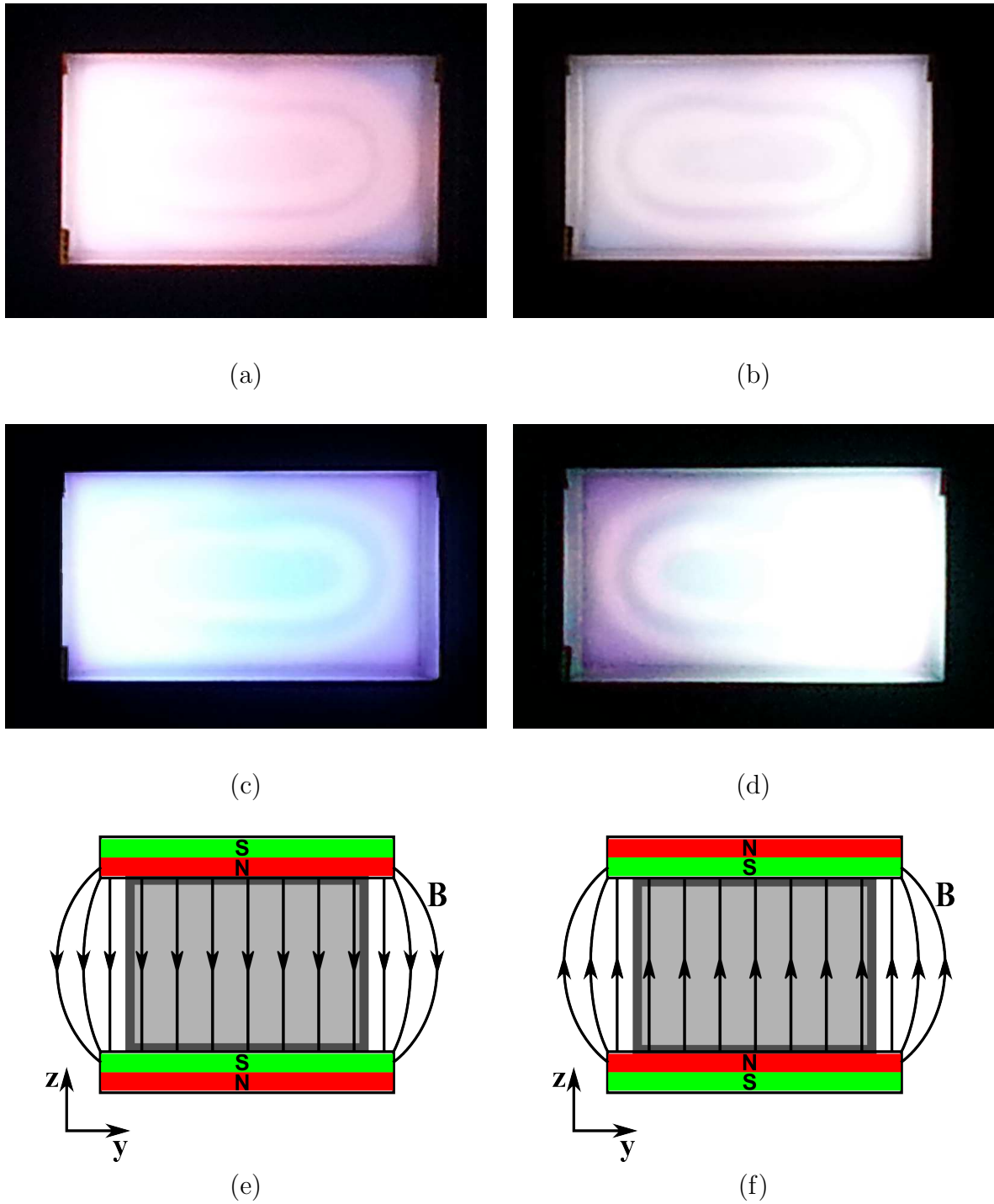
Figure 6.29: The asymmetrical structure in the PEGASES discharge chamber at a magnetic field strength of 190 G (a) and (b) in SF6 at a discharge power of 200 W, (c) and (d) Xe at a discharge power of 150 W. The schematics in (e) and (f) show the magnetic field of the pictures above.

(a)

(b)

(c)

Figure 6.30: The asymmetrical structure in the PEGASES discharge chamber in a 150 W xenon discharge at a magnetic field strength of (a) 62 G, (b) 109 G and (c) 190 G.
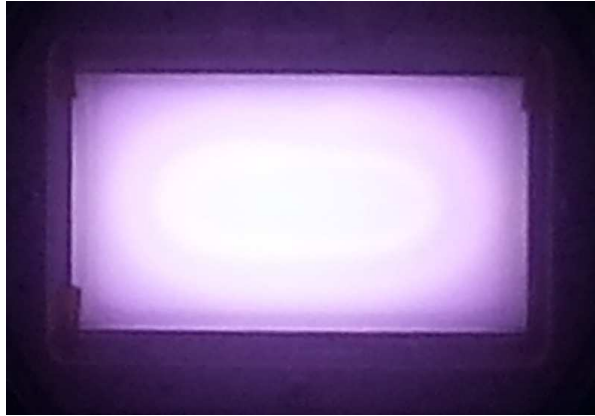
Figure 6.31: Picture of the PEGASES thruster without grids an magnets in a Xe discharge of 150 W.
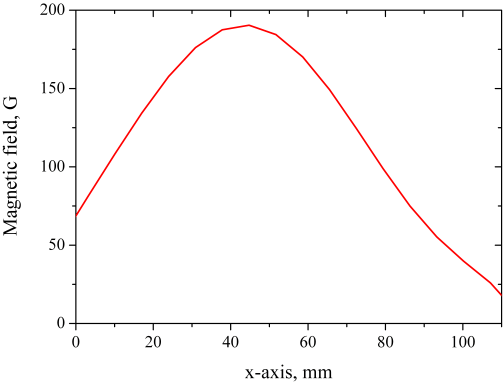
Figure 6.32: Magnetic field inside the PEGASES discharge cavity along the x-axis. x=0 mm is the grid plane and x=119 mm is the plane of the ceramic window.

crossing the magnetic barrier. To be sure we would need a measurement in all three dimensions. This might lead to a homogenous plasma in the plane of the grid (x=0). The measurement of the plasma potential in part (a) and (b) of the figure show that there is a potential drop of around 10 V from the back of the thruster where the coil is located to the front where the cavity ends into the vacuum chamber. It can be seen that the luminous part in the cavity has a plasma potential roughly 5 V higher than the non luminous part close to the coil. The electron temperature presented in part (c) and (d) of the figure shows the same trend than the plasma potential. The hot electrons are close to the coil in the back part of the discharge chamber and seem to be pressed into the corner by the magnetic field. The electron temperature is around 12 eV in the luminous part of the plasma and drops to around 2 eV down flow of the magnetic barrier at the exit of the cavity. The magnetic barrier works as intended and cools down the electrons.

The measurements of the electron density presented in part (e) and (f) of Fig. 6.33 show that the density is roughly 10 times higher in the luminous part in the back of the chamber than at the exit. The magnetic field seems to confine the plasma to the back of the discharge cavity close to the RF coil.

The measurements have been performed for the same conditions without a magnetic field. Figure 6.34 shows the electron density inside the discharge cavity for a 125 W, 5 sccm xenon discharge measured with the Langmuir probe. The plasma turned off half way through the measurement and had to be restarted. It is hard to reproduce the exact same discharge conditions when restarting a plasma. This is the reason why the upper and the lower part of the graph show suddenly different electron densities. There is no jump of the electron density. The rest of the graph shows the plasma density as expected. The density decreases towards the walls on the side and on the back. There is a decrease of the electron density from the back of the thruster where the RF coil is located to the front where the plasma enters into the vacuum chamber. This effect is not clearly visible in this graph due to the interpolation of the data.

In order to estimate the influence of the RF fluctuations on the potential of the plasma, measurements with a capacitive probe have been performed inside the discharge cavity along the x-axis. The measurements have been performed in a 10 sccm SF_6 discharge at the power of 125 W. The grid position is x=0 mm and the ceramic window is at x=119 mm. The measurements presented ing Fig. 6.35 reveal that the fluctuations in the plasma potential are between $4 - 12$ V inside the cavity.
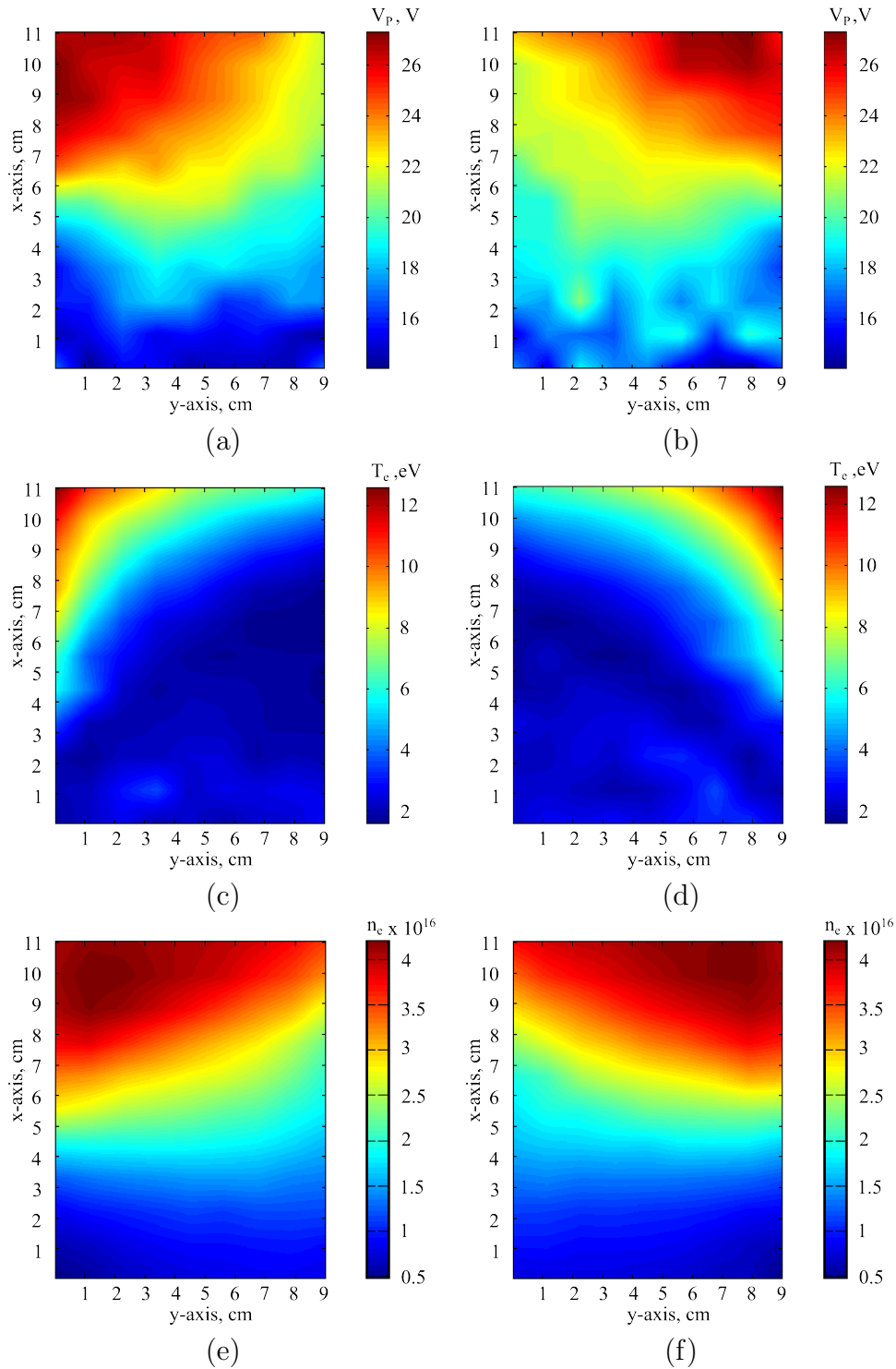
Figure 6.33: Figure (a) and (b) show the plasma potential, figure (c) and (d) show the electron temperature and (e) and (f) show the electron density. In figures (a), (c) and (e) the magnetic north pole is on top off the cavity and the magnetic field lines go into the picture. For (b), (d) and (f) the magnetic north pole is below the cavity and the field lines come out of the picture. The zero of the axes corresponds to the left corner at the exit of the cavity when viewed from the top. Measured in a 125 W, 5 sccm xenon discharge.
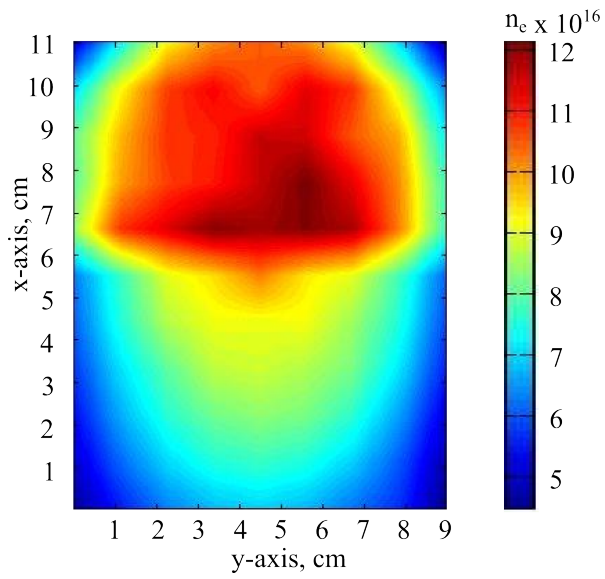
Figure 6.34: Measurement of the electron density inside the PEGASES thruster cavity without magnetic field in a 125 W, 5 sccm xenon discharge.
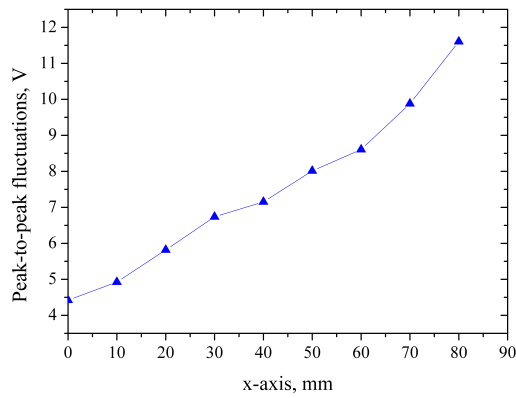
Figure 6.35: Measurements of the RF fluctuations in a 10 sccm SF_6 plasma.

The performed measurements are in agreement with the results from in Ch. 5. To refresh the memory, the drift is composed of two components, the B×E drift, $\mathbf{v_{E \times B}}$, and the diamagnetic drift, $\mathbf{v}_{\text{dia}}$,

$$\mathbf{v_{E \times B}} = \frac{\mathbf{E} \times \mathbf{B}}{B^2} \qquad \text{and} \qquad \mathbf{v}_{\text{dia}} = \frac{\nabla p_e \times \mathbf{B}}{e n_e B^2}. \tag{6.12}$$

The electron drift current is:

$$\mathbf{j}_e = -e n_e (\mathbf{v_{E \times B}} + \mathbf{v}_{\text{dia}}). \tag{6.13}$$

The electric field inside the PEGASES thruster is weak compared to the experiments performed in Ch. 5.

An estimation of the drift velocities shows,

$$\mathbf{v_{E \times B}} = \frac{E}{B} = \frac{10 \text{ V/cm}}{200 \text{ G}} = 5 \cdot 10^4 \text{ m/s}, \tag{6.14}$$

for the E×B drift when using a magnetic field of 200 G and an electric field of 10 V/cm. For the diamagnetic drift an electron pressure of $\nabla p = k T_e \nabla n_e$ with an electron temperature of 8 eV and a difference in the electron density of $5 \cdot 10^{16}$ is used. The diamagnetic drift is then,

$$\mathbf{j}_e = \frac{\nabla p}{e n_e B} = \frac{0.064 \text{ Pa}}{e \, 3 \cdot 10^{16} \cdot 200 \text{ G}} = 665 \text{ m/s}, \tag{6.15}$$

for a magnetic field of 200 G and an electron density of $3 \cdot 10^{16}$. This shows us that the E×B drift is clearly dominant in our case and origins in the residual electric field.

Observations made by the LPP laboratory show also an asymmetric structure inside the discharge chamber. The LPP uses an advanced matchbox which reduces the capacitive coupling effect and therefore the RF fluctuations in the plasma. They could also observe the drift structure in the case of a stronger magnetic field. Both, the E×B drift and the diamagnetic drift lead to an electron current orthogonal to both fields as displayed in Fig. 6.36. The electrons are confined between the magnetic barrier and the end of the discharge chamber where the RF coil is. This leads to an local increase of electron temperature, electron density and the plasma potential. As can be observed the plasma emits more light in the region where a high electron temperature is measured. The high
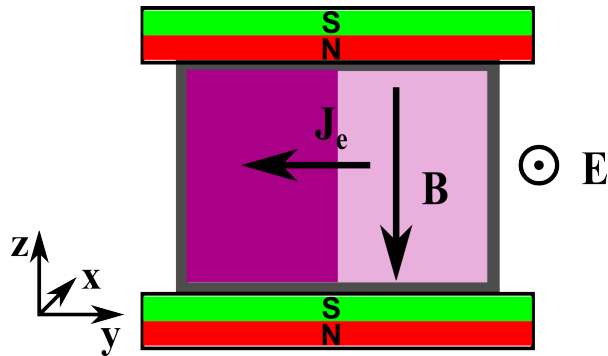
Figure 6.36: Electron drift inside the PEGASES thruster.

electron temperature leads to the production of a large amount of excited atoms. The light they emit when they decay is then localized in the hot region.

6.3 Conclusion

It has been shown that the PEGASES thruster can be used as an efficiency RF plasma source in xenon. The source is not yet optimized and the efficiency leaves still a margin for improvement. Measurements have been performed inside the discharge cavity in order to investigate the plasma parameters and obtain the ion flux. An acceleration of the plasma with a two grid system has been demonstrated. The accelerated ions in the plume of the PEGASES thruster have been analyzed with a variety of probes. The ion flux has been measured with a planar probe over a variety of conditions. The plasma potential has been measured with the help of a Langmuir probe. The ion velocity distribution function has been measured with the help of an E×B probe. Multiply charged ions have been observed in the plume of the thruster as well as other gases which probably come from a small leak in the system. Measurements with a RPA probe have shown the ion energy distribution function which has been used to verify the results of the E×B probe. The measurements of the E×B probe agree with the expected velocity except for a small deviation which can probably be solved by a calibration of the E×B probe with a well known ion source. An estimate of the thrust and the total efficiency of the thruster reveal a low efficiency at the moment with a huge margin for improvements.

An asymmetric plasma structure has been optically observed in the open discharge cavity of the PEGASES thruster with a magnetic barrier. The structure has been identified as an electron drift. The dominating factor is most likely an E×B drift due to the residual

118

electric field. The structure has been investigated with the help of a Langmuir probe and has been found to occur in the back of the thruster close to the RF coil. The drift seems to have no influence on the homogeneity of the plasma down flow of the magnetic barrier in the plane where the acceleration grids are usually mounted.

7 Conclusion

7.1 Overview of the Works

7.1.1 Goals of the Thesis

The goal of the thesis were to investigate the PEGASES thruster with a variety of probes inside the discharge cavity and in the plume. The investigation was aimed to establish the PEGASES as an efficient plasma source for electric space propulsion in xenon. For this preliminary numbers of the power transfer efficiency, thrust generation and total efficiency of the thruster are needed.

7.1.2 PEGASES Thruster

The concept of the PEAGSES thruster relies on an ion-ion plasma, that means an electron free plasma. The positive and negative ions are then extracted and accelerated alternately by means of a high-voltage grid assembly. PEGASES therefore belongs to the family of gridded ion engines. Using electronegative gases like SF_6 in combination with a magnetic barrier allows to create a strong electronegative plasma. The positive and negative ions can then be extracted by alternately biasing a pair of extraction grids. As the RF source of the PEGASES thruster is an efficient ions source, it has been decided to investigate its use as a classical ion thruster operating in xenon.

A prototype of the PEGASES thruster similar to the ones in use at the LPP has been installed onto the EPIC vacuum test bench at the ICARE laboratory. The thruster has been operated with a xenon discharge in order to obtain comparable values to other ion thruster. The plasma inside the discharge chamber has been investigated to obtain values for the electron temperature, electron density and plasma potential for different discharge conditions. The ion flux has been measured at the position of the grids to find the extractable ion current. An acceleration of xenon ions with a set of two grids has

been demonstrated. The resulting plasma plume has been investigated with a variety of probes over a large parameter range at different positions. The ion flux in the plume has been measured with the help of a planar probe. The plasma potential has been measured with a Langmuir probe. Measurements with the E×B probe reveal the VDF of the ions in order to obtain fundamental quantities that can be compared with values available in the open literature for other RF ion engines. The ion energy distribution function has been measured with the help of a RPA probe.

After adding a magnetic barrier to the PEGASES thruster, in order to investigate the thruster in SF_6 for its original purpose, that means the creation and acceleration of negative and positive ions, an asymmetric luminous structure has been observed. This structure has been observed in several gases like Ar, Xe and SF_6. It has been shown by changing the direction of the magnetic field and observing a change in the location of the structure, that the origin of this phenomenon does not lie in asymmetries in the PEGASES thruster. Performing a two dimensional measurement inside the discharge cavity of the PEGASES thruster with a Langmuir probe reveals the plasma parameters. The electron temperature, the electron density and the plasma potential reveal the location and the consistency of the structure. The observed asymmetric luminous structure is confined between the magnetic barrier and the end of the discharge chamber where the RF coil is located. The plasma in this region shows an elevated electron temperature and plasma potential as well as a higher density compared to its surroundings. The origin of the structure lies most probably in an electron drift. The potential fluctuations in the plasma are low compared to the one observed in the previous experiments, as the PEGASES thruster is an inductive source with a low capacitive coupling. The resulting electric field between the plasma and the grounded vacuum chamber is also low. An estimation of the drift velocities reveals the E×B drift due to the residual electric field is probably the dominating factor in the formation of this structure. The magnetic barrier however seems to confine the electron drift to the back of the chamber where the RF coil is located and the plasma in the plane where the acceleration grids are usually mounted seems to be homogenous. This is important for ion extraction and acceleration of plasma as an inhomogeneous plasma in front of the grid assembly leads to a lower efficiency.

7.1.3 Performances

I has been shown that the power transfer efficiency of the PEGASES RF source can reach up to 87 % in xenon. This number reveals that the PEGASES thruster in its current

state is an efficient ion source and comes close to numbers of other RF ion thrusters like the RIT family. The measured thrust on the other hand is with 0.5 mN very low compared to other ion thruster which are typically between $10 - 50$ mN at a power of $400 - 1500$ W. It has been shown that this is mainly a result of unoptimized grids and can be improved. The resulting total efficiency is very low with 0.08 % and even when the energy consumption of the neutralizing filament is neglected, it increases just to 0.15 %. The acceleration with the grids has to be optimized in order to extract and accelerate a larger amount ions and increase the thrust. If the complete Bohm current would be accelerated the total efficiency would increase to 29 % and 52 % neglecting the power consumption of the neutralizer and beam divergence. This could increase the total efficiency close to the 67 % which is reached by the RIT15 thruster.

7.1.4 E×B Probe

An E×B probe system has been developed and added to the diagnostic tools already available at the ICARE laboratory. The E×B probe allows to measure the ion velocity distribution function (VDF) in the plume of electric thrusters such as Hall thrusters and ion thrusters. The probe allows to measure the velocity of the ions in the plume as well as to identify multiply charged ions. By analyzing the obtained VDF the ratio between the different ion species can be calculated. The VDF can also reveal the presence of other gases in the plume of the thruster and can help to identify leaks or impurities. The signal strength of the developed E×B probe system can be adjusted by switching the entrance and the exit collimator to account for different plasma conditions. It is also possible to increase the resolution of the E×B probe at the cost of signal strength if a more precise measurement is required.

The E×B probe has been tested in the plume of a Hall thruster and of the PEGASES thruster. The obtained results have been compared to the measurements of other probes such a planar probe and a RPA probe. The tests show that a calibration of the E×B probe is necessary in order to obtain better values. Finally the E×B probe has been used to analyze the plume of the PEGASES thruster operating as a classical ion thruster in xenon. The probe delivered valuable data for understanding acceleration mechanism and the physics in the plume.

7.1.5 Strip Structure

While investigating magnetic field layouts for the PEGASES thruster, an asymmetrical luminous strip structure has been discovered in a RF generated plasma. It has been shown that the structure is present in a variety of gases such as Ar, Xe, O_2, SF_6, Kr and N_2. The structure has been shown to exist over a broad band of RF frequencies, in strength varying magnetic fields and over a large pressure range. An investigation revealed plasma drifts, especially the E×B drift, as a possible origin for the strip structure. The spiral coil located behind the discharged tube used in the experiments is not purely inductive but couples the power to the plasma also capacitively. This results in strong RF fluctuations inside the plasma which create an electric field between the plasma inside the discharge tube and the grounded vacuum chamber. The electric field together with the magnetic field create a drift of the electrons which probably lead to the observed structure. The capacitive coupling and therefore the resulting electric field can be reduced by introducing a Faraday shield between the RF coil and the discharge chamber. In leads in most cases to a disappearance of the strip structure.

7.2 Prospects

Many accomplishments have been presented in this thesis but a several points remain still to be investigated. This section gives some objectives for future research.

7.2.1 PEGASES

The PEGASES thruster was originally not intended for the use with xenon as a classical ion thruster. We have demonstrated that the source is efficient and with some effort can be developed into an ion thruster which operates in xenon and accelerates only positive ions.

The grids of the PEGASES thruster show the larges margins for optimization do exist. Therefore the grid assembly must be redesigned. This probably requires a large amount of work. After this has been accomplished it would be interesting to measure the real thrust with the help of a pendulum or redesign the thruster to a point where it can be mounted onto a thrust balance. At the moment the thruster is mounted to the outside of a vacuum chamber and the coil-matchbox assembly is not in the vacuum. In order

to be mounted onto a thrust balance the whole thruster assembly would have to work inside a vacuum chamber.

One of the main goals should be to demonstrate steady alternate and efficient positive and negative ion acceleration and investigate the plasma plume with the available probes and tools.

7.2.2 E×B Probe

The original plans for the E×B probe included a section for the separation of negative an positive ions as the probe was to be used in the plasma plume of the PEGASES thruster. This has not yet been included into the experimental setup as an acceleration of negative ions has not yet been attempted in the ICARE laboratory. So far it has only been demonstrated by the team of the LPP. Including this section into the design of the E×B probe would create a powerful tool in the investigation of the plasma plume of the PEGASES thruster when operating in alternative acceleration mode with an electronegative gas.

A calibration of the E×B probe with a well known plasma source would increase the precision of the probe and the obtained data. E×B probe results should be compared to RPA and LIF measurements. This makes the E×B probe a valuable probe for all kinds of plasma thruster.

An improvement of the E×B probe data can also be obtained by adding differential pumping to the probe system. This would decrease the pressure and the mean free path for momentum and charge exchange inside the probe which leads to less collisions and a better signal.

7.2.3 Strip Structure

The discovery of the strip structure lead to a better understanding of the plasma drift inside the plasma. It turns out that drift structures can be found in other plasma sources as well. As the probable origin of the structure is now known, a dedicated plasma source could be designed to investigate this phenomena. The more we know about this effect the better we can design future magnetized low-pressure plasma sources which can avoid this effect or even profit from its properties.

Bibliography

[1] T. M. Tikhonravov. *Works on Rocket Technology by E. K. Tsiolkowsky.* NASA, 1965.

[2] D. M. Goebel and I. Katz. *Fundamentals of Electric Propulsion: Ion and Hall Thrusters.* Wiley & Sons, 1 edition, 2008.

[3] M. J. L. Turner. *Rocket and Spacecraft Propulsion.* Springer Verlag, Praxis Publishing, 2001.

[4] H. Kuninaka, K. Nishiyama, Y. Shimizu, I. Funaki, H. Koizumi, S. Hosoda, and D. Nakata. Hayabusa asteroid explorer powered by ion engines on the way to earth. In *Proceedings of the 31st Intern. Electric Propulsion Conferce, Ann Arbor, MI, Sept. 2009*, IEPC-2009-267.

[5] N. Wallace, P. Jameson, C. Saunders, M. Fehringer, C. Edwards, and R. Floberghagen. The GOCE ion propulsion assembly - lessons learnt from the first 22 months of flight operations. In *IEPC - Proceedings*, 2011.

[6] H. J. Leiter, R. Killinger, H. Bassner, J. Müller, and R. Kukies. Development of the radio frequeny ion thruster RIT XT - A status report. In *Proceedings of the 27th Intern. Electric Propulsion Conferce, Pasadena, California, USA , Oct, 2001*, IEPC-01-104.

[7] H. J. Leiter, R. Killinger, H. Bassner, J. Müller, R. Kukies, and T. Fröhlich. Development and performance of the advanced radio frequency ion thruster RIT-XT. In *Proceedings of the 28th Intern. Electric Propulsion Conferce, Toulouse, France , USA , Mar, 2003*, IEPC-03-115.

[8] W. J. Larson and J. R. Wetz. *Space Mission Analysis and Design.* Microcosm Press, 1999.

125

[9] R. Killinger, H. Bassner, R. Kukies, and H. Leiter. Results of the 15000 hours lifetime test for the RITA ion propulsion an ESA's ARTEMIS satellite. In *Proceedings of the 27th Intern. Electric Propulsion Conferce, Pasadena, California, USA , Oct, 2001*, IEPC-01-082.

[10] J. R. Anderson, K. D. Goodfellow, J. E. Polk, V. K. Rawlin, and J. S. Sovey. Performance characteristics of the NSTAR ion thruster during an on-going long duration ground test. In *Aerospace Conference Proceedings, 2000 IEEE. Vol. 4. IEEE pp. 99-122*, 2000.

[11] P.Chabert. Electronegative plasma motor, US 2008/0271430A1, 2007.

[12] G. Leray. *PEGASES Plasma Propulsion with Electronegative Gases*. PhD thesis, École Polytechinque Paris, 2009.

[13] L. Popelier. *Développement du propulseur PEGASES : source inductive à haute performance et accélération successive de faisceaux d'ions positifs et d'ions négatifs*. PhD thesis, École Polytechnique, 2012 (in French).

[14] P. Colpo, T. Meziani, and F. Rossi. Inductively coupled plasmas: Optimizing the inductive-coupling efficiency for large-area source design. *Journal of Vacuum Science & Technology A*, 23:270, 2005.

[15] D. J. Economou. Fundamentals and applications of ion-ion plasmas. *Appl. Surf. Sci.*, 253:6672–6680, 2007.

[16] S. G. Walton, D. Leonhardt, R. F. Fernsler, and R. A. Meger. Extraction of positive and negative ions from electron-beam-generated plasmas. *Appl. Phys. Lett.*, 81:987–989, 2002.

[17] S. G. Walton, D. Leonhardt, R. F. Fernsler, and R. A. Meger. On the extraction of positive and negative ions from electron-beam-generated plasmas. *Appl. Phys. Lett.*, 83:626–628, 2003.

[18] A. Aanesland, A. Meige, and P. Chabert. Electric propulsion using ion-ion plasmas. *J. Phys. Conf. Ser.*, 162(1):012009, 2009.

[19] A. Aanesland, J. Bredin, P. Chabert, and V. A. Godyak. Electron energy distribution function and plasma parameters across magnetic filters. *Applied Physics Letters*, 100:044102, 2012.

[20] L. Popelier, A. Aanesland, and P. Chabert. Response of an ion-ion plasma to dc biased electrodes. *J. Phys. D: Appl. Phys.*, 44(31):315203, 2011.

[21] M. Irzyk. *Génération de faisceaux d'ions à partir de plasmas à haute densitié*. PhD thesis, Université d'Orléans, 2001 (in French).

[22] D. Gerst, M. Cirisan, S. Mazouffre, and A. Aanesland. Investigation of ion-ion plasmas for application in electric thrusters. In *Proceedings of the 32nd Intern. Electric Propulsion Conferce, Kurhaus, Wiesbaden, Germany , Sept, 2011*, IEPC-2011-127.

[23] F. F. Chen. Lecture notes on langmuir probe diagnostics. *IEEE-ICOPS meeting, Jeju, Korea, June 5, 2003*, 2003.

[24] R. R. J. Gagné and A. Cantin. Investigation of an RF plasma with symmetrical and asymmetrical electrostatic probes. *J. Appl. Phys.*, 43(6):2639–2647, 1972.

[25] H. M. Mott-Smith and I. Langmuir. The theory of collectors in gaseous discharges. *Phys. Rev.*, 28(4):727–763, Oct 1926.

[26] J. P. Sheehan and N. Hershkowitz. Emissive probes. *Plasma Sources Sci. Technol.*, 20:22, 2011.

[27] C. Ionita, J. Grünwald, C. Maszl, R. Stärz, M. CerCek, B. Fonda, T. Gyergyek, G. Filipic, J. Kovacic, C. Silva, H. Figueiredo, T. Windisch, O. Grulke, T. Klinger, and R. Schrittwieser. The use of emissive probes in laboratory and tokamak plasmas. *Contributions to Plasma Physics*, 51:264–270, 2011.

[28] K. Dannenmayer. *Scaling laws and electron properties in Hall effect thrusters*. PhD thesis, Université d'Orléans, 2012.

[29] Y. Raitses, D. Staack, A. Smirnov, and N. J. Fisch. Space charge saturated sheath regime and electron temperature saturation in Hall thrusters. *Phys. Plasmas*, 12: 073507, 2005.

[30] I. H. Hutchinson. *Principles of Plasma Diagnostics*. Cambridge University Press, second edition edition, 2002.

[31] C. Böhm and J. Perrin. Retarding-field analyzer for measurements of ion energy distributions and secondary electron emission coefficients in low-pressure radio frequency discharges. *Rev. Sci. Instrum.*, 64:31–44, 1993.

[32] G. J. Williams, M. T. Domonkos, and J. M. Chavez. Measurement of doubly charged ions in ion thruster plumes. In *Proceedings of the 27th Intern. Electric Propulsion Conferce, Pasadena, California, USA , Oct, 2001*, IEPC-01-310.

[33] S.-W. Kim. *Experimental Investigations of Plasma Paramaters and Species-Dependent Ion Energy Distribution in the Plasma Exhaust Plum of a Hall Thruster.* PhD thesis, The University of Michigan, 1999.

[34] R. R. Hofer. *Development and Characterization of High-Efficiency, High-Specific Impulse Xenon Hall Thrusters.* PhD thesis, University of Michigan, 2004.

[35] R. R. Hofer, R. S. Jankovsky, and A. D. Gallimore. High-specific impulse Hall thrusters, part 1: Influence of current density and magnetic field. *J. Propul. Power*, 22:721–731, 2006.

[36] B. M. Reid, R. Shastry, A. D. Gallimore, and R. R. Hofer. Angularly-resolved ExB probe spectra in the plumeof a 6-kW Hall thruster. In *Proceedings of the 44th AIAA/ASME/SAE/ASEE Joint Propulsion Conference & Exhibit*, pages 1–21, AIAA 2008-5287, 2008.

[37] B. M. Reid. *The Influence of Neutral Flow Rate in the Operation of Hall Thrusters.* PhD thesis, The University of Michigan, 2009.

[38] R. Shastry, R. R. Hofer, B. Reid, and A. D. Gallimore. Method for analyzing ExB probe spectra from hall thruster plumes. *Rev. Sci. Instrum.*, 80, 2009.

[39] M. E. Arciaga, A. G. Mendenilla, and H. J. Ramos. Characteristics of an ExB probe for extraction of h ions from a magnetized sheet plasma source. *Rev. Sci. Instrum.*, 74:951–955, 2003.

[40] A. Kieckehafer, D. Massey, and L. B. King. Probe diagnostics in a bismuth Hall thruster. In *Proceedings of the 30th Intern. Electric Propulsion Conferce, Florence, Italy, Sept, 2005*, IEPC-05-129.

[41] S. Mazouffre, G. Bourgois, K. Dannenmayer, and A. Lejeune. Ionization and acceleration processes in a small, variable channel width, permanent magnet Hall thruster. *J. Phys. D: Appl. Physics*, 45:185203, 2012.

[42] J. Ekholm and W. Hargus Jr. Exb measurements of a 200 w xenon hall thruster. In *41st AIAA/ASME/SAE/ASEE Joint Propulsion Conference & Exhibit, Tucson, Arizona, paper AIAA 2005-4405*, 2005.

[43] M. A. Lieberman and A. J. Lichtenberg. *Principles of plasma discharges and materials processing.* John Wiley & Sons, 1994.

[44] R. Hemsworth. Positive and negative ion sources for magnetic fusion. *IEEE Transactions on Plas*, 33:1799–1813, 2005.

[45] A. Aanesland, S. Mazouffre, and P. Chabert. Space exploration technologies pegases - a new promising electric propulsion concept. *Europhysics News*, 423:28–31, 2011.

[46] D. Gerst, M. Cirisan, and S. Mazouffre. Strip-like structure in a low-pressure magnetized RF discharge. *IEEE Transactions on Plasma Science*, 39(11):2570–2571, 2011.

[47] D. Gerst, M. Cirisan, and S. Mazouffre. Strip-like plasma drift in a magnetized RF discharge. In *Proceedings of the 30th International Conference on Phenomena in Ionized Gases, Belfast, Ireland, 2011*, A4-328.

[48] D. Gerst, S. Cuynet, M. Cirisan, and S. Mazouffre. Plasma drift in a low-pressure magnetized radio frequency discharge. *Plasma Sources Sci. Technol.*, 22(1):015024, 2013.

[49] L. J. Mahoney, A. E. Wendt, E. Barrios, C. J. Richards, and J. L. Shohet. Electron-density and energy distributions in a planar inductively coupled discharge. *J. Appl. Phys.*, 76:2041–2047, 1994.

[50] K. Dannenmayer, P. Kudrna, M. Tichy, and S. Mazouffre. Measurement of plasma parameters in the far-field plume of a Hall effect thruster. *Plasma Sources Sci. Technol.*, 20:065012, 2011.

[51] W. Baumjohann and R. A. Treumann. *Basic space plasma physics.* Imperial College Press, 1997.

[52] K. Dannenmayer and S. Mazouffre. Elementary scaling relations for Hall effect thrusters. *J. Propul. Power*, 27:236–245, 2011.

[53] G. J. M. Hagelaar and N. Oudini. Plasma transport across magnetic field lines in low-temperature plasma sources. *Plasma Phys. Control. Fusion*, 53:124032, 2011.

[54] P. Chabert, J. Arancibia Monreal, J. Bredin, L. Popelier, and A. Aanesland. Global model of a gridded-ion thruster powered by a radiofrequency inductive coil. *Physics of Plasmas*, 19:073512, 2012.

[55] H. J. Leiter and K.-H. Loeb, Horst W. ahd Schartner. The RIT15 ion engines-a survey of the present state of radio frequency ion thruster technology and its future potentiality. In *Proc. 3rd International Conference on Spacecraft Propulsion, Cannes*, 2000.

[56] R. G. Jahn. *Physics of Electric Propulsion*. McGraw-Hill Book Company, 1968.

[57] J. Vaudolon, S. Mazouffre, D. Gerst, and S. Tsikata. Experimental study of acceleration processes in Hall effect thrusters. In *63rd International Astronautical Congress, Naples, Italy, Paper IAC 12-E218*, 2012.

Appendices

A Flow Meter Conversion Factors

Two AERA FC-7700 flow meters are used to regulate the mass flow rate into the discharge chamber. The flow meters are calibrated to a maximum flow rate of 20 sccm SF_6 and to 50 sccm argon. The flow meters can be used with other gases if a conversion of the maximum flow rate is performed. Table A.1 gives the conversion factor a with respect to nitrogen. The flow rate can be converted,

$$Q_x = Q_{N_2}a, \tag{A.1}$$

where Q_x is the flow rate for the respective gas and Q_{N_2} the flow rate in nitrogen.

Symbol	Name	Conversion factor
Ar	argon	1.410
He	helium	1.410
Kr	krypton	1.410
N_2	nitrogen	1.000
O_2	oxygen	0.989
SF_6	sulfur hexa flouride	0.263
Xe	xenon	1.410

Table A.1: Conversion factors for AERA FC-7700 flow meter in respect to nitrogen.

B Version Française

B.1 Introduction générale

"Une fusée dans l'espace cosmique" était le nom d'un article publié par K.E. Tsiolkovski en 1903. C'est la date maintenant considérée comme le début de la science moderne des fusées et de l'astronautique. La partie la plus importante de cet article est probablement ce qu'on appelle l'équation de la fusée ou équation de Tsiolkovski. Cette équation, basée sur la conservation de la quantité de mouvement décrit le déplacement d'un véhicule lié à l'éjection d'une certaine masse de matière transportée dans le véhicule. Cette équation indique que le changement maximal de la vitesse est une fonction du rapport entre la masse initiale de la masse finale et la vitesse d'éjection de la masse d'appui. Tsiolkovski lui-même avait identifié les limites de la vitesse d'échappement dans la propulsion chimique. Il écrira 8 ans plus tard : " Il est possible que dans le temps, nous pourons utiliser l'électricité pour produire une vitesse gigantesque pour les particules éjectées de la fusée " dans son article " Enquête sur l'espace universel par des dispositifs à réaction ".

Le développement de moteurs-fusées chimiques a commencé à la fin des années 40 du 20ème siècle. La vitesse de développement accélère rapidement dans les années 50 où le lancement du satellite Spoutnik par l'Union soviétique le 4 Octobre 1957 a déclenché la course à l'espace. A partir de ce moment-là, l'Union soviétique et les états-Unis sont en compétition pour la suprématie dans l'espace avec des objectifs tels que la première sortie extravéhiculaire humaine dans l'espace. La lutte se termine lorsque Neil Armstrong pose le pied sur la lune le 20 Juillet 1969.

à partir du moment de la prédiction de Tsiolkovski, il s'est écoulé plus de 50 ans jusqu'en 1964, année où la NASA a lancé SERT-1, première mission avec un propulseur ionique de type Kaufman, qui a prouvé que Tsiolkovski avait raison. La NASA a ainsi démontré la faisabilité de la propulsion d'une sonde spatiale au moyen de particules accélérées électrostatiquement. A partir de ce moment, la propulsion électrique se développe rapi-

dement. Alors que les premières missions emploient du mercure ou du césium comme carburant, le xénon est désormais la norme pour la plupart des propulseurs électriques modernes. Un grand nombre de concepts de propulseurs électriques ont été développés au cours des 50 dernières années. Sur l'ensemble de ces concepts, deux types de moteurs se sont montrés plus prometteurs : le moteur ionique et le propulseur de Hall. Ces deux concepts, qui ont fait leur preuve au cours de plusieurs missions, monopolisent désormais le marché. Ces deux technologies offrent des performance en termes d'efficacité de poussée et d'impulsion spécifique qui ne peuvent physiquement pas être atteintes avec la propulsion chimique. Ceci permet des scénarios de missions jusqu'ici inenvisageable.

La mission Deep Space 1 de la NASA a réalisé un survol de l'astéroÃ¯de Braille et de la comète Borrelly avec l'aide de son propulseur ionique NSTAR. La mission japonaise Hayabusa a utilisé un micro propulseur ionique pour un rendez-vous avec l'astéroÃ¯de Itokawa et un retour d'échantillon vers la terre. La mission GOCE de l'ESA utilisait une paire de propulseurs ioniques T5 pour contrer la force de traînée de l'atmosphère afin de mesurer avec précision le champ gravitationnel de la Terre.

Les deux types de propulseurs, le propulseur de Hall et le propulseur ionique, bien que s'appuyant sur différentes architectures et principes physiques, partagent un point commun : ils accélèrent seulement des ions positifs. Il est donc nécessaire d'employer une cathode externe pour fournir des électrons et équilibrer ainsi les charges positives du faisceau. Les ions positifs et des électrons ont une longueur de recombinaison de plusieurs centaines de mètres. En conséquence, l'interaction avec des composants du véhicule spatial tels que les panneaux solaires ou les optiques ne peut être évitée.

Le propulseur PEGASES (Plasma Propulsion with Electronegative Gases) suit une autre voie. Le concept est en cours d'élaboration par la LPP (Laboratoire de Physique des Plasmas) de l'Ecole Polytechnique de Paris depuis 2005. Le propulseur PEGASES accélère des ions positifs et négatifs. Les ions sont produits par une source radiofréquence (RF) avec un gaz électronégatif tel que le SF_6. Le plasma passe à travers un champ magnétique qui favorise le refroidissement des électrons et augmente donc la création d'ions négatifs. Le plasma fortement électronégatif est ensuite fortement accéléré par des grilles polarisées alternativement. Une cathode de neutralisation n'est pas nécessaire puisque les charges positives et négatives quittent le propulseur ensemble : la quasineutralité est ainsi maintenue en permanence. La longueur de recombinaison entre les ions positifs et négatifs est seulement une fraction de celle entre les électrons et les ions

positifs. Cela permet de fortement limiter la rétrodiffusion des particules chargées qui peuvent conduire à une dégradation des panneaux solaires ou des optiques.

B.1.1 Motivation et objectifs

Malgré la simplicité apparente du concept beaucoup de travail restait à faire. Nous avons commencé nos expériences avec une décharge RF capacitive à 13.56 MHz générée à l'intérieur d'un tube de quartz. Le but était alors d'étudier différentes topologies du champ magnétique pour le propulseur PEGASES. En effectuant des expériences nous avons découvert une structure en forme de bande à l'intérieur du plasma. Une structure similaire venait juste d'être prédite dans des simulations numériques. Cela nous a conduit à une nouvelle priorité dans nos recherches. Nous avons alors essayé de répondre aux questions suivantes : d'où vient cette structure ? Qu'est-ce que cela signifie pour le propulseur PEGASES ? Peut-elle être supprimée ? En fin de compte, il s'est avéré que cette structure était aussi présente à l'intérieur du propulseur PEGASES.

Nous avions besoin d'un outil de mesure de la fonction de distribution de la vitesse des ions (VDF), ainsi que de la fraction d'ions moléculaires et de la quantité d'ions multi-chargés dans la plume du propulseur. Pour cela, nous avons développé une sonde en champs croisés E×B. Une telle sonde est nettement plus petite qu'un spectromètre de masse et peut ainsi être placée à l'intérieur de la chambre à vide. Elle est aussi plus facile à utiliser. L'objectif était d'utiliser la sonde avec une variété de gaz et finalement dans du SF_6, l'ergol proposé pour le prototype PEGASES.

B.1.2 Résumé du chapitre

Le chapitre 2 donne une introduction aux principes fondamentaux de la propulsion spatiale, suivie d'une présentation du propulseur de Hall et du propulseur ionique. Une description plus détaillée est donnée pour les propulseurs ioniques puisqu'ils sont étroitement liés à l'objet des recherches. Le chapitre se poursuit par une description du concept PEGASES et de ses éléments : la source de plasma RF, la barrière magnétique et le système d'accélération. Le chapitre se termine par une description du banc d'essai à vide utilisé pour les expériences.

Le chapitre 3 présente les sondes de plasma utilisées dans le cadre des travaux. Il introduit brièvement la sonde plane, la sonde capacitive, la sonde de Langmuir, la sonde

émissive et l'analyseur à champ retardateur. De plus on donne les éléments théoriques utilisés pour traiter les données obtenues.

Le chapitre 4 donne une présentation plus détaillée dans la théorie et la construction de la sonde E×B. Des simulations numériques de champ magnétique et électrique à l'intérieur de la sonde sont présentées, ainsi que des simulations de trajectoires d'ions. Une description détaillée de la construction du système de sonde est donné. Le chapitre se termine par la présentation des premières mesures qui ont été effectuées dans un propulseur de Hall et le propulseur ionique PEGASES.

Le chapitre 5 décrit l'étude sur une structure en forme de bande trouvée dans un plasma RF avec un champ magnétique perpendiculaire à l'écoulement. Des mesures avec une variété de sondes révèlent les propriétés du plasma. La dérive E×B est identifiée comme l'origine la plus probable de la structure. Un écran de Faraday est utilisé pour modifier les conditions de couplage de l'onde RF (transition capacitif vers inductif) afin d'atténuer la formation du ruban lumineux.

Le chapitre 6 contient les expériences réalisées avec le propulseur PEGASES. Les propriétés du propulseur sont caractérisées à l'intérieur de la cavité et l'efficacité de transfert de puissance est donnée. Des mesures avec la sonde E×B, une sonde plane et un RPA dans le faisceau du propulseur fonctionnant en xénon sont présentées. Une estimation de la poussée est donnée sur la base du flux d'ions mesuré. Le chapitre se termine par des expériences réalisées avec la barrière magnétique dans le SF_6 et le xénon.

Le chapitre 7 présente la conclusion du travail effectué et donne une des perspectives pour la recherche future sur le propulseur PEGASES.

B.2 Propulsion Électrique

Le but d'un système de propulsion est la génération et la livraison de la poussée afin de le déplacer. Le principe de la génération de la poussée d'un moteur-fusée est de créer un échange de quantité de mouvement entre le gaz propulseur qui est éjecté à une vitesse élevée et de la fusée ou engin spatial. Le Δv le changement de vitesse de l'engin spatial par son système de propulsion quand aucune autre force supplémentaire est appliquée.

Il provient de l'équation de fusée Constantin Tsiolkovski,

$$\Delta v = v_e \cdot \ln \frac{m_0}{m_1}, \tag{B.1}$$

où m_0 est la masse initiale de l'engin spatial et m_1 dont la masse à la fin de la manœuvre. La seule solution possible pour augmenter l'inductance de mission au dessus d'un certain niveau est d'augmenter la vitesse d'échappement propulseur. Cela peut être fait en utilisant des propulseurs électromagnétiques qui permettent d'accélérer un gaz propulseur ionisé soit par la force de Lorentz ou par un champ électromagnétique.

Sur une variété de différentes idées de propulsion électrique deux concepts clairement émergé et ont déjà été utilisés sur plusieurs missions, le propulseur salle et le propulseur ionique quadrillée. Propulseurs ioniques fonctionnent en accélérant de manière électrostatique des ions extraits d'un générateur de plasma et en les neutralisant.

Le propulseur PEGASES (acronyme de Plasma Propulsion with Electronegative Gases) est une nouvelle conception d'un système de propulsion ionique. Le concept de propulseur PEGASES a été créée par P. Chabert dans le laboratoire LPP de l'Ecole Polytechnique de Paris en 2005. Le plasma dans le propulseur est inductif généré par une bobine RF plane à l'arrière de l'étrave. Un gaz électronégatif tel que le SF_6 est utilisé comme propulseur. Les électrons dans le plasma sont refroidies en raison de la collision à l'intérieur du champ magnétique de la barrière. Il en résulte la création de plus d'ions négatifs à un point où l'on peut parler d'un plasma ion-ion. Les ions négatifs et positifs sont ensuite accélérés par un ensemble de grilles alternativement biaisées.

B.3 Diagnostics

Une sonde de Faraday plane offre la possibilité de mesurer le flux d'ions avec une grande précision. Un inconvénient des sondes cylindriques, tels que la sonde de Langmuir, est que la zone de collecte dépend fortement de la taille de la gaine. Si la taille de la gaine est de l'ordre du diamètre du fil une erreur importante peut être introduite. Une sonde plane permet d'éviter ce problème.

Une sonde capacitive peut être utilisée afin de déterminer les fluctuations RF du potentiel à l'intérieur du plasma. La connaissance des variations RF du potentiel est utile pour identifier le caractère de la décharge. Un haut niveau d'oscillation indique un couplage

capacitif de l'énergie RF vers le plasma même si une bobine d'induction est utilisée.

La sonde de Langmuir est probablement la méthode la plus simple pour obtenir une grande variété d'informations sur un plasma. Une sonde de Langmuir de base se compose simplement d'un fil métallique qui est plongé dans un plasma et collecte du courant pour une série de tensions de polarisation. La conception de la sonde influe cependant sur le plasma.

Une sonde émissive a l'avantage d'être peu sensible à un champ magnétique, contrairement à une sonde de Langmuir. Le filament de la sonde d'émission en tungstène est chauffé avec une source d'alimentation DC jusqu'à un régime d'émission d'électrons. Le potentiel flottant d'une sonde chaude émettant suffisamment est pratiquement égal au potentiel du plasma car le courant d'électrons allant du plasma vers la sonde est compensé par l'émission d'électrons due au chauffage : la gaine plasma est ainsi fortement atténuée et $V_s \approx V_p$.

Un analyseur à champ retardateur (RPA), également connu sous le nom d'analyseur d'énergie à champ répulsif (RFEA), est utilisé pour mesurer la fonction de distribution en énergie des ions (FDEI) dans un plasma. Une grille, dite de filtrage, à l'intérieur de la sonde est polarisée à partir d'une valeur légèrement négative à une valeur positive jusqu'à ce que le courant d'ions collecté soit nul. La FDEI est proportionnelle à la dérivée de la courbe courant-tension du RPA. Notez que d'autres grilles sont utilisées pour l'écrantage du plasma et pour le filtrage des électrons. Un RPA est généralement composé de 4 grilles.

B.4 Sonde E×B

Une sonde E×B, également appelé un filtre de Wien, est une sonde électromagnétique en champs E et B croisés qui fonctionne comme un filtre passe-bande pour les ions. Elle recueille et mesure des ions arrivant dans une très étroite gamme de vitesse correspondant au rapport E/B. Les ions qui arrivent avec une vitesse en dehors de cette gamme sont déviés. Par conséquent, la sonde E×B est un outil de diagnostic qui peut être utilisée pour mesurer la fonction de distribution en vitesse (VDF) des ions dans a plume des propulseurs électriques.

Dans une sonde E×B un champ électrique est appliqué orthogonalement à un champ magnétique. Une particule arrivant perpendiculairement aux deux domaines ne traverser

la zone en ligne droite uniquement si sa vitesse correspond à E/B. Cet effet est décrit par la force de Lorentz.

Pour être en mesure de balayer une plage de vitesses soit le champ magnétique soit le champ électrique peut être modifié. Dans notre cas, le champ magnétique est fixe et généré avec des aimants permanents en SmCo et le champ électrique varie via l'application de tensions de polarisation opposés sur deux plaques parallèles à l'intérieur de la sonde.

Un modèle numérique de la sonde E×B a été construit avec COMSOL. Le modèle comprend le champ électrique et magnétique généré par les aimants et les électrodes, ainsi que la structure et les matériaux de la sonde. Des simulations ont été effectuées pour déterminer la trajectoire des particules à travers la sonde E×B.

Des mesures ont été effectuées dans le jet d'un propulseur Hall et dans le propulseur PEGASES. Une trace de la sonde E×B avec le propulseur PEGASES montre les différentes espèces ions et peut aider à les identifier. On peut voir que la vitesse des ions est toujours supérieure à la valeur attendue calculée à partir de la tension de polarisation. Cela est dû au fait que le potentiel du plasma contribue à l'accélération des ions.

B.5 Etude de la structure en bande

Une barrière magnétique est un élément crucial pour la génération d'ions négatifs dans les sources de plasma à basse pression fonctionnant avec des gaz électronégatifs. Le champ magnétique est utilisé pour piéger les électrons et les refroidir ensuite les par collisions avec des particules lourdes. Une basse température électronique conduit à un taux d'attachement plus élevée, augmentant ainsi la production d'ions négatifs.

Lors de l'étude de configurations de champ magnétique différentes pour le piège du propulseur PEGASES en utilisant une décharge radiofréquence à couplage capacitif, on a observé la formation d'un motif bidimensionnel stationnaire dans la région où l'intensité du champ magnétique est élevée.

Lorsque l'on superpose un champ magnétique à la décharge RF, la structure du motif en forme de S est observée sur une large gamme de paramètres avec la décharge fonctionnant en mode capacitif. Les mesures des propriétés électroniques ont été réalisées avec une sonde de Langmuir compensée pour les oscillations RF à la sortie du tube de décharge avec de l'argon comme gaz. Ces mesures montrent que la structure de type bande agit comme un pont pour les électrons : ces derniers peuvent ainsi traverser la barrière

magnétique.

Une façon de réduire le couplage capacitif de l'onde RF consiste à placer un écran de Faraday branché à la terre entre l'antenne et le plasma. L'écran de Faraday localise le champ électrostatique entre la bobine et l'écran. Introduire un écran de Faraday dans notre configuration permet d'atténuer très fortement, voir d'éliminer, la structure de bande. Cela renforce l'hypothèse que la bande trouve son origine dans une dérive E×B.

La structure de type bande semble correspondre à une dérive "ouvert" des électrons magnétisés qui interagit avec les parois du réacteur. En mode capacitif, la bande est très lumineuse du fait des collisions entre les électrons chauds et les particules de gaz. La lumière est émise lorsque les atomes se désexcitent.

La bande d'une source de plasma à couplage inductif est faible ou inexistante. Très probablement, le plasma est homogène dans la zone oú les ions sont extraits et accélérés, c'est-à-dire dans la zone où les grilles sont placées dans le propulseur PEGASES.

B.6 Le propulseur PEGASES

Le propulseur PEGASES est non seulement une source pour créer un plasma d'ions négatifs à forte densité ou même un plasma ion-ion. Il peut également être utilisé comme propulseur ionique classique. Cela signifie qu'un plasma est créé dans un gaz neutre et que les ions positifs sont extraits et accélérés, ce qui rend nécessaire la neutralisation du faisceau derrière les grilles. Les performances du propulseur PEGASES ont été étudiées principalement dans du xénon afin de comparer les résultats obtenus avec les propriétés d'autres propulseurs ioniques.

Il a été démontré que le propulseur PEGASES peut être utilisé comme une source de plasma RF efficace dans du xénon. La source n'est pas encore optimisée et il existe encore une marge d'amélioration pour l'efficacité. Les mesures ont été effectuées à l'intérieur de la cavité de décharge afin d'étudier les paramètres du plasma et obtenir le flux d'ions. Une accélération du plasma a été produite avec un système à deux grilles. Les ions accélérés dans le jet du propulseur PEGASES ont été analysés avec une variété de sondes. Le flux d'ions a été mesuré avec une sonde plane pour une variété de conditions. Le potentiel du plasma a été mesuré à l'aide d'une sonde de Langmuir. La fonction de distribution de la vitesse des ions a été mesurée à l'aide d' une sonde E×B. Les ions multichargés ont été observées dans le jet du propulseur. On a aussi trouvé des

traces d'autres gaz qui proviennent probablement d'une petite fuite dans le système. Les mesures avec un RPA ont montré la fonction de répartition de l'énergie des ions. Ces mesures ont été utilisées pour vérifier les résultats de la sonde E×B. Les mesures de la sonde E×B sont en bon accord avec la vitesse théorique. Une petite déviation est cependant observée ce qui indique qu'une calibration de la sonde E×B est indispensable. Une estimation de la poussée et de l'efficacité totale du propulseur révèlent un faible rendement. Le bas niveau de performance provient de l'emploi d'un système de grilles non optimisé. Il existe donc une importante marge pour le rendement. Lorsque ce dernier est calculé en supposant une extraction du courant de Bohm, on retrouve un niveau similaire à celui des meilleurs RIT.

Une structure de plasma asymétrique a été observée de façon optique dans la cavité du propulseur PEGASES avec une barrière magnétique. La structure a été identifiée comme une dérive des électrons. Cette instabilité est probablement du même type que celle découverte au début de cette thèse dans une décharge RF capacitive. Le facteur dominant pour PEGASES est probablement la dérive E×B due au champ électrique résiduel. La structure a été étudiée à l'aide d'une sonde de Langmuir. On a montré qu'elle se situait principalement à l'arrière du propulseur à proximité de l'antenne RF. La dérive ne semble avoir aucune influence sur l'homogénéité du plasma au niveau des grilles d'extraction.

B.7 Conclusion

B.7.1 Vue d'ensemble des travaux

Objectifs de la thèse

Le but de la thèse était d'étudier le propulseur PEGASES avec une variété de sondes à l'intérieur de la cavité de décharge et dans le faisceau d'ions. L'étude visait à confirmer que PEGASES est une source de plasma efficace pour la propulsion électrique dans du xénon. Pour cela, il était nécessaire d'obtenir des valeurs préliminaires de l'efficacité de transfert de puissance, de la génération de poussée et de l'efficacité totale du propulseur.

Propulseur PEGASES

Le concept du propulseur PEAGSES s'appuie sur un plasma ion-ion, ce qui signifie un plasma dépourvu d'électrons libres. Les ions positifs et négatifs sont extraits et accélérés alternativement au moyen d'un assemblage de grilles à haute tension. PE-GASES appartient donc à la famille des moteurs ioniques à grilles. L'emploi de gaz électronégatifs comme SF 6 combinés avec une barrière magnétique permet de créer un plasma électronégatif à forte densité. Les ions positifs et négatifs peuvent ensuite être extraits en polarisant alternativement une paire de grilles d'extraction. Comme la source RF du propulseur PEGASES est une source d'ions efficaces, il a été décidé d'étudier son utilisation en tant que propulseur ionique classique fonctionnant en xénon.

Un prototype du propulseur PEGASES similaire à celui en usage au LPP a été installé sur le banc d'essais à vide EPIC au laboratoire ICARE. Le propulseur a été opéré avec une décharge au xénon afin d'obtenir des valeurs comparables à d'autre propulseurs ioniques RF. Le plasma à l'intérieur de la chambre de décharge a été étudié pour obtenir des valeurs pour la température des électrons, la densité des électrons et pour le potentiel du plasma pour différentes conditions de décharge. Le flux d'ions a été mesuré à la position des grilles pour trouver le courant d'ions extrait. Une accélération des ions xénon avec un ensemble de deux grilles a été démontrée. Le jet de plasma résultant a été étudié avec une variété de sondes sur une large gamme de paramètres à des positions différentes. Le flux d'ions dans le faisceau a été mesurée à l'aide d' une sonde plane. Le potentiel du plasma a été mesuré avec une sonde de Langmuir. Les mesures avec la sonde E×B révèlent la FDV des ions afin d'obtenir des quantités fondamentales qui peuvent être comparées avec les valeurs disponibles dans la littérature pour d'autres moteurs ioniques RF. La fonction de répartition en énergie des ions a été mesurée à l'aide d' une sonde RPA.

Après l'ajout d'une barrière magnétique au propulseur PEGASES, afin d'étudier le propulseur en SF_6 son carburant initial, ce qui signifie la création et l'accélération d'ions négatifs et positifs, une structure lumineuse asymétrique est apparue. Cette structure a été observée avec plusieurs gaz tels que Ar , Xe et SF_6. Il a été montré que la direction du champ magnétique influe sur la localisation de la structure. Nous avons vérifié que l'origine de ce phénomène ne se situe pas dans une éventuelle asymétrie dans le propulseur PEGASES. Une mesure en deux dimensions à l'intérieur de la cavité de décharge du propulseur PEGASES avec une sonde de Langmuir révèle les paramètres du plasma. La température des électrons , la densité d'électrons et le potentiel du plasma

font apparaître l'emplacement et la cohérence de la structure. La structure lumineuse asymétrique observée est confinée entre la barrière magnétique et l'arrière de la chambre de décharge où se situe la bobine RF. Le plasma dans cette région présente une température électronique élevée et un fort potentiel du plasma ainsi que d'une densité plus élevée par rapport à la moyenne. L'origine de la structure se trouve probablement dans une dérive des électrons. Les variations du potentiel plasma sont faibles par rapport à celles observé dans les expériences précédentes avec une décharge RF capacitive puisque le propulseur est une pratiquement purement inductive. Le champ électrique au sein du plasma est donc faible. Une estimation des vitesses de dérive E×B révèle que la dérive due au champ électrique résiduel est probablement le facteur dominant dans la formation de cette structure. La barrière magnétique semble cependant limiter la dérive des électrons au niveau de l'arrière de la chambre. Le plasma, dans le plan où les grilles d'accélération sont généralement montées semble être homogène. Ceci est important pour l'extraction d'ions et l'accélération des ions car un plasma inhomogène en face des grilles conduit à une réduction de l'efficacité globale.

Performances

I a été montré que l' efficacité du transfert de puissance de la source RF PEGASES peut atteindre jusqu'à 87 % en xénon. Ce nombre révèle que le propulseur PEGASES dans son état actuel est une source d'ions efficace et se rapproche des autres propulseurs ioniques RF comme la famille RIT. D'un autre côté, la poussée mesurée, de l'ordre de 0.5 mN, est très faible par rapport aux autres propulseurs ioniques qui ont généralement des poussées de 10 à 50 mN pour une puissance de 400 W à 1500 W. La faible poussée est principalement due au fait que la géométrie des grilles n'est pas optimisée. Le rendement total obtenu est très faible avec 0.08 %. Même quand la consommation d'énergie du filament de neutralisation est négligée, il augmente seulement à 0.15 %. La configuration des grilles doit être optimisée afin d'extraire et d'accélérer un plus grand nombre d'ions. On a montré que si le courant extrait correspond au courant de Bohm alors le rendement total passerait à 29 % et 52 % en négligeant la consommation d'énergie du neutraliseur et la divergence du faiseau. Cela pourrait accroître l'efficacité totale au voisinage des 67 % qui est atteint par le propulseur RIT15.

Sonde E×B

Un système de sonde E×B a été développée et ajoutée aux outils de diagnostic déjà disponibles au laboratoire ICARE. La sonde E×B permet de mesurer la fonction de distribution en vitesse des ions (FDV) dans le jet de propulseurs électriques tels que les propulseurs de Hall et les propulseurs ioniques. La sonde permet aussi d'identifier des ions à charge multiple. En analysant la FDV obtenue, le rapport entre les différentes espèces d'ions peut être calculé. LA FDV peut également révéler la présence d'autres gaz dans le jet du propulseur et peut ainsi aider à identifier les fuites ou les impuretés. Le niveau de signal en sortie de la sonde E×B développée peut être ajustée en jouant sur la géométrie des collimateurs d'entrée et de sortie pour tenir compte des différentes conditions de plasma. Il est également possible d'augmenter la résolution de la sonde E×B si une mesure plus précise est requise mais au détriment du niveau de courant.

La sonde E×B a été testée dans le jet d'un propulseur Hall et du propulseur PEGASES. Les résultats obtenus ont été comparés à des mesures d'autres sondes telle qu'une sonde plane et une sonde RPA. Les tests montrent qu'un étalonnage de la sonde E×B est nécessaire afin d'obtenir de meilleures valeurs. Enfin la sonde E×B a été utilisée pour analyser le faisceau du propulseur PEGASES fonctionnant comme un propulseur ionique classique en xénon. La sonde a fourni des données précieuses pour comprendre le mécanisme d'accélération et la physique de la plume.

Structure de bande

Lors de l'étude sur la topologie magnétique pour le propulseur PEGASES, une structure en forme de bande lumineuse asymétrique a été découverte dans un plasma RF. Il a été démontré que la structure est présente dans une grande variété de gaz tels que Ar, Xe, O_2 , SF_6 , N_2 et Kr. La structure est présente sur une large bande de fréquences RF, quelle que soit l'intensité du champ magnétique et sur un large domaine de pression. L'étude a identifié des dérives de plasma , en particulier la dérive E×B , comme une origine possible de la structure de bande. L'antenne en spirale située derrière le tube à décharge utilisé dans les expériences n'est pas purement inductive mais un couplage capacitif existe. Il en résulte des fluctuations RF à l'intérieur du plasma qui peuvent créer un champ électrique entre le plasma à l'intérieur du tube à décharge et la chambre à vide reliée à la terre. Le champ électrique ainsi que le champ magnétique créent une dérive des électrons qui conduit probablement à la structure observée. Le couplage

capacitif, et donc le champ électrique résultant, peut être réduit par l'introduction d'un écran de Faraday entre la bobine RF et la chambre de décharge. Dans ce cas, l'écran conduit à une disparition de la structure de bande.

B.7.2 Perspectives

Beaucoup de réalisations ont été présentés dans cette thèse mais un plusieurs points restent encore à étudier. Cette section donne des objectifs pour la recherche future.

PEGASES

Le propulseur PEGASES n'était pas initialement destiné à un fonctionnement avec du xénon comme un propulseur ionique classique. Nous avons néanmoins démontré que la source est efficace. Avec un peu d'efforts, PEGASES pourraient devenir un propulseur ionique au xénon qui accélère seulement des ions positifs et rivaliser avec les RIT.

Les grilles du propulseur PEGASES offrent actuellement de grandes marges d'optimisation. Par conséquent, l'étage d'extraction/accélération à grilles doit être repensée. Cela nécessite probablement une grande quantité de travail. Par la suite, il serait intéressant de mesurer la véritable poussée du propulseur à l'aide d'un pendule ou de réaliser une nouvelle version du prototype pour qu'il puisse être monté sur une balance de poussée. Actuellement, le propulseur est monté à l'extérieur d'une chambre à vide et l'ensemble bobine - bpîte d'accord ne se trouve pas dans le vide.

L'un des principaux objectifs devrait être de démontrer l'extraction et l'accélération alternée d'ions positifs et négatifs et d'étudier le faisceau de plasma ainsi crée avec les sondes et les outils disponibles.

Sonde E×B

Les plans originaux der la sonde E×B incluaient une section pour la séparation d'un des ions positifs et négatifs puisque la sonde devait être utilisée dans le jet de plasma du propulseur PEGASES. Ceci n'a pas encore été inclus dans le dispositif expérimental car une accélération d'ions négatifs n'a pas encore été tentée au laboratoire ICARE. Jusqu'à présent,seule l'équipe du LPP l'a réalisée. Introduire cette section dans la conception de la sonde E×B créerait un outil puissant pour l'étude du jet de plasma du

propulseur PEGASES lors du fonctionnement en mode d'accélération alternée avec un gaz électronégatif.

Une calibration de la sonde E×B avec une source de plasma bien connue permettrait d'augmenter la précision de la sonde et les données obtenues. Les résultats de la sonde doivent être comparés à ceux obtenus par RPA et LIF. Une calibration de la sonde E×B en ferait un outil de grande valeur pour toutes sortes de propulseur à plasma.

Une amélioration des données de la sonde E×B peut également être obtenue en ajoutant un système de pompage différentiel de la sonde. Cela diminuerait la pression à l'intérieur et les libres parcours moyen de collision et d'échange de charge ; en conséquence le signe serait de meilleur qualité.

Structure de bande

La découverte de la structure de bande a mené à une meilleure compréhension de la dérive électronqiue à l'intérieur du plasma. Il s'avère que les structures liées à des dérives peuvent être trouvées dans d'autres sources de plasma magnétisées. Comme l'origine probable de la structure est maintenant connue, une source de plasma dédiée pourrait être conçue pour étudier ce phénomène. Plus nous en savons sur cet effet, plus nous pouvons concevoir des sources de plasma magnétisé à basse pression qui peuvent limiter cet effet ou bien profiter de ses propriétés.

Jan Dennis GERST

Sources plasma RF magnétisées : Applications à la propulsion spatiale

Résumé :

Le propulseur PEGASES (Plasma Propulsion with Electronegative Gases) est un nouveau type de propulseur électrique pour la propulsion spatiale. Il utilise des ions négatifs et positifs créés par une décharge radiofréquence à couplage inductif pour générer la poussée. L'accélération électrostatique des ions est assurée par un ensemble de grilles polarisées. Un filtre magnétique est utilisé pour augmenter la quantité d'ions négatifs dans la cavité du propulseur.

Le propulseur PEGASES est non seulement une source qui permet de créer un plasma d'ions négatifs à forte densité, et même un plasma d'ion-ion, mais il peut également être utilisé comme un propulseur ionique classique. Cela signifie qu'un plasma est créé dans un gaz électropositif (e.g. Xe) et que les ions positifs sont extraits et accélérés. Dans ce cas, il est nécessaire de neutraliser le plasma derrière la zone d'accélération, comme dans d'autres propulseurs ioniques. Les performances du propulseur PEGASES ont été étudiées principalement dans du xénon afin de comparer les résultats obtenus avec les propulseurs ioniques de type RIT.

Le propulseur a été étudié à l'aide d'une série de sondes telles qu'une sonde de Langmuir, une sonde plane, une sonde capacitive et un RPA (pour Analyseur à Champ Retardateur). De plus, une sonde en champs croisés ExB a été développée pour mesurer la vitesse des ions quittant le propulseur ainsi que la fraction des différentes espèces ioniques présentes dans le plasma.

Mots clés : plasma, propulsion électrique, propulseur ionique

Investigation of Magnetized Radio Frequency Plasma Sources for Electric Space Propulsion

Abstract :

The PEGASES thruster (Plasma Propulsion with Electronegative Gases) is a novel type of electric thruster for space propulsion. It uses negative and positive ions produced by an inductively coupled radio frequency discharge to create the thrust by electrostatically accelerating the ions through a set of grids. A magnetic filter is used to increase the amount of negative ions in the cavity of the thruster.

The PEGASES thruster is not only a source to create a strongly negative ion plasma or even an ion-ion plasma but it can also be used as a classical ion thruster. This means that a plasma is created and only the positive ions are extracted and accelerated making it necessary to neutralize the plasma behind the acceleration stage like in other ion thrusters. The performances of the PEGASES thruster have been investigated mainly in xenon in order to compare the obtained results with RIT-type ion thrusters.

The thruster has been investigated with the help of a variety of probes such as a Langmuir probe, a planar probe, a capacitive probe and a RPA (Retarding Potential Analyzer). In addition, an ExB probe has been developed to measure the velocity of the ions leaving the thruster and to differentiate between the ion species present in the plasma.

Keywords : plasma, electric propulsion, ion thruster

Institut de Combustion Aérothermique Réactivité et Environnement - ICARE

1C avenue de la. Recherche Scientifique, 45071 Orléans